# Identifying Erosional Hotspots in Duluth-Area Streams after the 2012 Flood Using High-Resolution Aerial Lidar Data

A Thesis
SUBMITTED TO THE FACULTY OF
UNIVERSITY OF MINNESOTA
BY

Pichawut Manopkawee

IN PARTIAL FULFILLMENT OF THE REQUIREMENTS
FOR THE DEGREE OF
MASTER OF SCIENCE

Dr. Karen Gran

August 2015

© Pichawut Manopkawee 2015

**Acknowledgements**

The project would not have been successful without the help from many people in many ways. It is an excellent opportunity to thank individuals and institutions that support me to reach the goals. First and foremost, I would like to thank my advisor, Professor Karen Gran, for her guidance, patience and encouragement, without this research would never have accomplished. Her efforts and ability helped me smooth out of my idea and grammatical constructions. Her felicitous style made my graduate studies a truly pleasant experience. To my committee, Professor John Swenson and Professor Tongxin Zhu, I am extremely grateful for their assistance and valuable suggestions throughout my project. Moreover, I cannot forget to thank all my new friends in fluvial geomorphology research group; Virginia Batts, Courtney Targos, Nathaniel Mitchell, and Edward Gazzetti, who support and give assistance on various aspects of this project.

I would highly appreciate Department of Earth and Environmental Sciences, University of Minnesota Duluth that gives me a great opportunity and excellent experience during my graduate studies. I must thank Department of Geological Sciences, Chiang Mai University, Thailand that fosters my strength, knowledge and experience in Geology during my undergraduate studies. In addition, I also highly appreciate the Royal Thai Government Scholarship provided by the Royal Thai Embassy, to support my life, research experience, and wonderful activities in the USA.

Finally, I would like to acknowledge with immense gratitude, the support and love from my family, my parents, my friends and other participants who provide so much love, motivation and encouragement throughout my entire education.

## Abstract

During June 19th to 20th, 2012, northeastern Minnesota experienced a high record rainfall event, causing soil saturation and inundation, slope failures, flash flooding, and damage to public infrastructures. Geomorphic effects of the flood included severe streambank and bluff erosion and landslides. The purposes of this study are to investigate erosional hotspots and channel reaches in Duluth-area streams that experienced significant geomorphic changes as a result of the 2012 flood and to determine the roles of human modifications to the stream networks on erosional hotspots at a reach scale.

Erosion occurred when driving forces, controlled by topography and precipitation, overcame resisting forces, controlled by shear strength of materials at the bed and banks. One-meter resolution lidar data, which were collected before and after the flood, were used to extract driving forces, predict erosional hotspots, and map out locations of significant geomorphic change in a GIS framework. Lidar data were first filtered in GeoNet to remove noise in low-gradient areas and enhance geomorphic features. The lidar-derived DEMs were then used to calculate a stream power-based erosion index (SP) and angle of impingement (AOI), to identify stream reaches with high bend curvature, and to identify stream reaches proximal to high bluffs. Bedrock exposure locations, which could significantly limit erodibility, were obtained from Minnesota Geological Survey maps (Hobbs, 2009a, b, c). These parameters were used to predict preliminary erosional hotspot locations. Field observations were done to verify the results of predicted erosional hotspots from the GIS-based predictive model and develop a new threshold model. The refined predicted erosional hotspots were classified into different types and were compared with valley types and channel-reach types to determine how susceptible different channel-reach types were to change.

The preliminary GIS-based predictive model had low accuracy of prediction due to misidentification of many erosional sites along the streams, compared to erosional sites from field observations. The refined threshold model improved the percent of accuracy for all points and for FEI $\geq 2$ to greater than 80%, with less than 10% of points over- and under-predicted on three sample streams. The Minnesota Geological Survey (MGS) bedrock exposure maps were verified and improved by field maps, resulting in 90-95%

accuracy in new bedrock exposure locations. In terms of types of erosional hotspots, more than 70% of erosional hotspots in the northern and the southern ends of Duluth are located in pool-riffle reaches within entrenched valleys; these hotspots are primarily classified as topographic erosional hotspots, which likely had significant geomorphic changes due to topography, substrate materials, and planform geometry. In the central area of Duluth, more than 70% of erosional hotspots are located in pool-riffle reaches within confined valleys; these hotspots are classified as topographic/anthropogenic erosional hotspots due to being located in the areas of significant anthropogenic influences. Pool-riffle reaches are identified as the most susceptible channel-reach type to change from the 2012 flood.

The GIS-based predictive model could locate erosional hotspots and susceptible reaches which were strongly affected by the 2012 flood. It also incorporates anthropogenic effects to describe the influences of human construction causing erosion in a particular area. The project offers the City of Duluth useful data on causes of the channel changes in the particular reaches, potentially helping with future stream restoration efforts.

## Table of Contents

## List of Tables

## List of Figures

## *Introduction*

From June 19th to 20th, 2012, Duluth and adjacent areas in northeastern Minnesota experienced 0.18 meter (7.25 inches) rainfall as measured at the Duluth International Airport, which was the greatest 2-day precipitation ever recorded (Graning & Hluchan, 2012). The Mississippi headwaters, the St. Croix River, and western Lake Superior streams experienced significant flooding causing geomorphic changes in stream corridors, including channel migration, changes in local slope, and adjustments to grain size distributions (Czuba et al, 2012). This rainfall event led to saturation of soil, significant runoff, and an increase in erosion of streambanks and bluffs along the streams. The heavy flood caused damage of more than $100 million to repair utilities, infrastructure, and recreational areas in Duluth and the surrounding areas in the St. Louis County (Schwartz, 2012).

After the flood, many people attempted to assess the impacts of geomorphic characteristics of the Lake Superior Stream because many of them experienced high magnitudes of erosion, which possibly affected communities and ecological systems. In terms of geological assessment, Neitzel (2013) determined the magnitude of erosion of selected bluffs in Amity Creek related to the flood events and quantified the amount of sediment distributed to the channels. Wick (2013) developed a GIS-based model to predict erosional hotspots at a reach scale along Amity Creek, Talmadge River, and French River, and compared predictions to impacts from the flood. In terms of chemical analysis of Lake Superior, Forsman (2014) estimated the effect of the severe flood on dissolved nutrients in western Lake Superior. She also found how lakes and their biota responded to the severe flood. This study focuses specifically on where erosion occurred along channels during the flood. Erosional hotspots are defined as areas of concern that are susceptible to erosion and have high potential to contribute a large amount of sediments to streams. These hotpots could cause significant geomorphic changes in stream corridors through time. In this study, we compare the locations of erosion that occurred during the flood with predicted erosional hotspots to develop and refine a predictive erosional model.

Theoretically, erosional hotspots at a reach scale can be predicted if an effective tool to see the topography of landscapes is available. Now, lidar data provided by Minnesota Geospatial Information Office (MnGeo) are available, so we can attempt to predict erosional hotspots remotely based on channel topography and geometry. Lidar is a laser scanning technique which has been widely used to generate precise measurements of surfaces and can be visualized as a three-dimensional raster digital elevation model (DEM) over landscapes. The collection of high-resolution aerial lidar data in the Arrowhead region during 2011 and 2012 was part of a publicly-funded statewide initiative. Because lidar was collected before and after the occurrence of flood, we could potentially use those lidar data from different time periods to demonstrate how a particular landscape has changed through time.

In order to qualitatively and quantitatively assess the impacts of the 2012 flood in Duluth, twelve streams ranging from the Lester River to Mission Creek were selected for erosional hotspots analysis. At each site, lidar data were used to determine shapes, sizes, elevations, slopes, and upstream areas of the channels. These parameters were used to calculate GIS-based predictors and locate high bluffs. Bedrock exposure location is another important parameter that was used to predict where erosional hotspots are located since bedrock exposure affects channel erodibility. Field observations were performed to check the results from predictions. Field-mapped erosion could be influenced by either topographic changes or human modifications on landscapes, such as infrastructure development in and around rivers. The identification of these hotspots could be valuable for the city of Duluth, MN, as people can monitor these sites and restore affected streams for the benefits of their communities and ecological systems.

The goals of this project are to document which areas in each channel in the Duluth area changed as a result of the 2012 flood, to predict types of erosional hotspots at the reach scale, and to quantify how much channel changes occurred as a result of natural and anthropogenic drivers. We used one year of lidar data coupled with Minnesota Geological Survey map and the field observation-based bedrock exposure data in order to map out topographic erosional hotspots. We used infrastructure maps to map out the

anthropogenic influences. We also checked the valley types and channel-reach types to assess the sensitivity of changes in channels with similar geomorphic features.

## *Background*

### *Fluvial Erosion Parameters*

Climate, topography, and geology are general factors that influence geomorphic processes. Channels can respond to factors by changing their geometry and slopes. The main processes by which channels respond to change are erosion and deposition of sediment and bedrock incision. The physical motion of sediments is controlled by both driving and resisting forces. Erosion usually occurs during peak flows because streams have high stream power that exceeds frictional forces and resistance of particles. Stream power is a measure of the driving forces, which are a function of potential energy expenditure per unit length of channel (Knighton, 1998). For erosion to occur, the frictional forces have to be less than the driving forces.

Nieber et al. (2008) noted that sediment sources in the North Shore streams include sediments from incision, bank erosion, and overland flow. The North Shore and Duluth-area streams are quite similar in the way that both have reaches flowing through bedrock, finer-grained glacial till, and glaciolacustrine sediments (Fitzpatrick et al., 2006). Erosion in tills and glaciolacustrine sediments provides most of the fine sediment load to Duluth-area streams.

Slumping is a common bank erosion process in North Shore and Duluth-area streams. This process depends on soil moisture conditions and hydraulic action (Hooke, 1979). Bank erosion usually occurs when soil is saturated, leading to high pore pressure and low cohesive force (American Society of Civil Engineers, 1998; Rinaldi & Casagli, 1998). Consequently, slumping will move sediments downslope in a single event. Hydraulic action also acts on the toe of a bluff, oversteepening and destabilizing it, and leading to bank erosion at the lower banks. However, upper banks are eroded by slumping (Hooke, 1979). Those processes are strongly dependent on both the intensity and the frequency of precipitation, since multiple peak flow events may erode more

sediments than a single event because saturated soil fails more readily (Hooke, 1979; Knighton, 1973).

Channel geometry is another factor affecting erosion by fluvial processes. Erosion typically starts by downcutting the valley, while extending headward erosion at channel tips, and enlarging the drainage basin. In the earliest stage of stream incision, streams have high erosive potential to vertically incise and make a typical v-shape valley. Lateral erosion can simultaneously occur with vertical incision when the bed is smothered by high sediment load. The valley geometry is controlled by the ratio between vertical incision and lateral erosion. For instance, entrenched valleys, which have wide depositional areas and floodplains and have meander bends in their valleys, have higher rates of lateral erosion than rates of vertical incision, but confined valleys, which have high erosive potential within a steep channel slope, are the opposite (Leopold et al., 1964).

Flow directed toward the outer banks has more energy to erode than the flow directed toward the inner banks. Sediments eroded from outer banks through lateral erosion are transported by faster-moving water to inner banks, depositing the sediments when stream energy declines (Knighton, 1998). Bedrock reaches are also eroded by sediment and flowing water, but erosion generally occurs much more slowly, causing geomorphic changes over longer timescales.

Erosion in streams usually occurs in an area where there is a steep channel slope, a high discharge and high stream power, along the outer banks rather than the inner banks, and in areas with erodible substrates. Bedrock reaches also experience erosion, but over longer timescale or slower rates than more erodible substrate reaches.

*Identifying Erosional Hotspots*

The possible natural variables, which control sediment loads and erosion potentials, are topography, planform geometry, soil or rock erodibility, and hydrology. Wick (2013) used lidar data to identify places where stream power and angle of impingement (AOI) were high and where bluffs as sources were plentiful, and used field data to map bedrock and surficial geology in order to identify substrate erodibility

(resisting forces).

Stream power describes the rate of potential energy expenditure per unit length of channel (Knighton, 1974). Sediment loads can be transported if a stream power exceeds bed resistance. An evidence of high stream power might be seen in the areas with scour of alluvium on the bed or the bedrock. If there is insufficient stream power, sediment loads will not be mobilized at the bed of the stream (Bull, 1979). Ferguson (2005) provided an equation to predict the value of stream power per unit width on the bed:

$$\omega = (\rho gQS)/w \qquad (1)$$

where $\rho$ refers to the density of water, g is the acceleration due to gravity, Q is water discharge, S is channel slope, and w is bankfull channel width. Those relationships were simplified as a series of hydraulic geometry relationships with both width and area being functions of water discharge: $w = c_1Q^b$and $Q = c_2A$. Those relationships are combined to generate a stream power-based erosion index (SP):

$$SP = kA^{(1-b)}S \qquad (2)$$

where k combines coefficients $c_1$, $c_2$, and is a function of hydrology, bedrock and substrate erodibility, and b = 0.5 for alluvial channels (Leopold & Maddock ,1953)

The channel planform geometry can also affect the rate of erosion. When streams flow toward outer banks, they increase shear stress and hydraulic action to the banks. Maximum shear stress and high migration rate generally occur in the outer bank just downstream of the bed apex (Knighton, 1998). The shear stress is a function of the bend curvature. Nanson and Hickin (1986) found that migration rates are affected by bend curvature obtained from radius of curvature divided by bankfull channel width. Where bend curvature ratio is relatively low, the hydraulic force, the shear stress and the migration rate are at peak (Begin, 1981; Furbish, 1988). High-resolution lidar data can provide remote data on bend curvature, which affects shear stress and erosion potential. Wick (2013) used the angle of impingement as a measure of erosion potential with a higher angle of impingement indicating a higher shear stress. The angle of impingement was calculated by measuring the flow direction at specific point of the channel (i):

$$AOI = |Va_{i-1} - Va_i| \quad (3)$$

where $Va_i$ is the vector direction of the main channel at point i, and $Va_{i-1}$ is the vector direction of the main channel at previous point i, some set distance upstream from point i.

The angle of impingement is directly related to the radius of curvature, which helps drive migration rates and erosion rates in the streams (Wick, 2013). However, the angle of impingement measured via equation 3 depends on the distance between points, challenging its utility in channels with changing meander wavelengths. Because of this, Wick (2013) found that AOI as measured in the equation 3 was not a strong predictor of stream erosion. One of the goals of this project was to develop and improve a method of measuring bend curvature.

Streambanks and bluffs are considered as potential sources of sediment, since erosion there is not balanced by deposition on the opposite side of channel. In particular, high bluffs, which are composed of erodible sediments and are adjacent to streams, are the potential sources of large volumes of sediments. Knowing where those high bluffs are located allows us to map out potential erosional hotspots. Wick (2013) mapped out bluffs greater than two meters over a 12 x 12 meters area. Because erodibility is important, knowing where bedrock outcrops lie is critical.

*Light Detection and Ranging (Lidar)*

Lidar is a remote sensing technique using light from a pulsed laser to measure surface topography on the Earth (National Oceanic and Atmospheric Administration, 2013). The results of the reflected light can provide accurate three-dimensional information about the shape of the earth and the characteristics of the target. Lidar equipment is composed of a laser, a scanner, and a GPS receiver. In principle, an airborne laser is assigned to point at surface topography on the ground. The beam illuminates and reflects a specific area on the surface. A sensor works with a GPS to get a precise location of points on the Earth's surface and records the time-interval from the pulse being sent to the return pulse being received. The results of a detail-rich group of elevation points are called a point cloud. Each point in the point cloud has a spatial coordinate (latitude and longitude), which is related to a specific reflected point on the

Earth's surface. The point can be displayed in several forms, such as digital elevation models, digital terrain models, and contour lines (Agarwal et al., 2006; Bandara et al., 2011).

Although lidar images are widely used in many fields of study because they are multifunctional application tools, there are some errors that reduce accuracy and precision of the lidar system measurement. Hodgson and Bresnahan (2004) described that positional error and lidar point labeling are two main sources of errors. The positional error in the lidar collection process is the first main source of the problems associated with the Global Positioning System (GPS) onboard the aircraft. Multiple over-flights over uneven roofs of buildings or different flow paths generate the horizontal error. There were two different flight paths in the Arrowhead region, including that one flew north-south, and the other one that flew northwest-southeast and northeast-southwest in a different time period. The divergence along with scan angle of horizontal error was diverted approximately 0.2 to 0.33$^{o}$ (Hodgson & Bresnahan, 2004). In addition, the second possible source of lidar's error is from the process of labeling the points. A single laser pulses toward a surface location, and a return pulse is recorded as time and intensity. The first return indicates vegetation, whereas the last return indicates bare earth topography. In this project, we used only the last return that reflected the ground and rock materials. However, the last return pulse has low intensity and exhibits an angular deviation from surface, which can cause a vertical error. The vertical error in elevation significantly influences the accuracy and the interpretation of gradients and curvatures of channel characteristics.

Errors in the Duluth-area lidar are not negligible. Since the repeat lidar data in Duluth were generated from two different time periods, horizontal and vertical offsets are found in the lidar data caused by different flightline directions, reducing the accuracy of channel changes. These offsets lead to an inaccurate measurement of net volumetric changes. Although we did several tests to document and remove the errors in Duluth lidar data (see Appendix 1 for details), we were unable to satisfactorily fix the data and thus did not use the repeat lidar data for quantitative analysis for this study.

## *Study Area*

### *Geologic History of Duluth Area*

Northeastern Minnesota is located in the Arrowhead region with more exposed bedrock than other parts of the state. Approximately 1,100 million years ago, North America started to split along a rift from Kansas through Lake Superior. This rift had a large magmatic plume that spilled out along the fissure on the surface along the North Shore of Lake Superior as primarily basaltic lava flows. These flows were known as the North Shore Volcanic Group, and had 60,000 meters thickness extending from Isle Royale to the Keweenaw Peninsula. Some of the magma crystallized beneath the lava flows, forming intrusive units known as the Duluth complex, composed of gabbro and other coarse-grained igneous rocks. The complex extended from Duluth northeastward to Ely and the northeastern tip of Minnesota. It contains valuable resources for mineral exploration, such as Copper-Nickel sulfide deposits (Green, 1983; Miller et al, 2001; Van Schmus, 1992).

The mid-continent rift system also created major normal faults that formed an elongated basin and affected flow directions of rivers. These rivers flowed to a topographic low and created a large amount of sediments overlying the volcanic flows beneath what is now Lake Superior. Eventually, there was a large tectonic plate that collided with the east coast of North America. As a result, the mid-continent rift system stopped and normal faults became reverse faults because of compression (Cannon, 1994).

From the Paleozoic to the Tertiary time, northeastern Minnesota experienced erosion rather than deposition because lands in this region were above sea level, and sediments were eroded and removed. No rocks were preserved in northeastern Minnesota from that time (Ojakangas & Matsch, 1982).

About 1.8 million years ago, glaciers moved into Minnesota and the northern United States. Drill hole data show that there were more than four major glacial episodes in Minnesota: the most recent one that affected Minnesota is the Wisconsinan glaciation. Duluth and northeastern Minnesota were mainly covered by the Superior lobe that contained a lot of fragments of basalt, volcanic rocks, and sedimentary rocks from the

mid-continent rift system. The Superior lobe last retreated about 11,500 years ago from the Superior basin (Attig et al., 1985; Lusardi, 1997).

Glacial Lake Duluth was formed as the Superior lobe melted and retreated 11,500 years ago. This created abundant glaciolacustrine and deltaic sediments mainly composed of silt and clay deposits from meltwaters flowing into the lake. Glacial Lake Duluth drained southward through the Kettle River and the Brule River that formed the St. Croix River. Moreover, 9,500 years ago, the Superior lobe eventually melted out of the Lake Superior basin, forming Lake Superior, and the drainage shifted to the Atlantic Ocean through the St. Lawrence River. When that happened, the water level in Lake Superior decreased at least 61 meters (200 feet) lower than the present level because the weight of ice had depressed the land where the outlet was at Sault Ste Marie. Since then the land has been rising up from isostatic rebound, causing rivers to vertically incise to water level, exposing rocks along lower ends of channels (Saarnisto, 1974).

In terms of bedrock exposure in the Duluth-area streams, bedrock is primarily composed of the Duluth complex and the North Shore Volcanic Group rocks (Miller et al., 2001). The Duluth complex and miscellaneous intrusive rocks are mainly gabbro, with varying amounts of anorthositic and granitic rocks (Fitzpatrick et al., 2006; Ojakangas, 2009). Layered series of gabbro are exposed from Stewart Creek to Miller Creek, where anorthositic gabbro is mostly found from Coffee Creek to the Lester River, and continues northeastward. The North Shore Volcanic Group is mostly composed of basalts, usually formed as amygdaloidal basalt, and is found on beaches of Lake Superior (Ojakangas, 2009). Mission Creek is mainly underlain by sedimentary rocks in the Animikie Group, including thick greywacke sandstone and mudstone (Ojakangas, 2009).

Quaternary surficial deposits are typically exposed in the upper reaches of all watersheds, while bedrock is dominantly exposed at the surface of the middle and lower main stems. The oldest glacial deposits from the last major advance in the upper watersheds composed of supraglacial drift with loamy sandy till of the Cromwell Formation (Fitzpatrick et al., 2006; Hobbs, 2004). The deposition of silty loam till to clay loam till in the Barnum Formation is a result of later glacial readvances (Hobbs, 2004).

Till plain deposits, which are modified, undulated, and rolled by the lake action, are extensively found along the western Lake Superior and the St. Louis River.

*Geomorphic Characteristics of the Duluth-Area Streams*

Duluth is located at the westernmost edge of Lake Superior and at the mouth of the St. Louis River. In terms of topography, Duluth is dominated by a steep hillside that ascends the elevation from Lake Superior to inland elevations (Fitzpatrick et al., 2006) (Figure 1A). These geomorphic characteristics resulted from scour of the Lake Basin and isostatic rebound after the Superior lobe retreated 11,500 years ago. The land surface has been rising up on the North Shore affecting the longitudinal profiles of the Duluth-area streams resulting in different longitudinal profiles from typical mountain streams. However, channel slopes are as high as those of the mountainous streams (Montgomery & Buffington, 1998), and many reach characteristics are similar to mountain channels. Figure 1B and 2 show the longitudinal profiles of all the Duluth-area streams; near the headwaters they are low-gradient and flow across glacial till. As they get closer to their outlets, they steepen exposing bedrock at the surface through river incision.

Bedrock and surficial geology and geomorphic characteristics and processes are consistent across the Duluth watershed. The main bedrock geology in Duluth-area streams are the Duluth Complex Intrusive Rocks and the North Shore Volcanic Group. In headwaters, streams flow over glacial deposits with little or no valley development. Many reaches have wetland vegetation. The middle reaches are underlain by gabbro and other intrusive rocks exposed from Stewart Creek to the Lester River, and typically located in confined valleys. The lower reaches from Stewart Creek to Chester Creek are underlain by gabbro and other igneous intrusions, whereas those from Tischer Creek to the Lester River are dominated by rhyolite and other volcanic rocks. Streams flow through bedrock bluffs and outcrop near the shore of Lake Superior. Streams in the southern area of the Duluth area that drain into the St Louis River estuary have till plain or lake-modified clays near the mouths (Fitzpatrick et al., 2006).

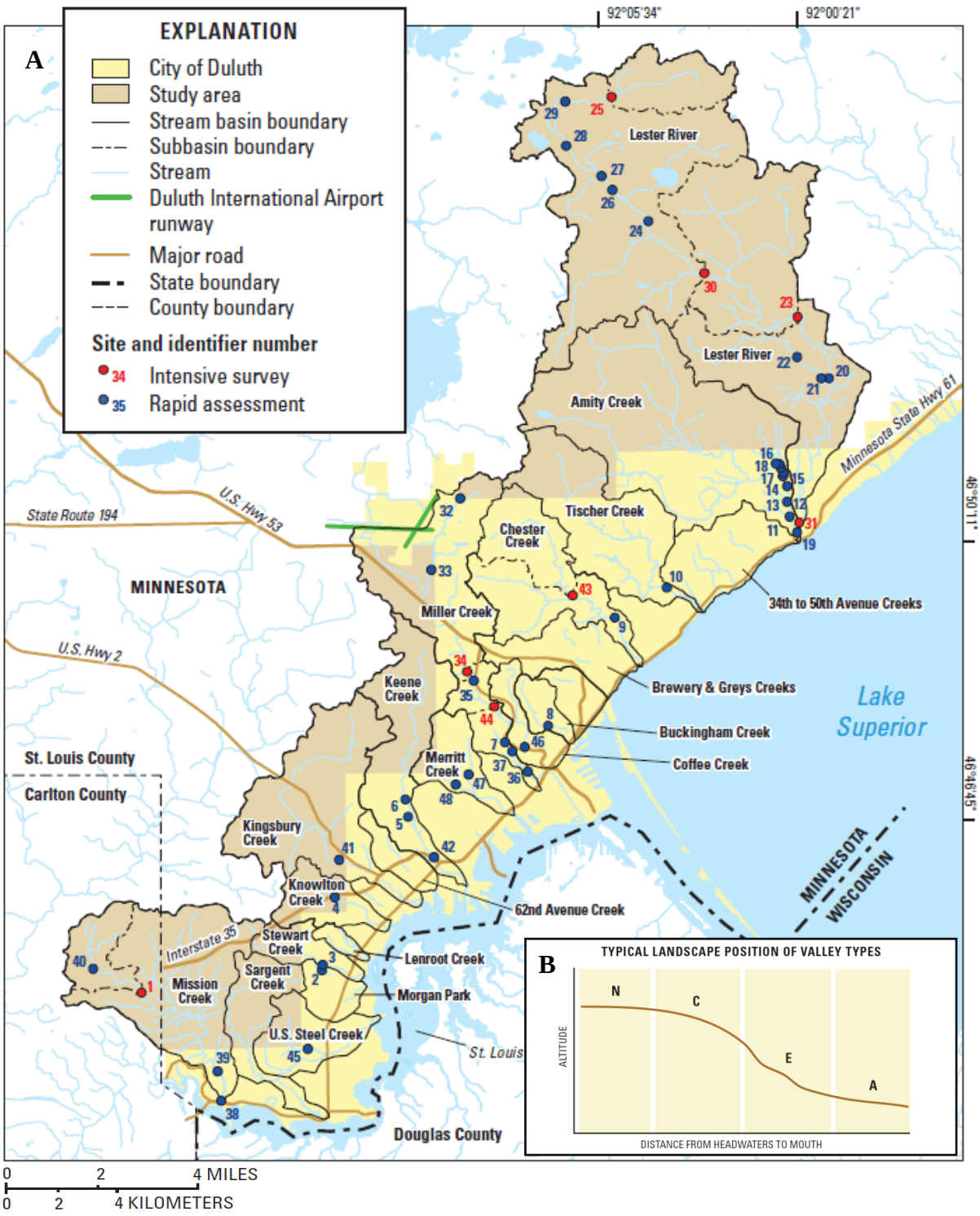


**Figure 1 A.** Study area and the City of Duluth, MN. Duluth is located on a steep hillside parallel to Lake Superior. Streams then flow southeastward into Lake Superior, the St. Louis River estuary, and the St. Louis River. **B.** a typical longitudinal profile showing the valley types from upstream to downstream (map modified from Fitzpatrick et al., 2006).

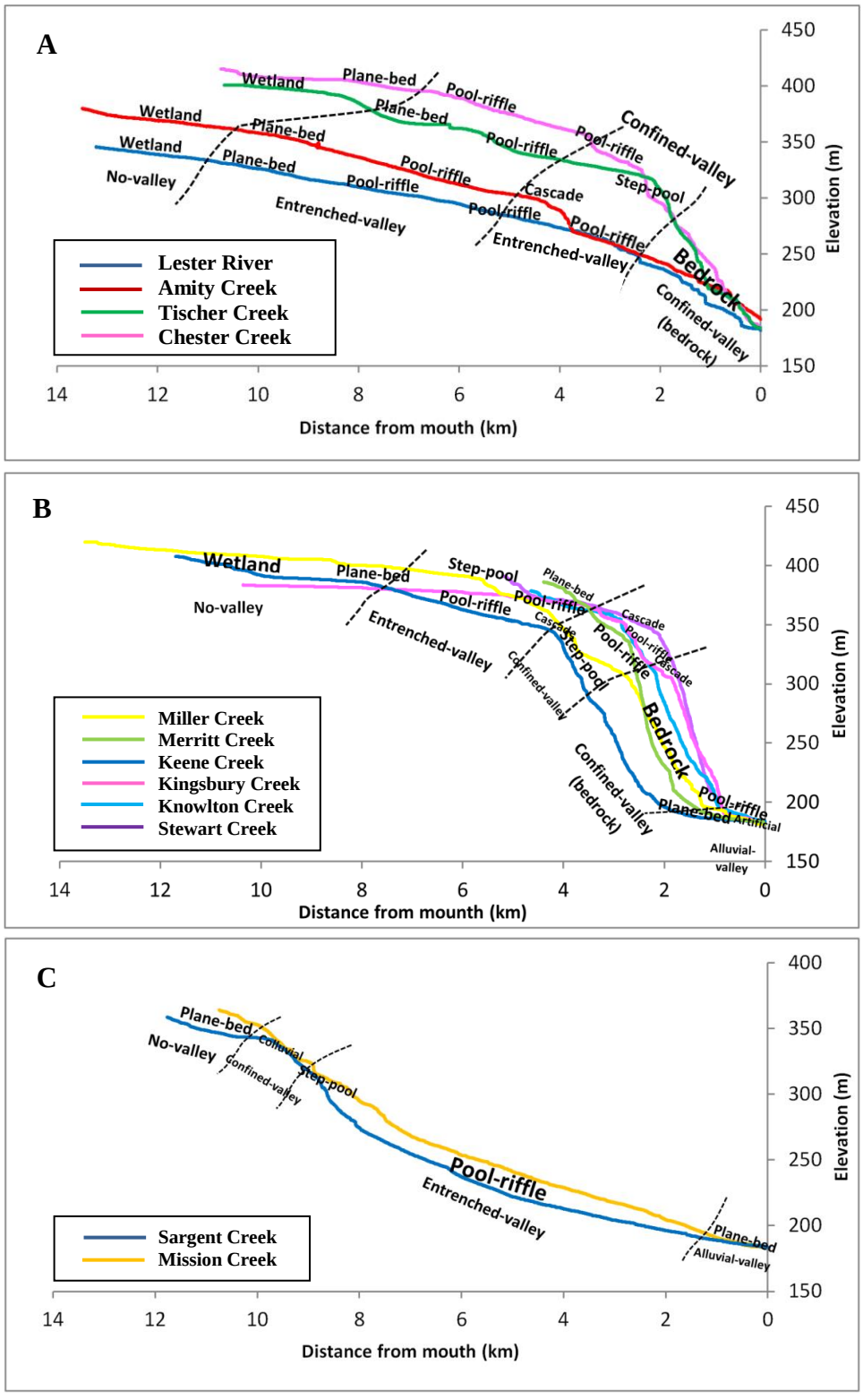


**Figure 2** Longitudinal profiles of all streams in each of three different areas of Duluth-area streams with their valley types and channel-reach types: **A.** the northern area, **B.** the central area, and **C.** the southern area (modified from Fitzpatrick et al., 2006)

Mission Creek and Sargent Creek have different valley types and drainage patterns due to their bedrock and surficial geology. Mission Creek and Sargent Creek are underlain by fine-grained sedimentary rocks, (i.e. sandstone, siltstone, shale, mudstone and greywacke) which are less resistant to erosion than igneous rocks. As a result, the drainage pattern of Mission Creek is more dense and dendritic than that of other watersheds (Fitzpatrick et al., 2006).

In terms of stream networks in the Duluth-area, most of them flow perpendicular to the shoreline of Lake Superior, but their flow characteristics are not the same throughout the Duluth watershed (Fitzpatrick et al., 2006). The main stem outlets from the Lester River to Chester Creek flow toward Lake Superior, through bedrock exposure with steep channel slope near outlets. Stream outlets from Miller Creek to Stewart Creek flow into the St. Louis River estuary and have a low channel slope with depositional areas of alluvial deposits near the mouth. Sargent Creek and Mission Creek flow directly into the St. Louis River and have alluvial deposits downstream near outlets with more graded profiles compared to the other streams (Figure 2).

From these commonalities of geology, geomorphic characteristics, and outlet locations, we classified the study area in to 3 different areas (Figure 2):

1. **The northern area** includes the Lester River, Amity Creek, Tischer Creek, and Chester Creek. The upper and middle reaches are mainly underlain by glacial deposits in reaches that lack alluvial valleys, whereas the lower reaches are exposed igneous rocks within confined valleys with steep slopes. The main stem outlets flow directly into Lake Superior.

2. **The central area** includes Miller Creek, Merritt Creek, Keene Creek, Kingsbury Creek, Knowlton Creek, and Stewart Creek. The middle and lower reaches have exposed Duluth Complex bedrock at the surface within confined valleys with steep slopes, whereas rivers flow through glacial deposits in the upper reaches. The city of Duluth and adjacent communities are located in the middle and lower reaches, so the channel morphology in this area is dominated by human constructions. All creek outlets flow directly into the St. Louis River estuary.

3. **The southern area** includes Sargent Creek and Mission Creek. These two creeks are mainly underlain by fine-grained sedimentary rocks within entrenched valleys. The drainage pattern is typically dendritic. The creeks eventually flow to the St. Louis River.

Fitzpatrick et al. (2006) classified geomorphic segments in Duluth-area streams into seven types, based on the locations of streams, channel slopes, valley types, and channel-reach types. These range from the headwaters to the lower reaches with details listed in Table 1. These geomorphic segments have different dominant processes in which each type would likely respond to a large-scale flood event differently. Thus, it is important to track valley types and channel-reach types when looking at the response of each type to the flood.

Valley confinement is the degree that topographic features limit the extent of a valley floor and floodplain formation along a river. Valleys can be typically classified as confined or unconfined based on their topographic gradients, stream characteristics, their appearances, and vegetation (Nagel et al., 2014). Confined valleys (C) are generally narrow located in v-shaped mountainous basins which have a steep channel slope, high erosive potential and high stream energy without floodplains, Entrenched valleys (E) have wider depositional areas and floodplains than those confined valleys (Nagel et al., 2014). Streams in entrenched valleys can meander within their valleys. Entrenched valleys can have the active channel migration and the development of channel sinuosity (Nagel et al., 2014). No valleys (N) are broad areas without a valley development, and alluvial valleys (A) are valleys which have a valley wider than meandering belts and floodplains, and have a gentle channel slope (Fitzpatrick et al., 2006) (Figures 1B and 2).

Montgomery and Buffington (1997) classified typical channel-reach types in mountainous drainage basins which are similar to the channel-reach types in Duluth-area streams. Cascade reaches (CA) are found on a steep channel slope within confined valleys. The substrate materials usually consist of cobbles and boulders, which cause smaller channel-spanning pool spacing than a channel width apart. Step-pool reaches (SP) have similar characteristics to cascade channels, but large clasts separate the areas of channel-spanning steps and pools, which have spacing of typically one to four channel

widths. The cascade and step-pool channels have large materials that are mobile only during large hydrologic events (Grant et al., 1990). Plane-bed reaches (PB) are areas that lack periodic bedforms and are characterized as long stretches of relatively characterless bed. Pool-riffle reaches (PR) are undulating sequences of bars, pools, and riffles (Leopold & Maddock, 1953). Bars are the high points within the channel and pools are the topographic depression. Pool-riffle reaches variably composed of sand to cobble usually occur at a moderate to low channel slope. Colluvial reaches (CO) are found in ephemeral

**Table 1** Geomorphic segment classification of Duluth-area streams, classified by Fitzpatrick et al., 2006

| No. | Geomorphic Segment Classification | Sub-Segment | Dominant Valley Type | Channel Type | Potential Geomorphic Change |
|---|---|---|---|---|---|
| 1 | Headwater channels with gentle slopes | W<br>W.3 | No-valley<br>No-valley | Wetland<br>Wetland | Channel Widening |
| 2 | Upper main stems with moderate slopes | U1<br>U2 | No-valley<br>Confined | Pool-riffle<br>Plane-bed | Vertical Incision<br>Bank Erosion |
| 3 | Middle main stems with gentle or moderate slopes | M.3<br>M1<br>M2 | Entrenched<br>Confined, Entrenched<br>Confined | Pool-riffle<br>Step-pool<br>Plane-bed | Bank/Bluff Erosion<br>Landslide<br>Lateral Migration/ Bar Formation |
| 4 | Bedrock main stems with steep slopes | B | Confined: Bedrock | Bedrock | Waterfall Recession<br>Knickpoint Migration |
| 5 | Lower main stems with moderate slopes | L1<br>L2 | Confined, Entrenched<br>Confined, Entrenched | Plane-bed<br>Plane-bed | Channel Widening<br>Lateral Migration<br>Bank/Bluff Erosion |
| 6 | Aggradational main stems with gentle slopes | *A | Alluvial | Pool-riffle<br>Artificial | Channel alteration |
| 7 | Tributaries with moderate to steep slopes | T1<br>T2<br>BT<br>**LT | Confined, Entrenched<br>Confined, Entrenched<br>Confined<br>Confined | Pool-riffle<br>Pool-riffle<br>Colluvial<br>Colluvial | Vertical Incision<br>Landslide |

**Explanation**

W: wetland, W.3: wetland slope with 0.3-1% slope, U1: upper main stems with 1-2% slope, U2: upper main stems with 2-4% slope, M.3: middle main stems with gentle slope, M1: middle main stems with 1-2% slope, M2: middle main stems with 2-4% slope, B: bedrock channel with steep slope, L1: lower main stems with 1-2% slope, L2: lower main stem with 2-4% slope, T1: tributary with 1-2% slope, T2: tributary with 2-4% slope, BT: tributary with confined bedrock valley and steep slope

* Aggradational lower main stems (A) are unusual in Duluth-area streams, found only in Mission Creek and the lower main stems of Sargent Creek

** Tributaries to lower main stems (LT) are mainly in Amity Creek and Mission Creek

tributaries with steep channel slopes in headwaters flowing though colluvial valleys. Bedrock reaches (B) lack an alluvial bed and flow across bedrock; they generally have steep channel slopes. Wetland (W) and anthropogenic (A) reaches are minor channel-reach types in the Duluth-area streams. Wetland reaches are headwater streams generally flowing through glacial deposits with no valley development (Fitzpatrick et al., 2006), and anthropogenic reaches are modified by human constructions in order to allow streams to flow through anthropogenic-controlled routes (Table 1). These are common channel-reach types in the Duluth-area streams, which respond differently to the flood.

Channels usually respond to changes in watersheds. The channel responses include the changes in sediment transport, rates of erosion and deposition, channel widening or narrowing, lateral erosion or vertical incision, and avulsion (Fitzpatrick et al., 2006). The levels and characteristics of channel responses result from both natural and human factors. The possible natural drivers, which influence channel responses in the Duluth-area streams, are the increase or decrease of runoff and flood peaks, the long-term base level change in Lake Superior, and substrate erodibility controls. Possible human activities, which affect geomorphic processes there, are clearance of riparian or upland forest, agriculture, urban development, road construction, gravel pits and quarries, and hiking trails (Fitzpatrick et al., 2006). For example, if vegetation is cleared from valley slopes due to urban development, runoff and flood peaks will increase, possibly eroding valley sediments into streams, and increasing the potential of channel erosion, particularly streambank and bluff erosion (Fitzpatrick et al., 2006).

***Methods: Data Sources and Collection***

The main sources of data used in the project are lidar-derived DEMs provided by the Minnesota Geospatial Information Office. These lidar data were collected between May 3rd to June 2nd, 2011, and October 29th to November 8th, 2012. They are available in 1 meter-resolution for Duluth. These data have a stated vertical accuracy of 0.05 m (0.16 feet) and 0.036 m (0.12 feet) Root Mean Square Error (RMSE) from pre- and post- lidar data, respectively, and a stated horizontal accuracy of +/- 1.16 m (3.8 feet) for both campaigns. They were used to determine stream networks and watersheds and to predict

erosional hotpots in the Duluth-area streams. The repeat lidar data were also processed with the intention of fusing them to quantify the channel geometry changes through time (see Appendix 1).

Stream shapefiles derived from the USGS 1:24000 scale topographic maps were used to guide channel delineation in the areas where roads blocked automatic delineation from lidar-derived DEMs. These files were obtained from the Minnesota DNR Data Deli (http://deli.dnr.state.mn.us/data_search.html), and can now be accessed from the MN Geospatial Commons (https://gisdata.mn.gov/).

For infrastructure maps, we used the major roads, inlets-outlets and water systems that were available to download from the Minnesota DNR Data Deli. For building and construction locations, we used the construction maps that were downloadable from the St. Louis County and Carlton County web services-GIS (http://www.stlouiscountymn.gov/LANDPROPERTY/Maps/WebServicesGIS.aspx).

For bedrock exposure locations, we downloaded them as a part of the GIS files provided by the Minnesota Geological Survey. The bedrock maps of the Duluth Heights, Duluth, and West Duluth quadrangles were available in the 1:24000 maps (Hobbs, 2009). The bedrock geology map of Mission Creek was downloaded from the C-19 Geologic atlas of Carlton County, Minnesota [Plate 2] (Boerboom, 2009).

***Methods: Erosional Hotspots Identification***

In order to identify erosional hotspots for each watershed, we used threshold criteria based on Wick (2013) to predict high erosional potential hotspots. We then conducted field observations to check those predicted erosional hotspots and map out where erosion occurred from the 2012 flood. The field observation-based data were used to refine the GIS-based predictive model and develop a refined threshold model. The field erosion maps were compared with the infrastructure maps in order to identify the potential drivers of erosion (Figure 3).

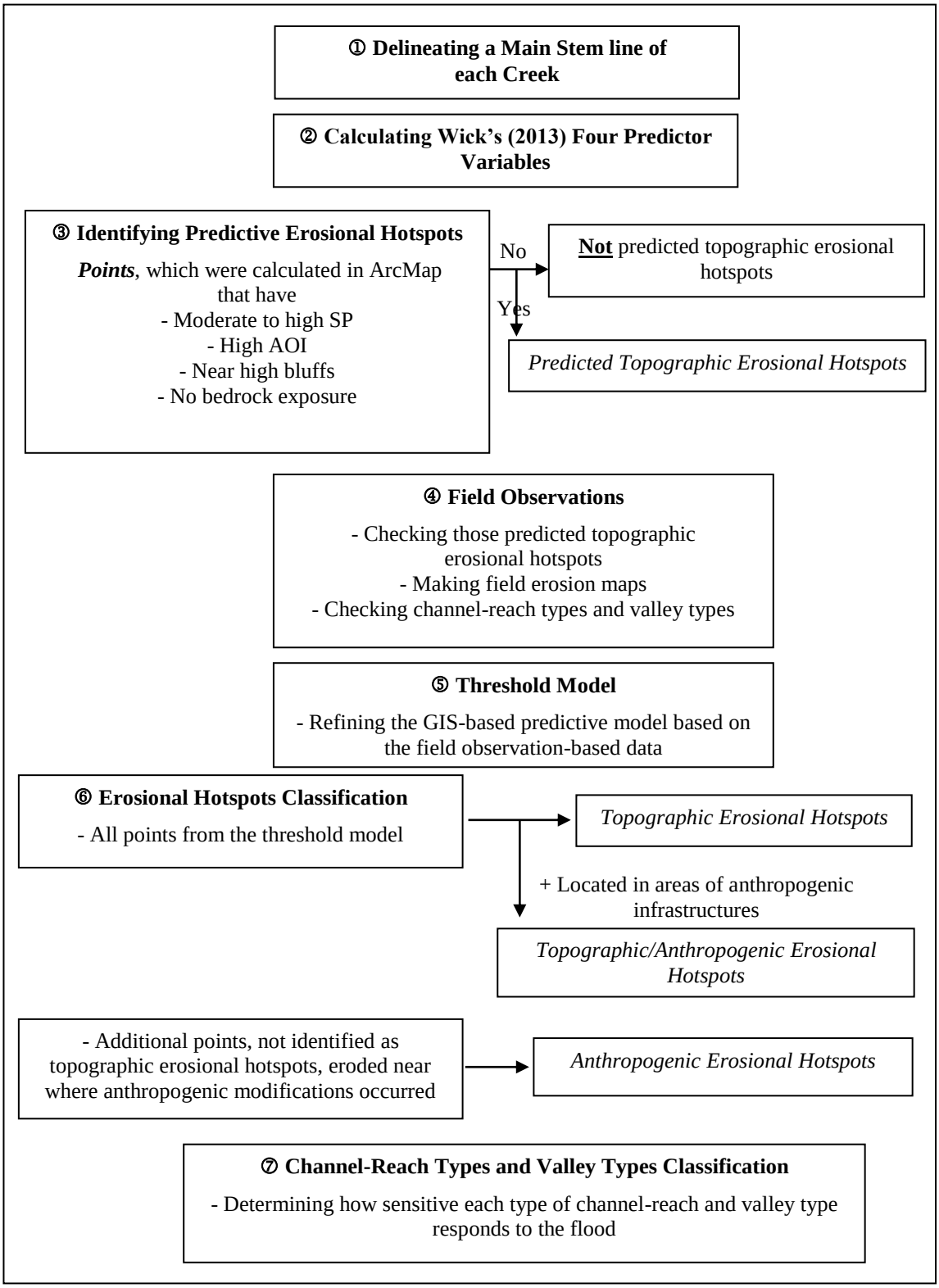


**Figure 3** Steps to identify erosional hotspots and susceptible channel-reach types and valley types.

*Delineating Stream Networks and Watersheds*

After downloading the1-meter resolution lidar-derived DEM data, we compared them to data from DNR 24K stream files to identify where main stems flow. We found that some flow routes were not well-correlated to the changes in elevation and topography. To improve the stream networks, we delineated main stem channels from the 1-meter DEMs based on topography using Hydological Toolbox in ArcMap. We then compared those results to the DNR 24K stream files to check road crossings. We found the topographic barriers (digital dams) from bridges, culverts, and road crossings on 1-meter DEMs which do not illustrate the elevation of the main stem itself. This resulted in the delineation of an erroneous stream networks.

Wick (2013) noted that there were two methods to correct this problem; GeoNet and the Hydrological Toolbox in ArcMap. GeoNet is a program that uses nonlinear filtering to reduce noise in low-gradient areas and enhance geomorphic features of interest, without changing landscape contours (Passalacqua et al., 2010). GeoNet ideally smoothes the high-frequency fluctuations of the ground surface and enhances geomorphic features, such as channel and bluff edges (Figure 4). This filter can remove some of the errors in main stem delineations, but the digital dams still exist in the 1-meter DEMs.

To remove the digital dams, we manually removed pixels at digital dams out of the DEMs using the Hydrology Toolbox in ArcMap. We made a line across each of the digital dams, and then assigned the lower elevation of the bottom of the dam on the line. After that, we converted the line to a raster and replaced the new elevation values crossing to each digital dam (Wick, 2013). However, the manual burned method is a time-consuming process that requires multiple iterations until an acceptable network is produced. We used an accumulation threshold of 100,000 $m^3$ to define the channel network.

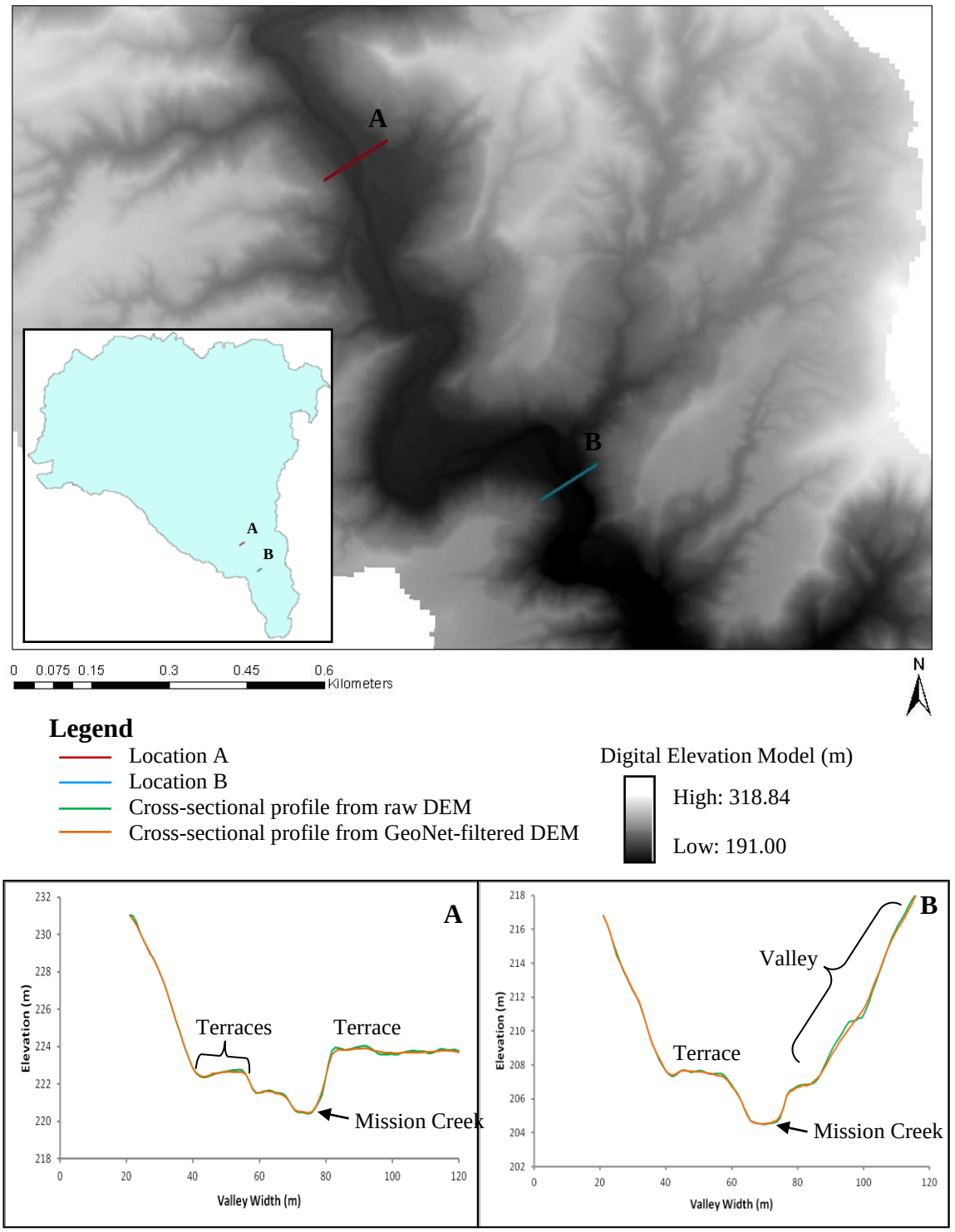


**Figure 4** A comparison between the raw lidar DEM and the GeoNet-filtered DEM cross-sectional profile from Mission Creek in location A and B. The GeoNet-filtered DEM reduces the high-frequency fluctuations of the ground surface and enhance channel and bluff edges.

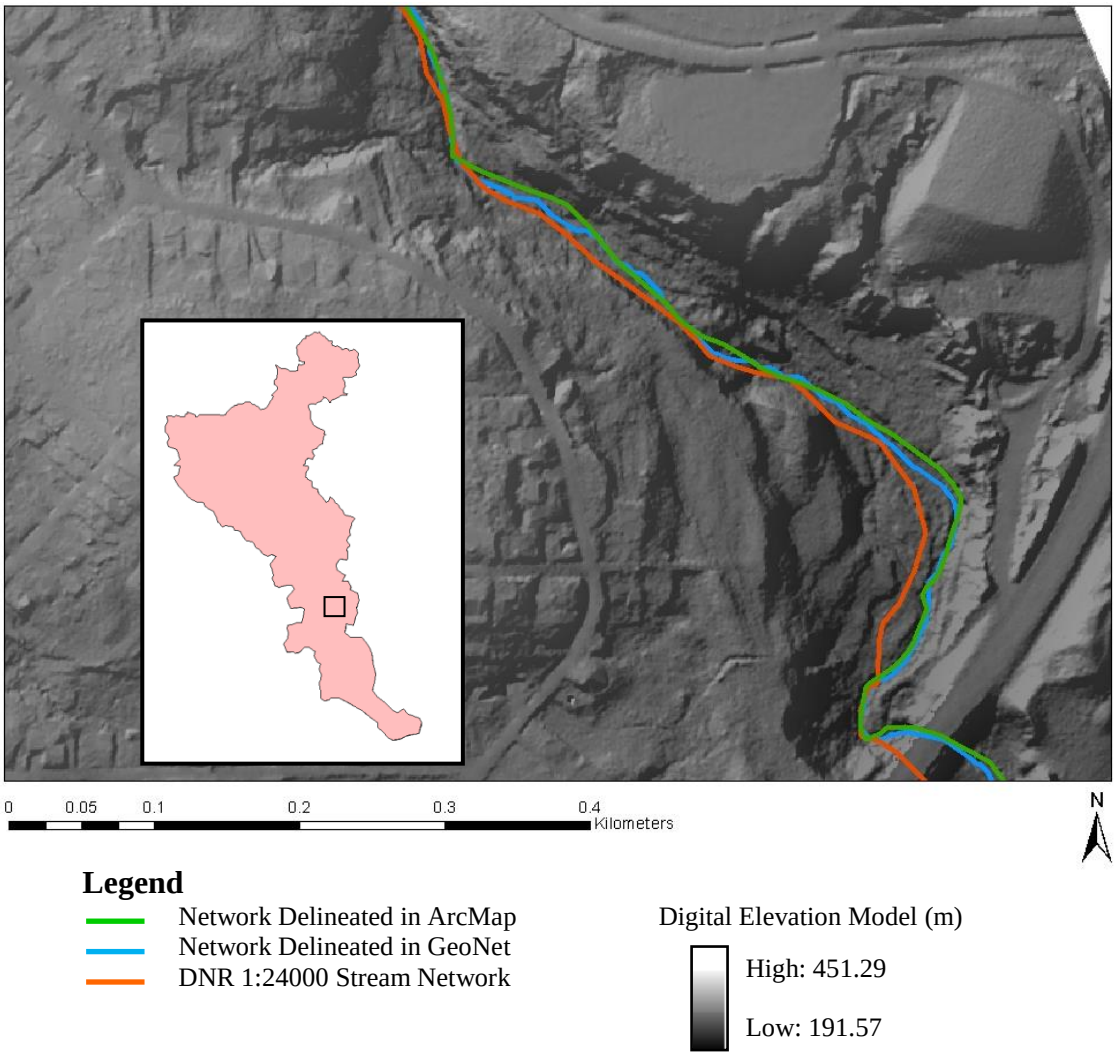


**Figure 5** A comparison between the DNR 24K, the GeoNet-derived, and the ArcMap-derived stream networks, along Miller Creek. Streams from both ArcMap and GeoNet networks were defined by thresholds for accumulation (100,000 $m^3$).

Figure 5 shows the comparison between stream networks from DNR 24K, GeoNet-derived and ArcMap-derived stream networks along Miller Creek. The data from DNR 24K stream files are less accurate than those from GeoNet-derived and ArcMap-derived stream networks. The main stems delineated from GeoNet method were accurate in the upper reaches, but were inaccurate downstream due to the digital dams. On the other hand, the ArcMap-generated networks throughout the main stems were more accurate than GeoNet networks because digital dams were burned out manually, causing streams to flow naturally downstream.

*Predicting Erosional Hotspots based on Channel Geometry Calculation*

After delineating stream networks and watershed boundaries, we started to calculate Wick's (2013) four predictor variables, including the stream power-based erosion index, angle of impingement, bluff proximity, and bedrock exposure locations. We also added a new predictor variable for channel planform: bend curvature ratio. The procedures for the GIS analyses were done following procedures from Wick (2013).

The stream power-based erosion index is the first parameter used to predict erosional hotspots along the streams. We extracted main stem lines and calculated the average slope over 100 meter reaches at 25 meter intervals along the main stems. The flow accumulation raster, which was created by the Hydrology Toolbox, provided the upstream area at each point along the streams. We exported those data with distance upstream and elevation to measure a stream power using equation 2.

The angle of impingement (AOI) is the angle at which a stream approaches the bank. We used the Planform Statistics Toolbox to measure the AOI (Lauer, 2006) via equation 3. We measured AOI every 5 meters because a longer ruler length would cause us to miss tight bends. The bend curvature ratio is an alternate measurement of the tightness of meander bends along the stream. We calculated the bend curvature ratio in order to compare to the results from the angle of impingement. We expect to see a high ratio of bend curvature in a relatively straight channel, and a low ratio at a tight bend. To calculate bend curvature ratio, we fit circles to meanders along the streams, measuring

the radius of curvature and bankfull channel width at each point in DEMs, and calculated the ratio using the following equation:

$$\text{Bend curvature} = R_c/w \quad (4)$$

where $R_c$ is a radius of curvature, and w is a bankfull channel width.

Although streambanks are often the sites of erosion, highly erodible bluffs provide much more sediments when they erode. Thus, identifying their locations as potential high contributors of sediment is important. We identified the areas with relief greater than 2 meters and 4 meters over a window of 12 meters by 12 meters because this height can separate bluffs from streambanks (less than 2 meters). We then identified the bluffs along the main stems that were within one channel-width from the stream centerline. This practice was performed because streams could erode at the toe of the bluffs and the bluff could collapse, providing abundant sediments to the streams. Bluffs not adjacent to streams are not major contributors of sediments to stream channels under current conditions.

MGS bedrock exposure as mapped on the 1:24000 bedrock maps were used to determine the locations of bedrock exposure along the main stems. Those maps were also used as the reference maps for field observations.

After we finished preparing all predictor variables, the data of SP and AOI were classified by using the Jenks natural breaks classification in ArcMap to partition data into different classes based on natural groups in data distribution. The SP values were classified into five different classes, whereas the AOI values were classified into three different classes ranging from low to high values. The GIS-based predictive model predicted erosional hotpots at sites that have moderate-high stream power, high angle of impingement, are located near high bluffs, and have no bedrock exposure.

### *Methods: Field Observations*

Field observation was done in summer 2014. We completed the field surveys to 1) check predicted erosional hotspots to identify whether erosion had occurred at sites at predicted points; 2) map erosion from the 2012 flood along the streams using the Field

Erosion Index (FEI) (Wick, 2013); 3) map and verify bedrock exposure locations; and 4) check valley types and channel-reach types in order to help determine what types of channel-reach morphology were sensitive to changes from the 2012 flood.

We assessed how much erosion occurred along the streams using the FEI. We assumed that the geomorphic characteristic changes and erosion in the Duluth-area streams were affected by the 2012 flood at different magnitudes comparing to the potential of erosion during a regular annual flood. Wick (2013) created a scoring system for rating the erosion, which is shown in Figure 6. A score of 0 depicts bedrock exposure indicating low erosional potential. A score of 1 indicates little or no erosion in reaches with sediment banks. A higher score denotes increasing erosional severity. A value of 7 indicates complete scour on bluffs higher than 4 meters. We walked along the streams and rated the erosion due to the flood. At the same time, we took notes of the bedrock exposure locations, and the valleys types and channel-reach types. Figure 7 shows the examples of sites with a different FEI score.

| Field Erosion Index (FEI) | |
|---|---|
| Score | Description |
| 0 | Bedrock, Little or No Erosion |
| 1 | Little or No Erosion |
| 2 | Bank Erosion/Undercutting, one bank |
| 3 | Bank Erosion/Undercutting, both banks |
| 4 | Slump, one bank |
| 5 | Slump, both banks, or on bank >4m |
| 6 | Complete scour, one bank |
| 7 | Complete scour, both banks, or one bank > 4m |

**Figure 6** Field observation scoring systems for estimating erosion classified by Wick, 2013.


**Figure 7** Images of sample FEI sites with different FEI Scores: **A**. FEI = 0 at Stewart Creek, **B.** FEI = 1 at Keene Creek, **C.** FEI = 2 Tischer Creek, **D.** FEI = 3 at Lester River, **E.** FEI = 4 at Chester Creek, **F.** FEI = 5 at Mission Creek. **G.** FEI = 6 at Amity Creek, and **H.** FEI = 7 at Kingsbury Creek.

### *Methods: Comparing GIS Predictors and Field Observations*

The Field Erosion Index data were used to refine the GIS-based predictive model. We plotted each of the predictor variables with the FEI score in order to determine statistically significant correlations. The average SP, AOI, bend curvature ratio, bluff proximity, and bedrock exposure locations were plotted versus the FEI score. We calculated $r^2$ and p-values for simple linear regressions: the $r^2$ value indicates how well the regressions fit the data, and the p-value indicates the level of significance of each of the regressions. In general, the higher the $r^2$, the better model fits the data. For the regression with p-value lower than 0.05, the correlations are significant. The new data were used to refine the predictive model and predict topographic erosional hotspots based on those additional data.

### *Results: Erosional Hotspots Predictors*

We geographically organized the data analysis based on the commonalities of geology, geomorphic characteristics, and outlet locations (Figure 8). We show examples of results from one stream in each area (Amity Creek from the northern area, Miller Creek from the central area, and Mission Creek from the southern area), although all twelve streams were mapped, analyzed and put into a digital archive for reference.

We calculated the stream power-based erosion index along the stream networks of all the study basins. Since the longitudinal profiles of Duluth-area streams are different from those of typical mountainous drainage basins (Montgomery & Buffington, 1998) (Figures 2), we expected that SP values are low in the upper reaches of the stream networks where slopes are low and drainage areas are small, and rapidly increase downstream as both slope and drainage area increase. Table 2 and Figure 9 show the average SP values per 2 kilometers throughout the main stems. Examples from each area are shown in Figures 10A, 11A, and 12A.

The channel planform geometry was calculated using the angle of impingement. The angle of impingement calculated by the Planform Statistics Toolbox is shown in Figures 10B, 11B, 12B for Amity Creek, Miller Creek, and Mission Creek, respectively.

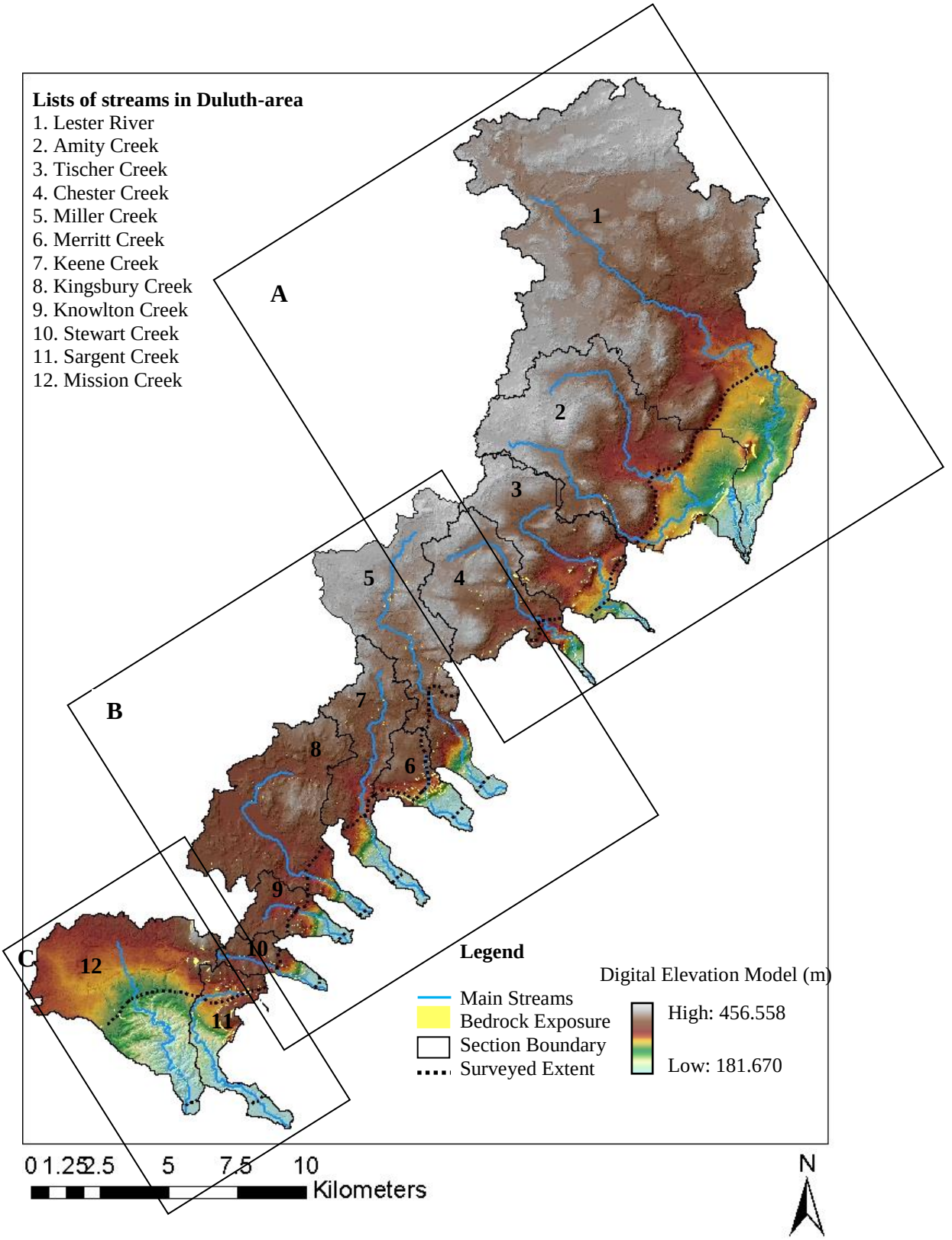


**Figure 8** Duluth-area streams were separated into three areas based on geology, geomorphic segment characteristics, and outlets: **A.** the northern area, **B.** the central area, and **C.** the southern area.

**Table 2** Average SP values in kg/ms$^2$ per 2 kilometers of spacing in Amity Creek, Miller Creek, and Mission Creek.

| Watershed / Distance from mouth (km) | Amity Creek | Miller Creek | Mission Creek |
|---|---|---|---|
| 0-2 | 13,8727 | 153,448 | 53,898 |
| 2-4 | 119,822 | 221,534 | 59,163 |
| 4-6 | 55,250 | 96,971 | 56,631 |
| 6-8 | 53,928 | 19,854 | 78,219 |
| 8-10 | 48,317 | 20,081 | 64,561 |
| 10-12 | 21,148 | 9,664 | 10,038 |
| 12-14 | 25,129 | 7,722 | - |
| 14-16 | 20,730 | 4,833 | - |
| 16-18 | 12,766 | - | - |
| 18-20 | 14,431 | - | - |

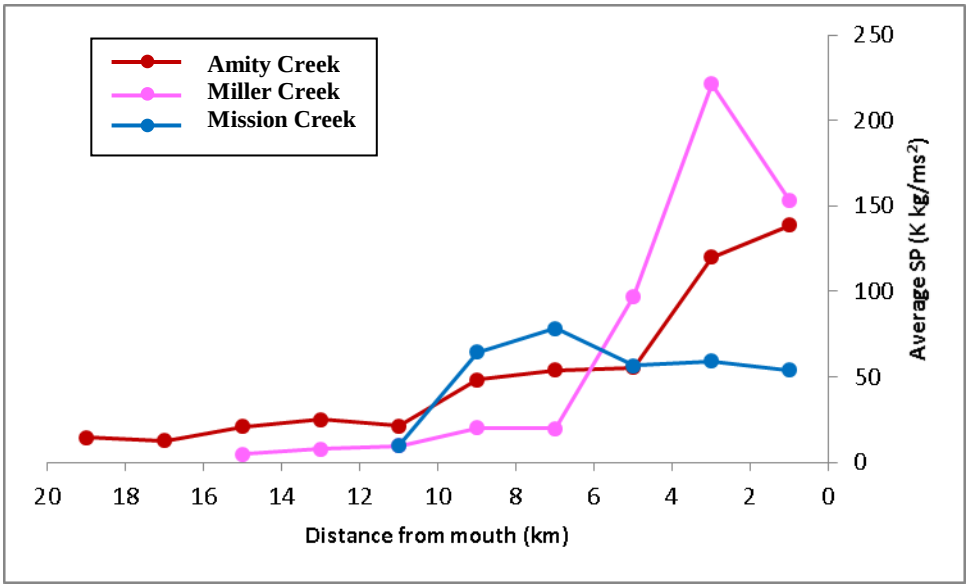


**Figure 9** Longitudinal profiles of the average SP values in kg/ms$^2$ per 2 kilometers of spacing in Amity Creek, Miller Creek, and Mission Creek, according to Table 2.

The AOI values range from 0 to 1.16 radians along Amity Creek, 0 to 1.34 radians along Miller Creek, and 0 to 1.20 radians along Mission Creek. High angle of impingement values occur where bends are tight and high energy goes toward the outside of the channel. In terms of the bend curvature ratio, we expect to have low values, whereas shear stress and migration rate are high. Therefore, the locations of high values of the angle of impingement would be similar to low values of the bend curvature ratio. These values and locations of the bend curvature measurements are shown in Figures 10C, 11C, and 12C for Amity Creek, Miller Creek, and Mission Creek, respectively.

We delineated two sizes of bluffs along the stream networks: 2 meters and higher bluffs and 4 meters and higher bluffs within 7 meters from the channel centerline in the Lester River to Stewart Creek and 20 meters from the channel centerline in Sargent Creek to Mission Creek, respectively. The bluffs within the stream buffer zone are shown in Figures 10D, 11D, and 12D. They can be seen in both lidar data and field observations along the length of the channels. We expected them to be more dense in the middle and lower reaches than in the upper reach due to an increase in relief, although they can be composed of different types of substrates, such as bedrock and glacial till.

Figure 10E shows the MGS bedrock exposure of Amity Creek at Hawk Ridge to the confluence with the Lester River. These bedrock exposures, which are more resistant to erosion, are found along the channel and are mostly located along Seven Bridges Road and particularly the uppermost three bridges. Figure 11E shows the MGS bedrock exposure of Miller Creek where bedrock is mostly found from W 3$^{rd}$ street (Lincoln Park) to Piedmont Avenue. Figure 12E also shows the MGS bedrock exposure of Mission Creek which is found at some areas in middle and lower reaches.

The GIS-based predictive model depends on the combination of predictor variables using the threshold values of Wick (2013). We classified the SP and AOI values as five and three different classes, respectively, using the Jenks natural breaks classification in ArcMap. This classification method seeks to partition data into classes based on natural groups in data distribution. This method automatically calculates the arrangement of whole values into classes and gives us the lowest value of each class. From the classification, we found that the upper 80$^{th}$ percentile of the SP values in Amity

Creek and Mission Creek was moderate-high SP thresholds. Likewise, the upper 45$^{th}$ percentile of SP value in Mission Creek was the moderate-high SP threshold. The high AOI threshold was a value which was greater than the 90$^{th}$ percentile. As a result, we predicted erosional hotspots as shown in a GIS-based predictive model located at sites that have moderate-high SP, high AOI, are located near high bluffs, and have no MGS bedrock exposure (Figure 13).

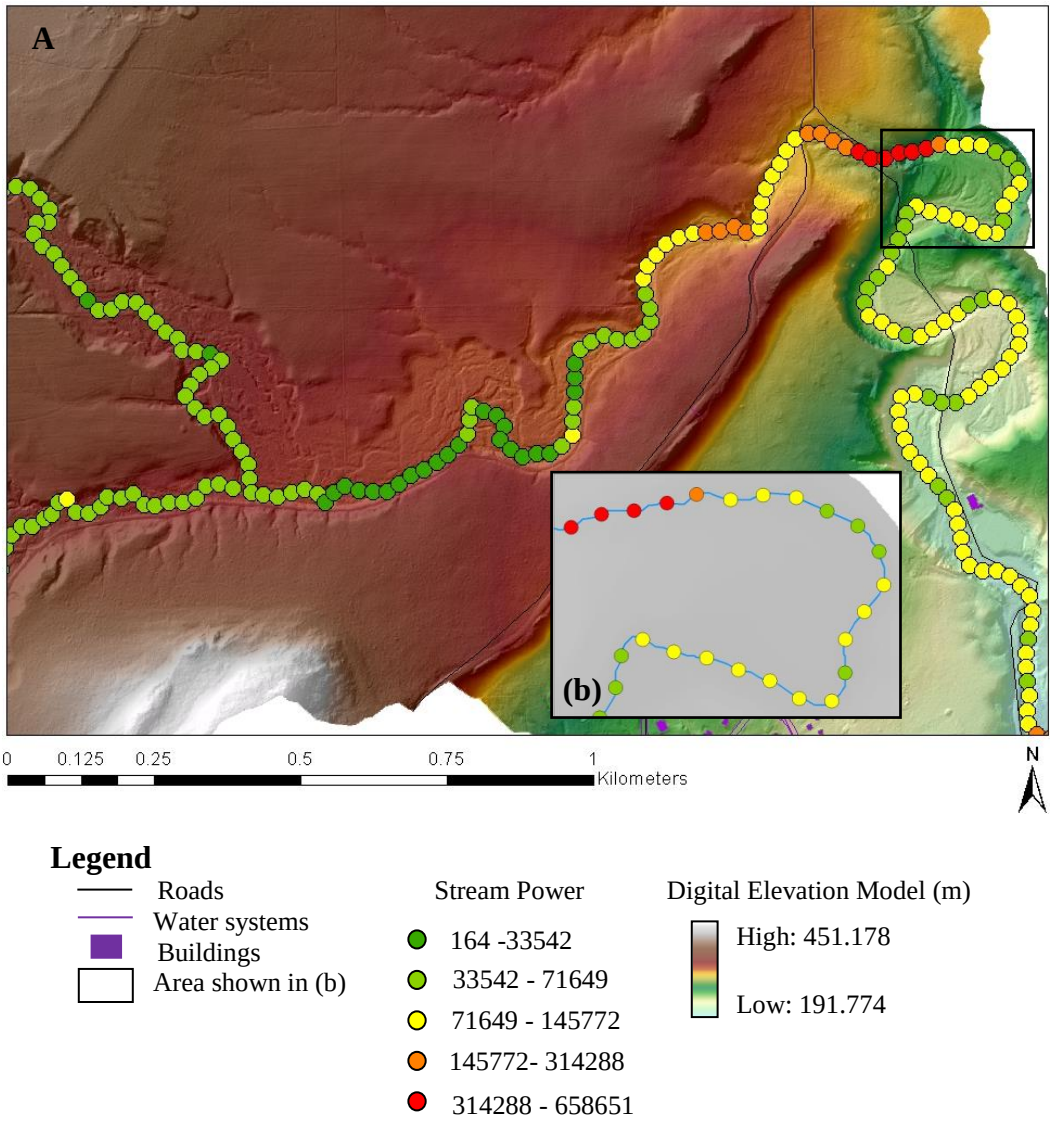


**Figure 10A** Predictors for Amity Creek watershed. SP in kg/ms$^2$, shown in every 25 meters, **(b)** the SP values for the outlined area in the larger map.

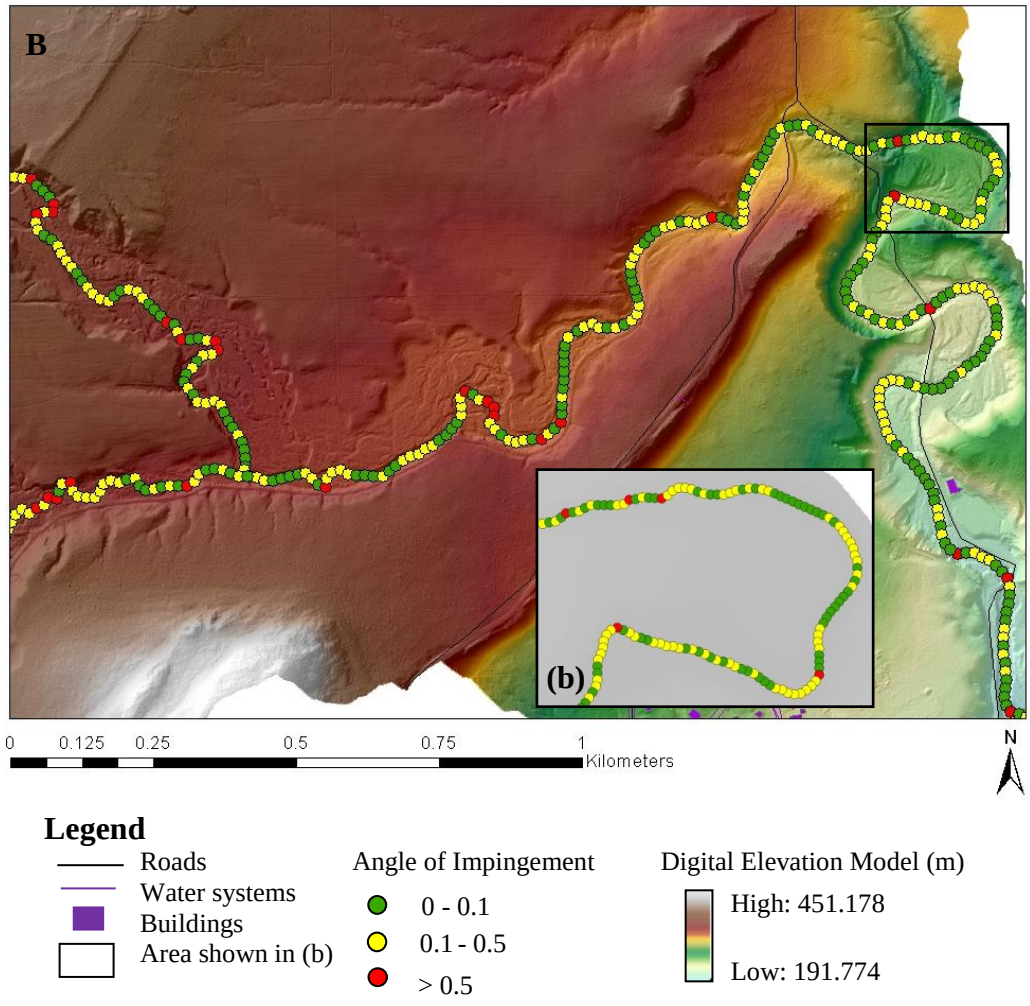


**Figure 10B** Predictors for Amity Creek watershed. Angle of impingement in radians, shown in every 15 meters in larger map, (**b**) angle of impingement in every 5 meters along the stream for the outlined area in the larger map.

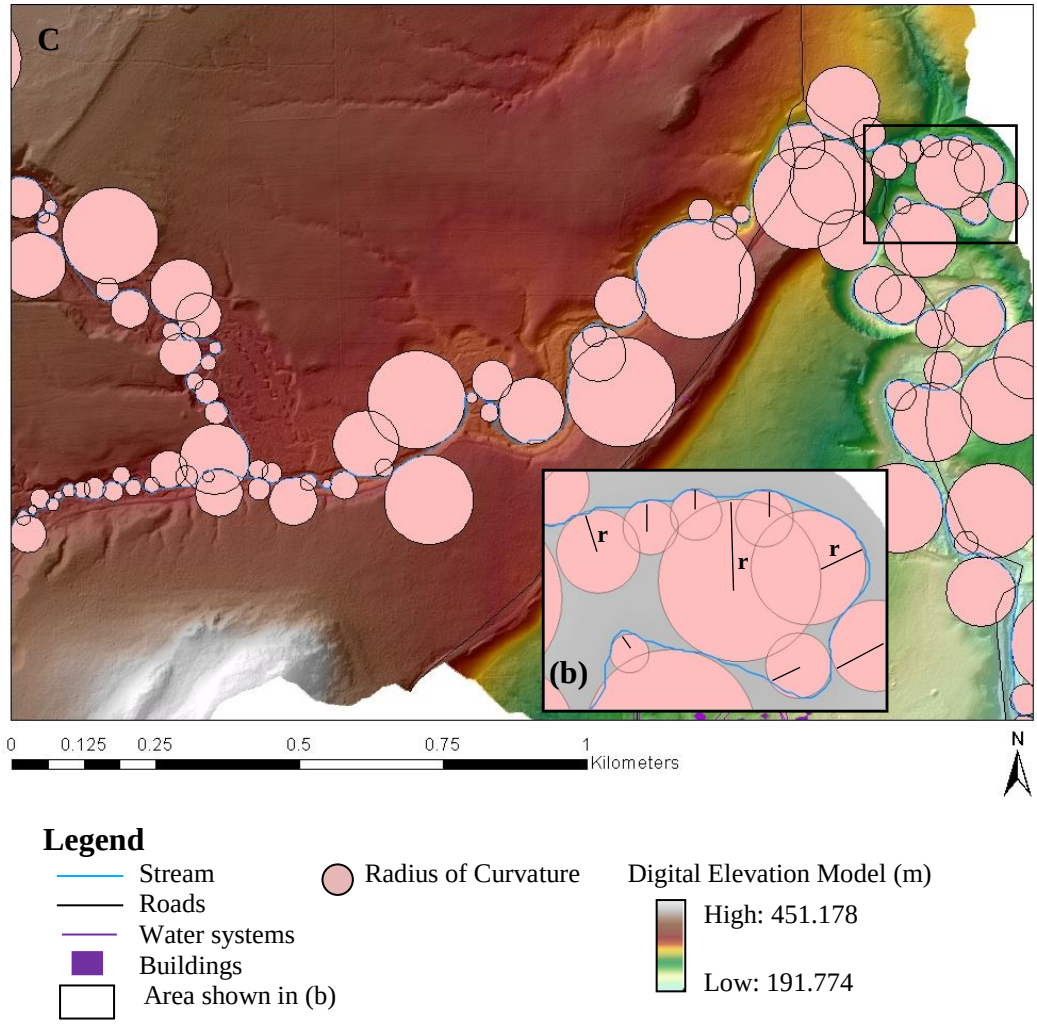


**Figure 10C** Predictors for Amity Creek watershed. Bend curvature (radius of curvature divided by bankfull channel width) shown throughout the creek, **(b**) the bend curvature for the outlined area in the larger map.

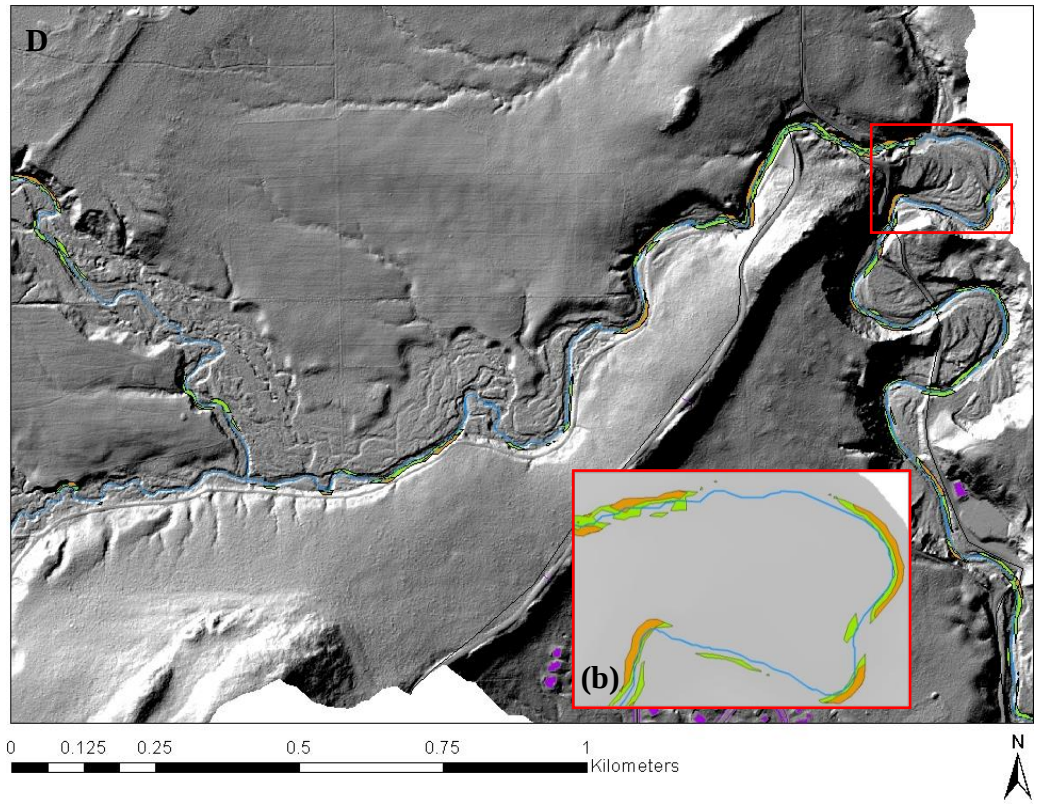


**Figure 10D** Predictors for Amity Creek watershed. 2 meters and higher bluffs (green) and 4 meters and higher bluffs (brown) within 7 meters from channel centerline, **(b**) the bluffs for the outlined area in the larger map.

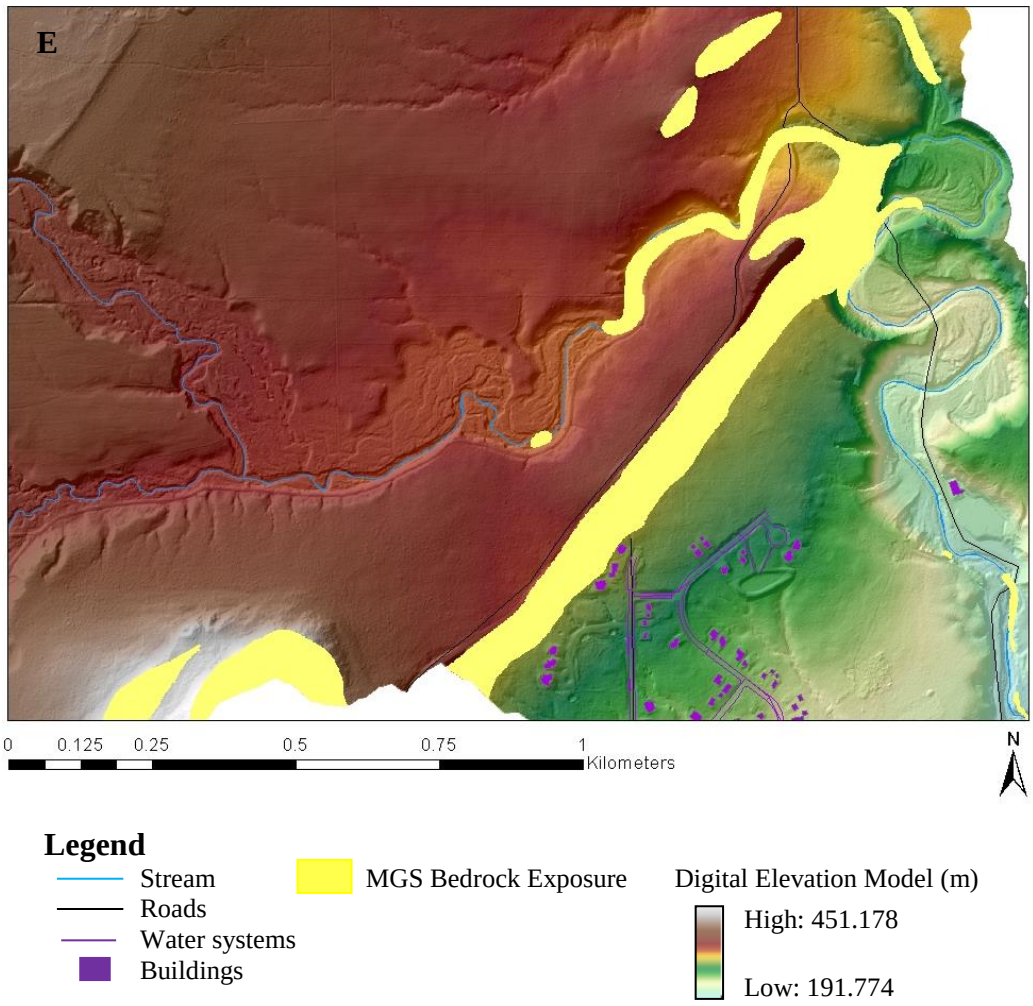


**Figure 10E** Predictors for Amity Creek watershed. Bedrock exposure map was downloaded from Minnesota Geological Survey (Hobbs, 2009b).

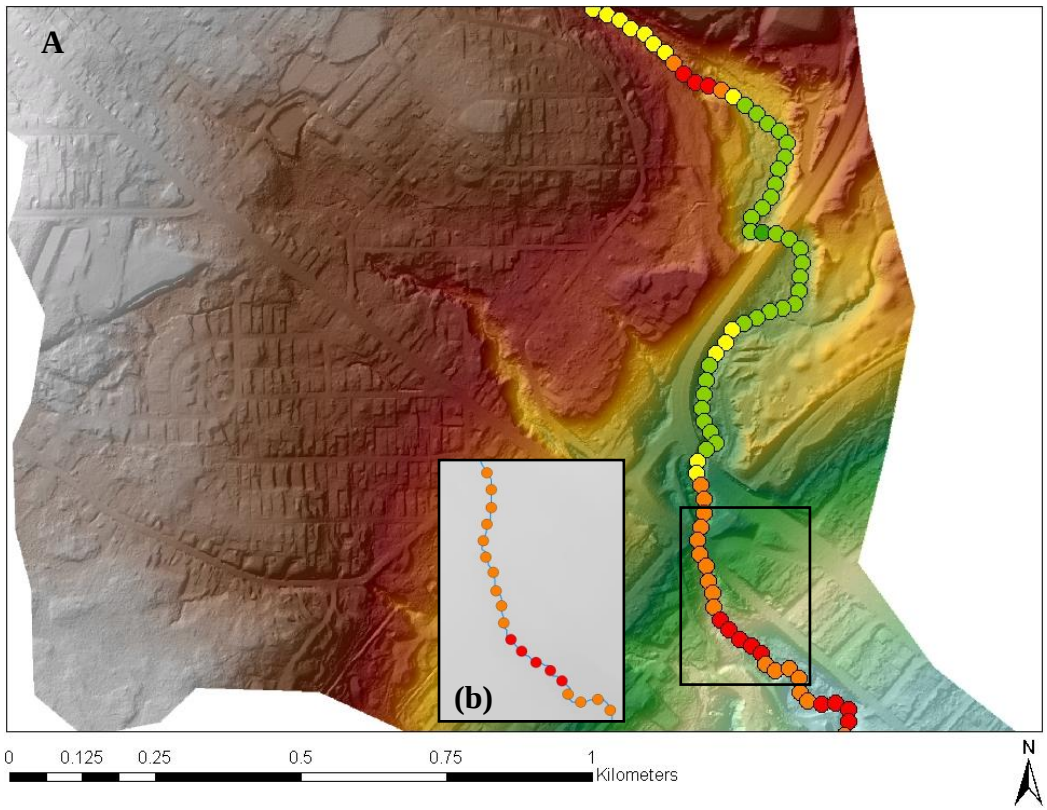


**Figure 11A** Predictors for Miller Creek watershed. SP in kg/ms$^2$, shown in every 25 meters, **(b)** the SP values for the outlined area in the larger map.

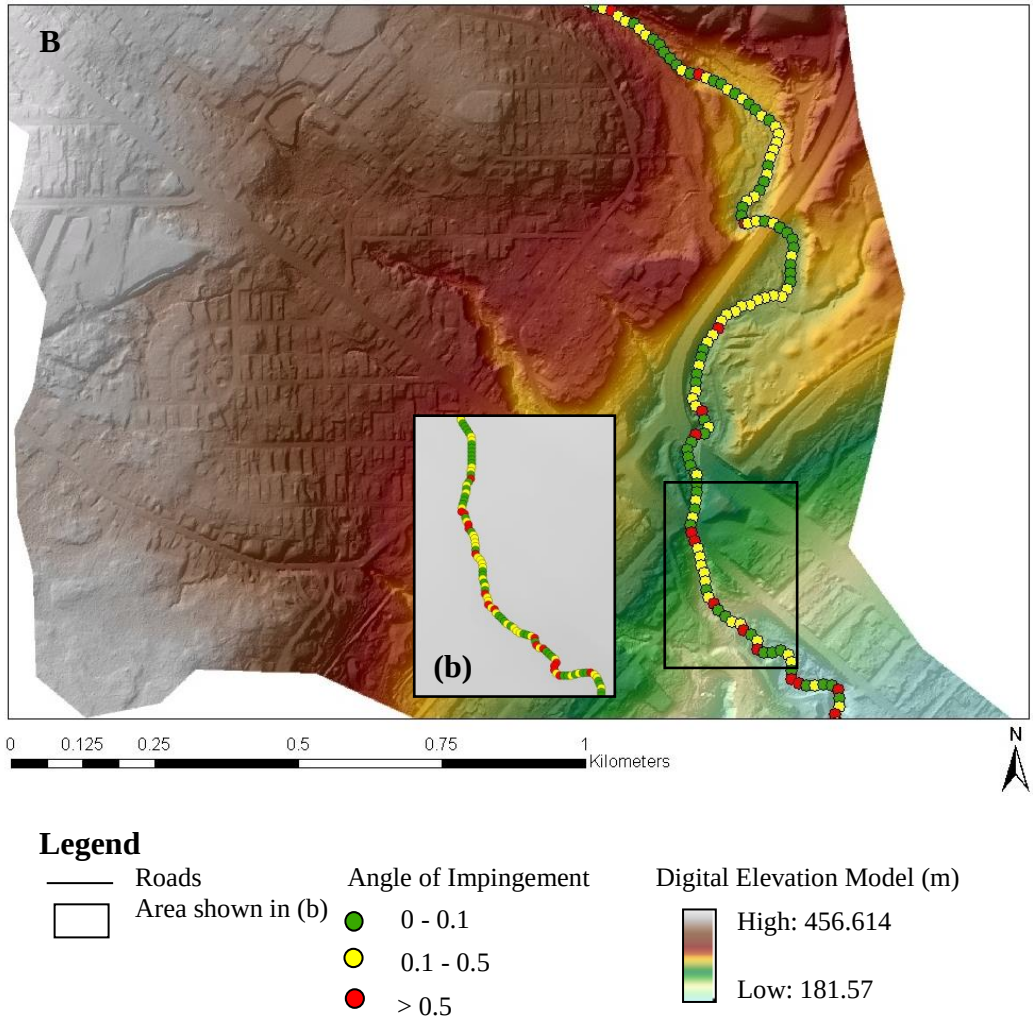


**Figure 11B** Predictors for Miller Creek watershed. Angle of impingement in radians, shown in every 15 meters in larger map, (**b**) angle of impingement in every 5 meters along the stream for the outlined area in the larger map.

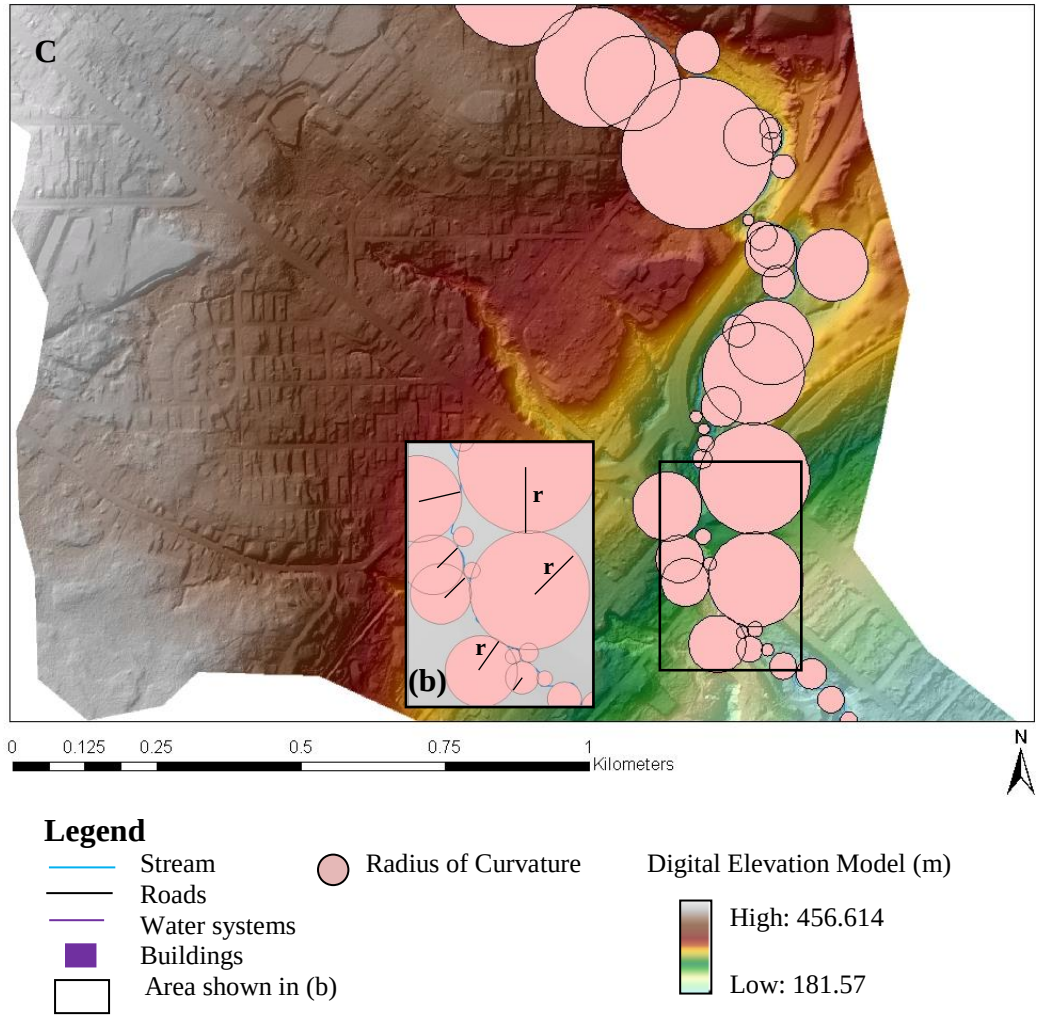


**Figure 11C** Predictors for Miller Creek watershed. Bend curvature (radius of curvature divided by bankfull channel width) shown throughout the creek, **(b)** the bend curvature for the outlined area in the larger map.

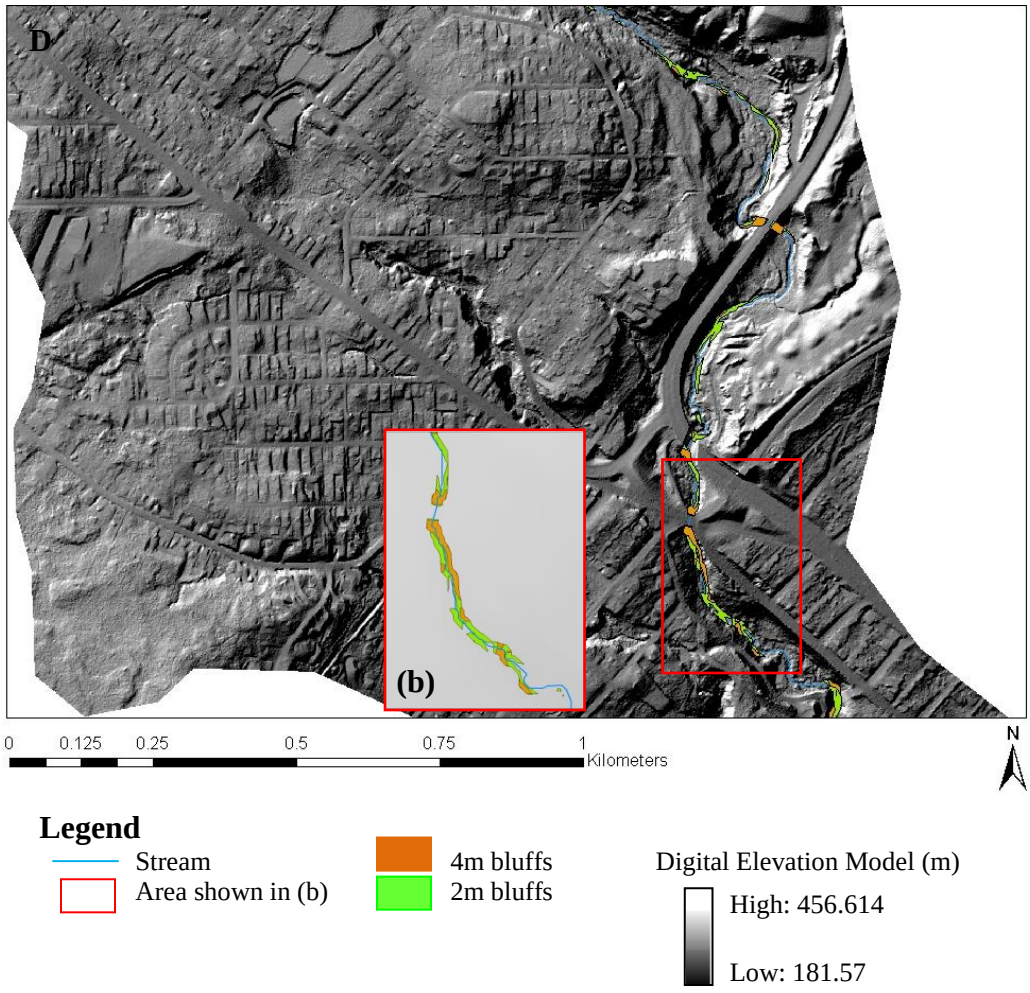


**Figure 11D** Predictors for Miller Creek watershed. 2 meters and higher bluffs (green) and 4 meters and higher bluffs (brown) within 7 meters from channel centerline, **(b**) the bluffs for the outlined area in the larger map.

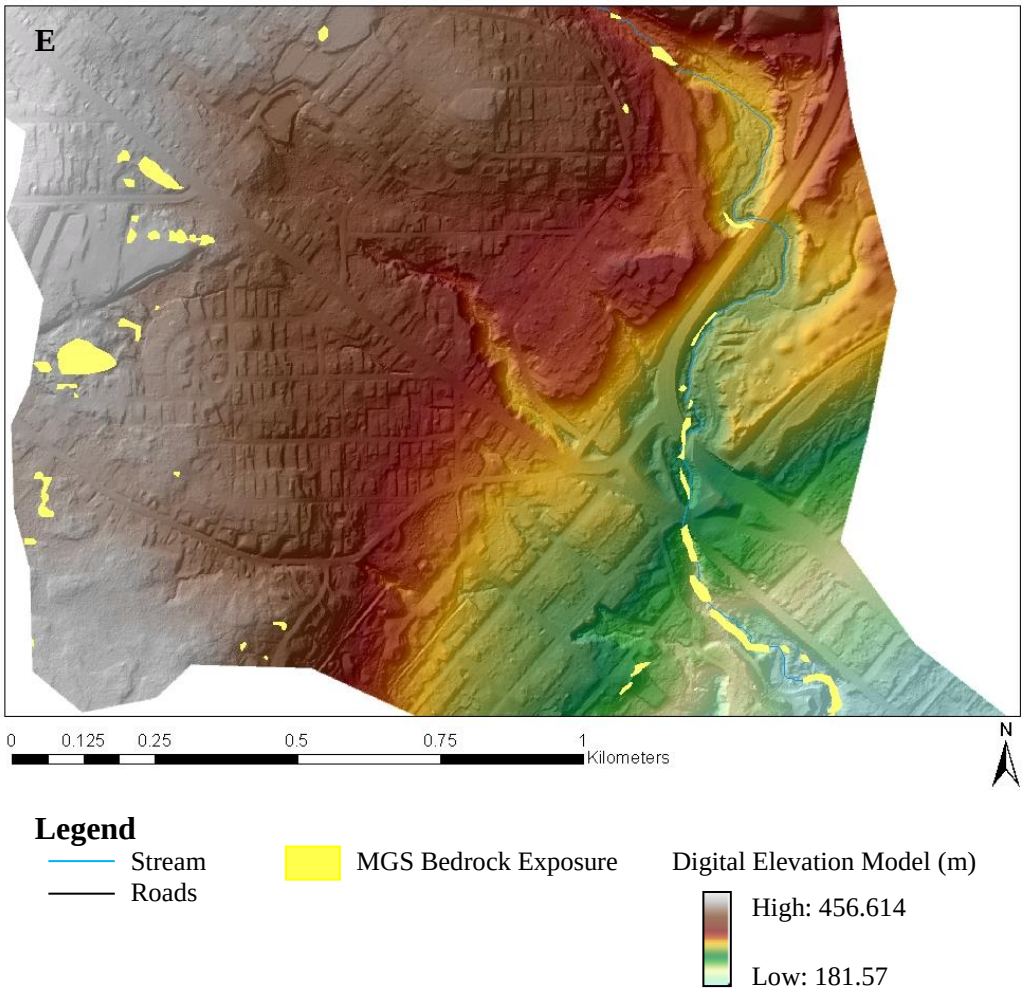


**Figure 11E** Predictors for Miller Creek watershed. Bedrock exposure map was downloaded from Minnesota Geological Survey (Hobbs, 2009a).

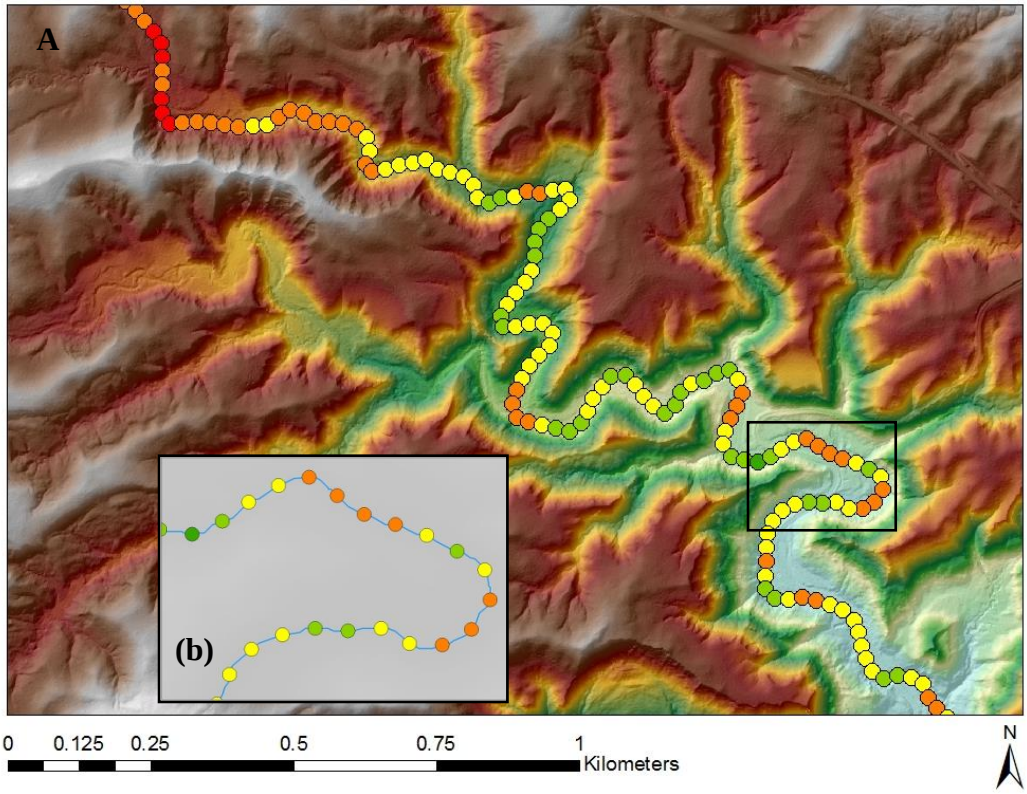


**Figure 12A** Predictors for Mission Creek watershed. **A.** SP in kg/ms$^2$, shown in every 25 meters, **(b)** the SP values for the outlined area in the larger map.

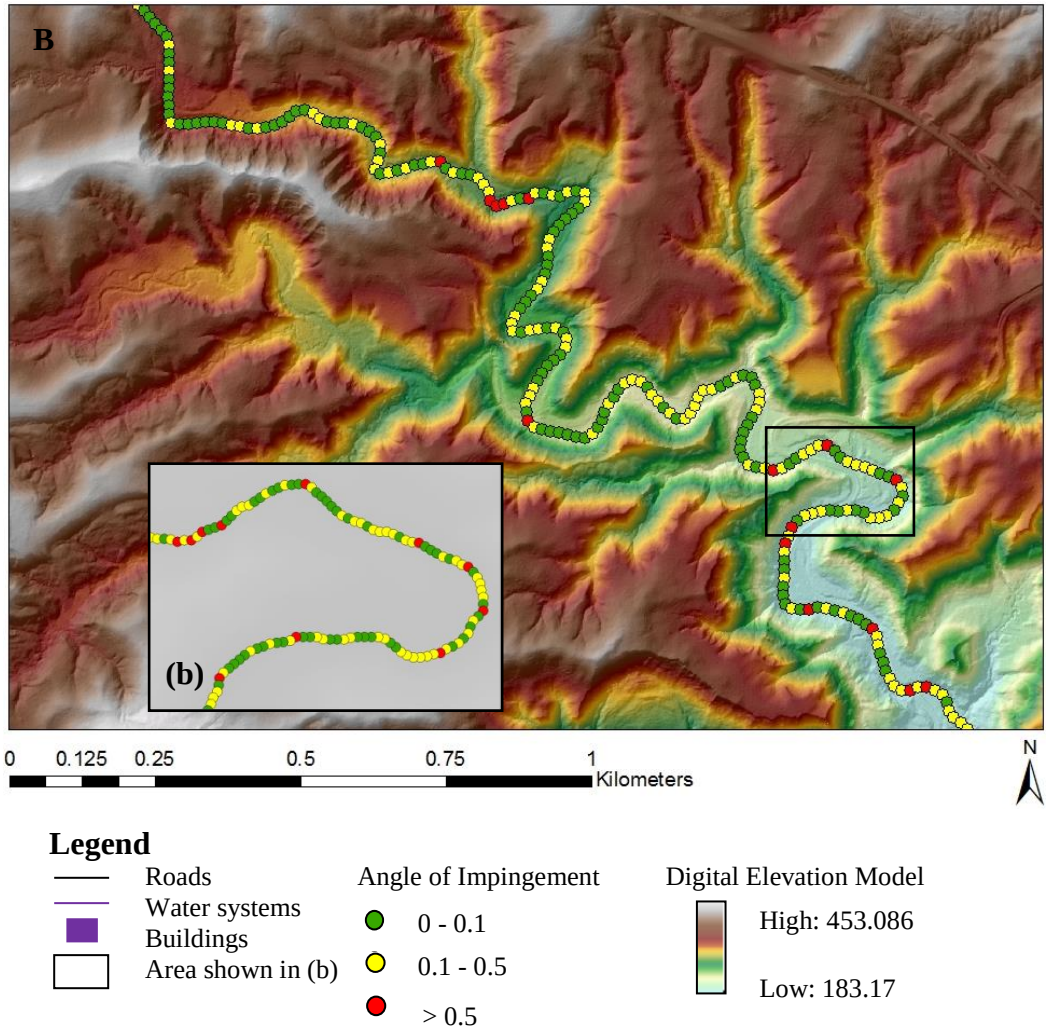


**Figure 12B** Predictors for Mission Creek watershed. Angle of impingement in radians, shown in every 15 meters in larger map, (**b**) angle of impingement in every 5 meters along the stream for the outlined area in the larger map.

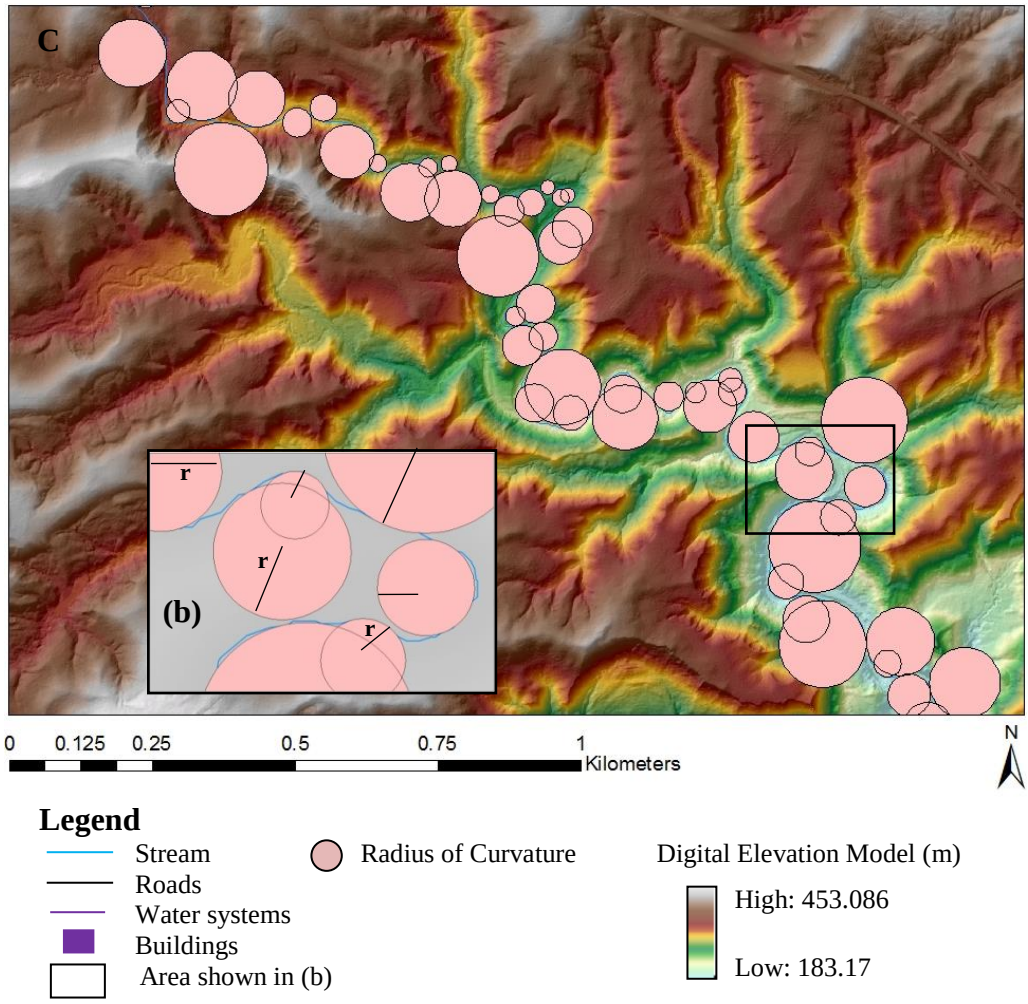


**Figure 12C** Predictors for Mission Creek watershed. Bend curvature (radius of curvature divided by bankfull channel width) shown throughout the creek, **(b**) the bend curvature for the outlined area in the larger map.

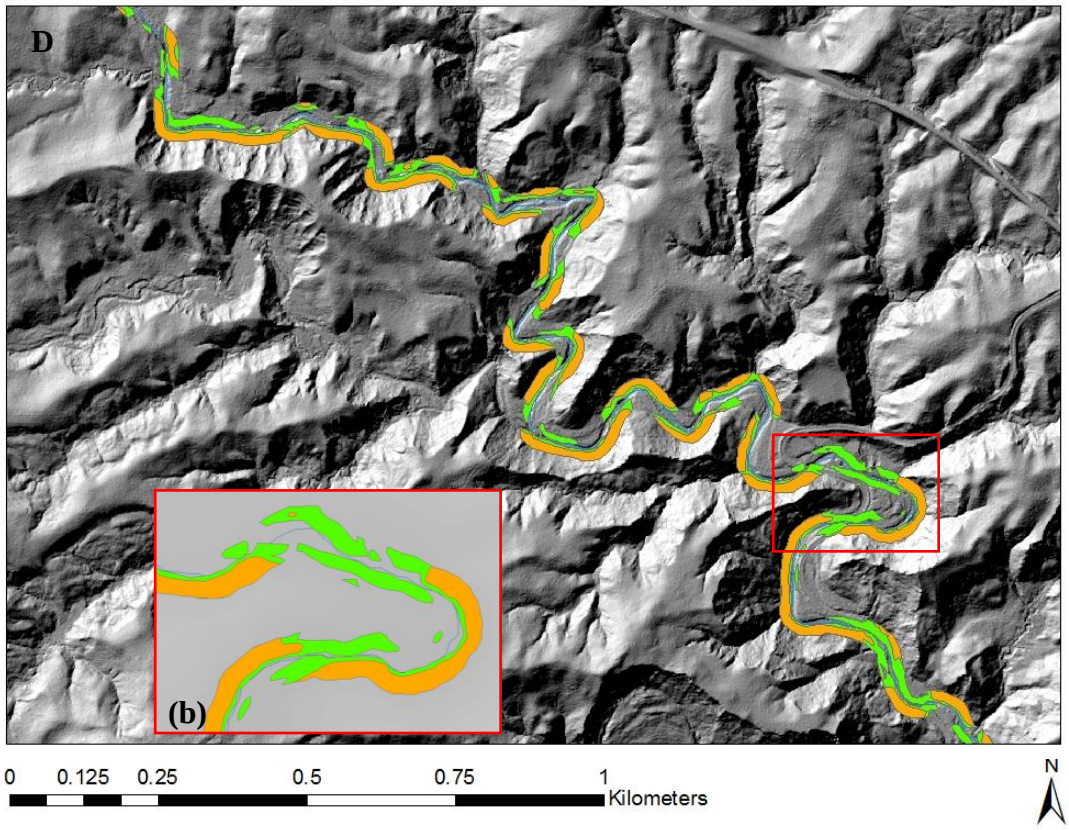


**Figure 12D** Predictors for Mission Creek watershed. 2 meters and higher bluffs (green) and 4 meters and higher bluffs (brown) within 20 meters from channel centerline, **(b)** the bluffs for the outlined area in the larger map.

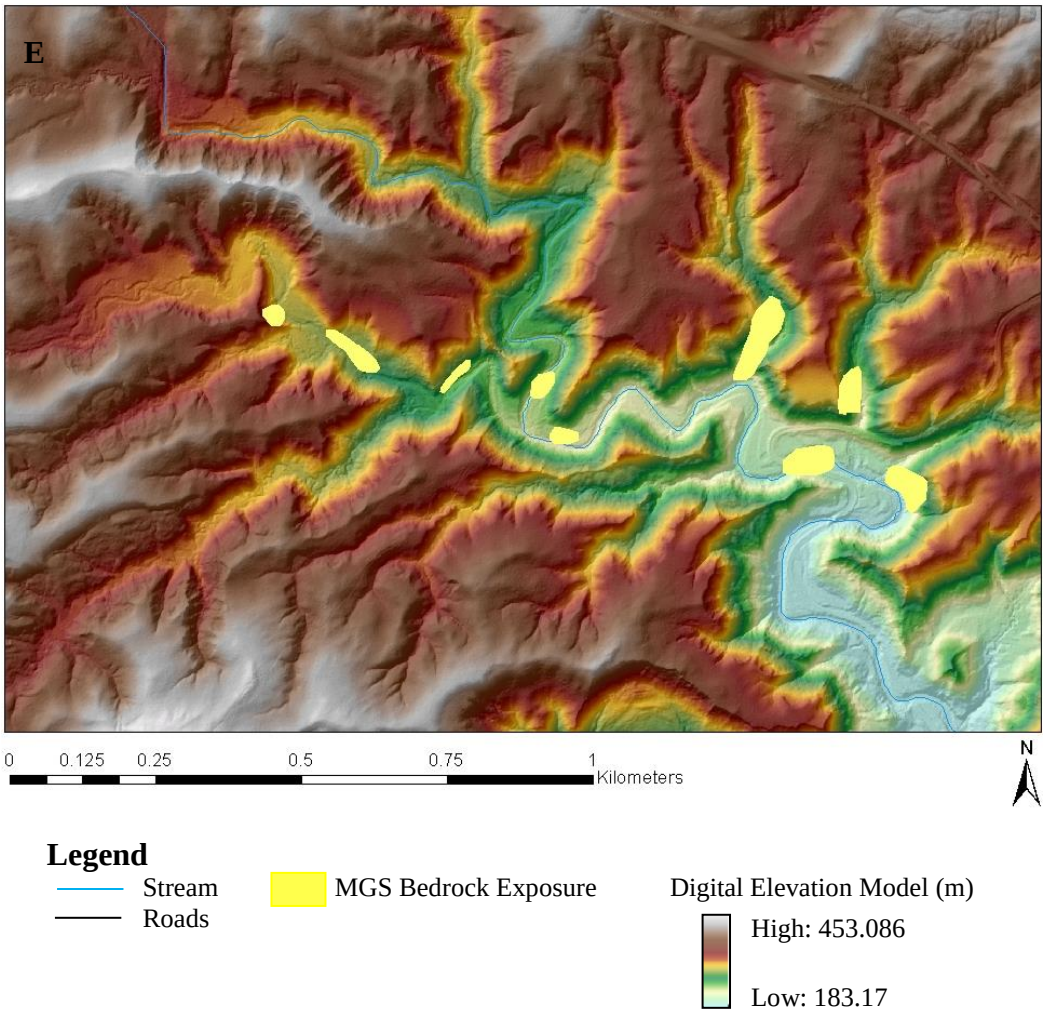


**Figure 12E** Predictors for Mission Creek watershed. Bedrock exposure map downloaded from Minnesota Geological Survey (Boerboom, 2009).

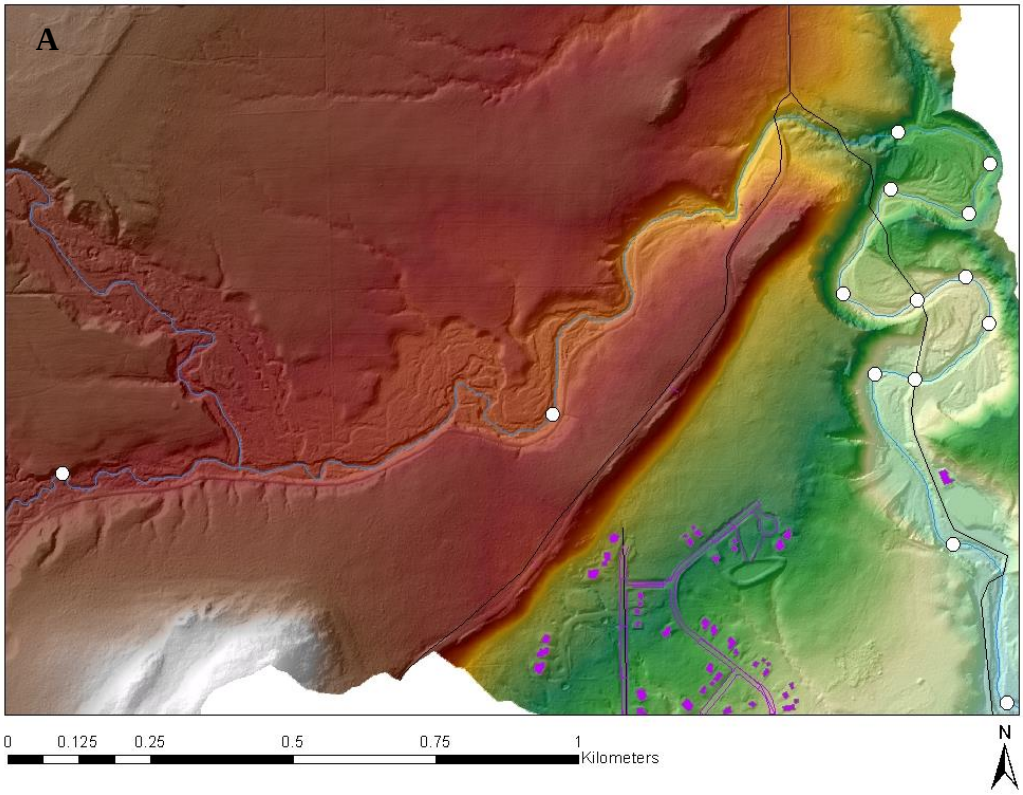


**Figure 13A** GIS-based predictive model of Amity Creek predicted erosional hotspots at the sites that have moderate-high SP, high angle of impingement, are located near high relief of bluffs, and have no MGS bedrock exposure.

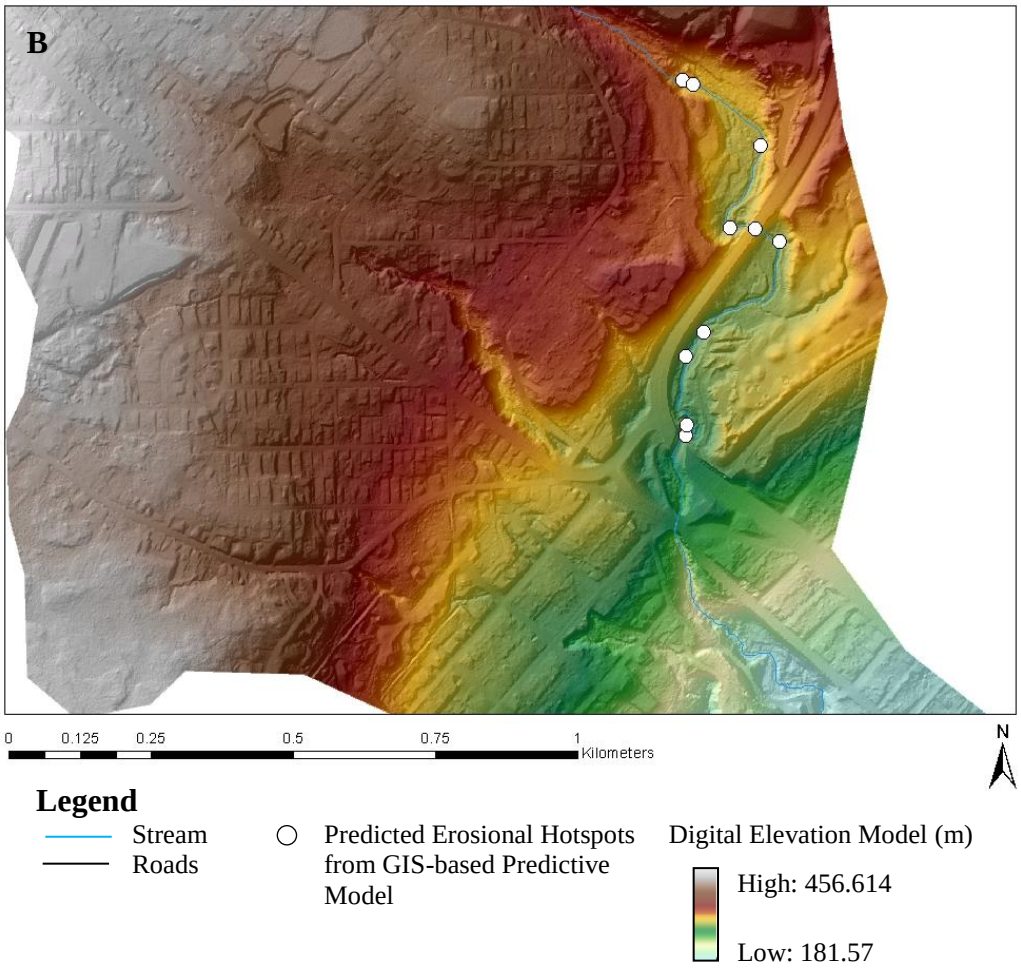


**Figure 13B** GIS-based predictive model of Miller Creek predicted erosional hotspots at the sites that have moderate-high SP, high angle of impingement, are located near high relief of bluffs, and have no MGS bedrock exposure.

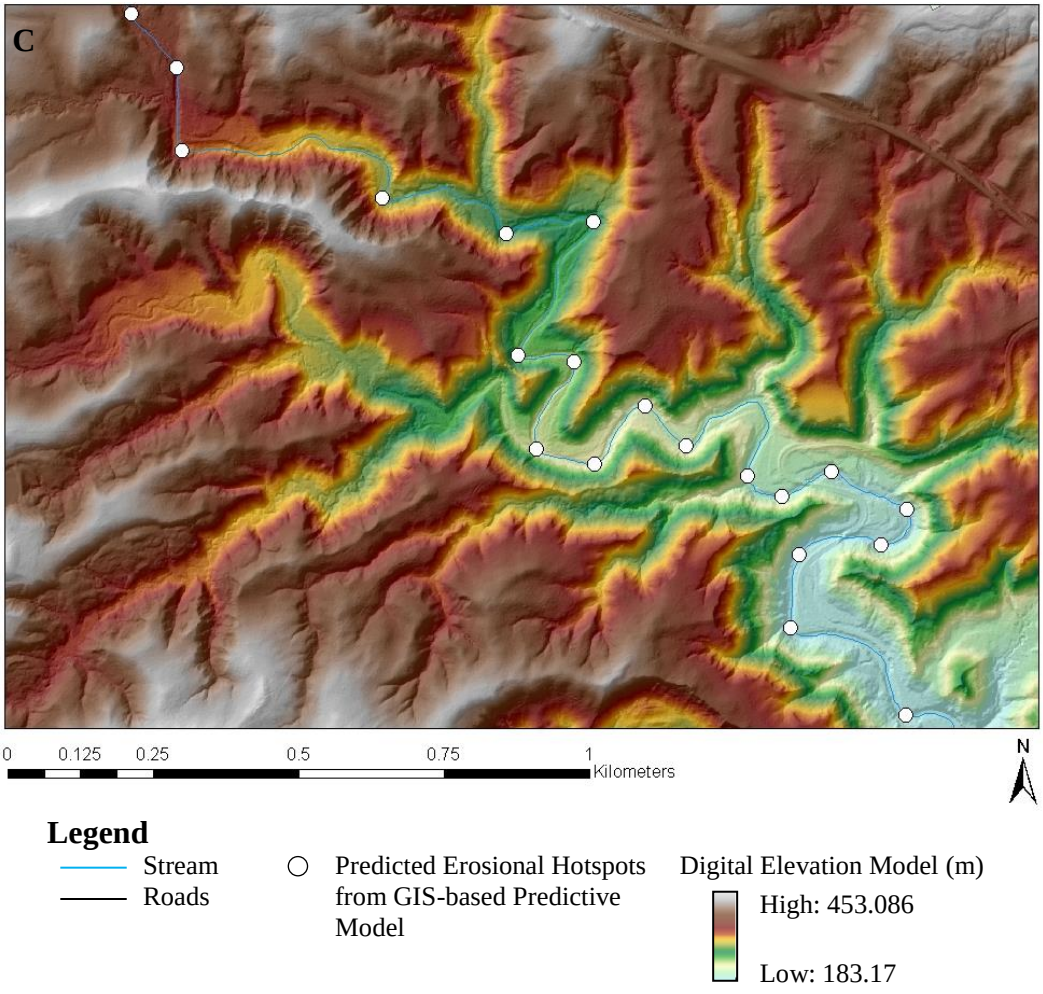


**Figure 13C** GIS-based predictive model of Mission Creek predicted erosional hotspots at the sites that have moderate-high SP, high angle of impingement, are located near high relief of bluffs, and have no MGS bedrock exposure.

***Results: Field Observations***

The GIS-based predictive model predicted erosional hotspots that were typically located in the middle and lower reaches. However, some erosional hotspots were not predicted in the lower reaches due to some reasons: 1) the lower reaches of the northern area are controlled by bedrock exposure which is difficult to erode, 2) the lower reaches of the central area are controlled by human constructions and bedrock exposure which could either increase or decrease the levels of erosion, and 3) the lower reaches of the southern area have very low-low SP which would predict less bank erosion.

During field observations, we checked those erosional hotspots that were predicted from the GIS-based predictive model, checked the valley types and channel-reach types along the streams compared to the classification of channel-reach types by Fitzpatrick et al. (2006), and mapped out the locations of bedrock exposure compared to the MGS bedrock exposure map. Moreover, we simultaneously conducted the Field Erosion Index surveys for all 12 watersheds.

Figures 14A, 14B show the field maps of bedrock exposure compared with the MGS bedrock exposure maps of Amity Creek and Miller Creek, respectively. The field map of bedrock exposure of Mission Creek is similar to the MGS bedrock exposure map and is not shown here. Figures 15A, 15B, 15C show the valley types and channel-reach types during field checking. Figures 16A, 16B, 16C show the results of FEI rating surveys from Amity Creek, Miller Creek, and Mission Creek, respectively. Low scores, which indicate bedrock exposure (0) and no or little erosion (1) were mainly found in the lower reaches of Amity Creek and Miller Creek. The moderate scores (2-5) were mainly found near predicted topographic erosional hotspots. High scores (6-7) were rare in Miller Creek, but were typically found in middle and lower reaches of Mission Creek.

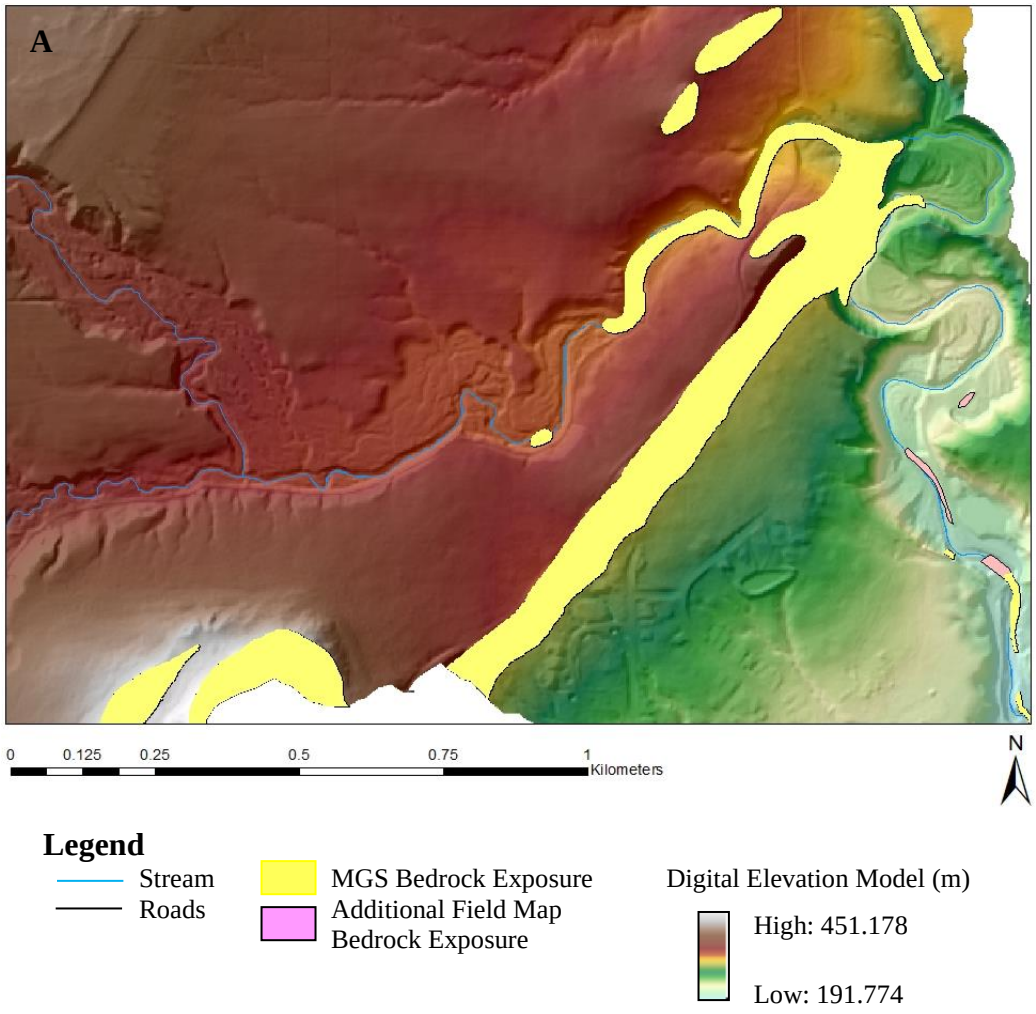


**Figure 14A** Bedrock exposure map of Amity Creek watershed: MGS bedrock exposure map and additional field map of bedrock exposure, based on field observation-based data.

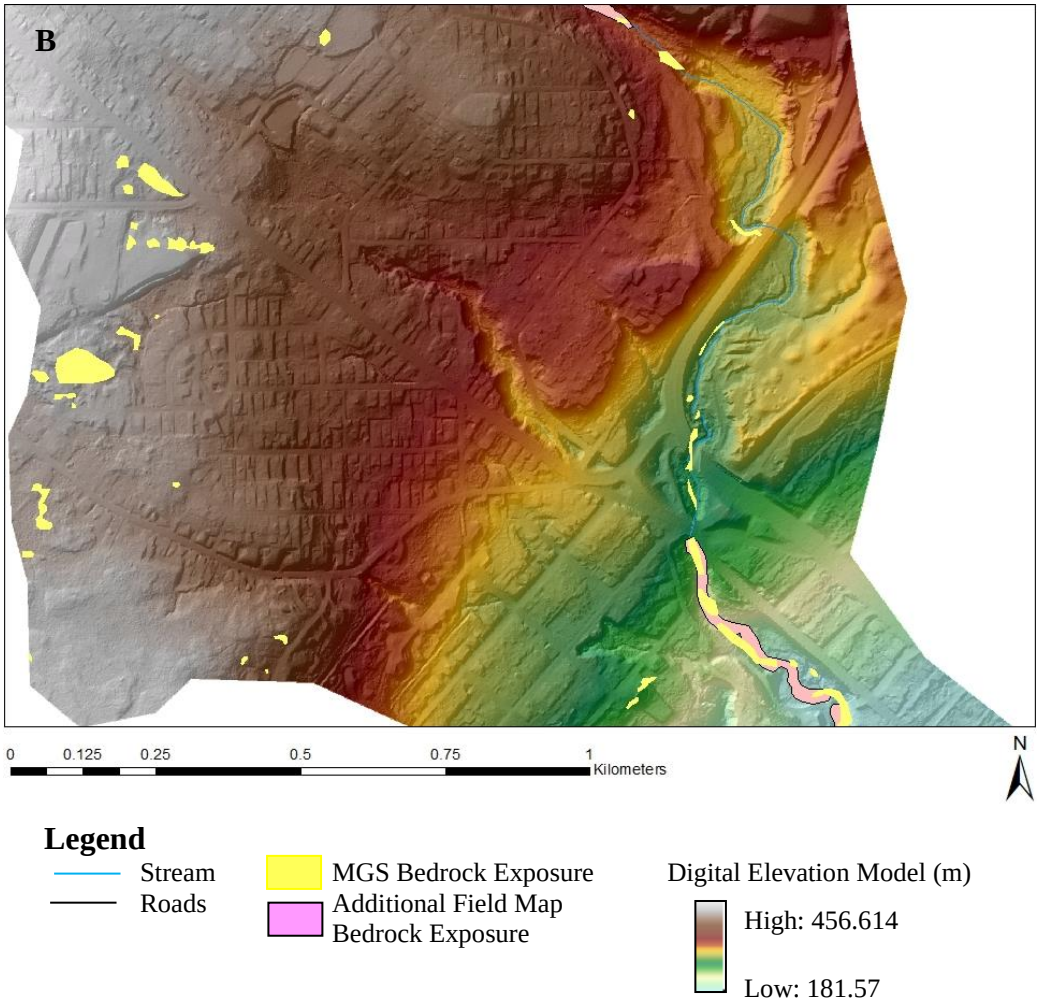


**Figure 14B** Bedrock exposure map of Miller Creek watershed: MGS bedrock exposure map and additional field map of bedrock exposure, based on field observation-based data.

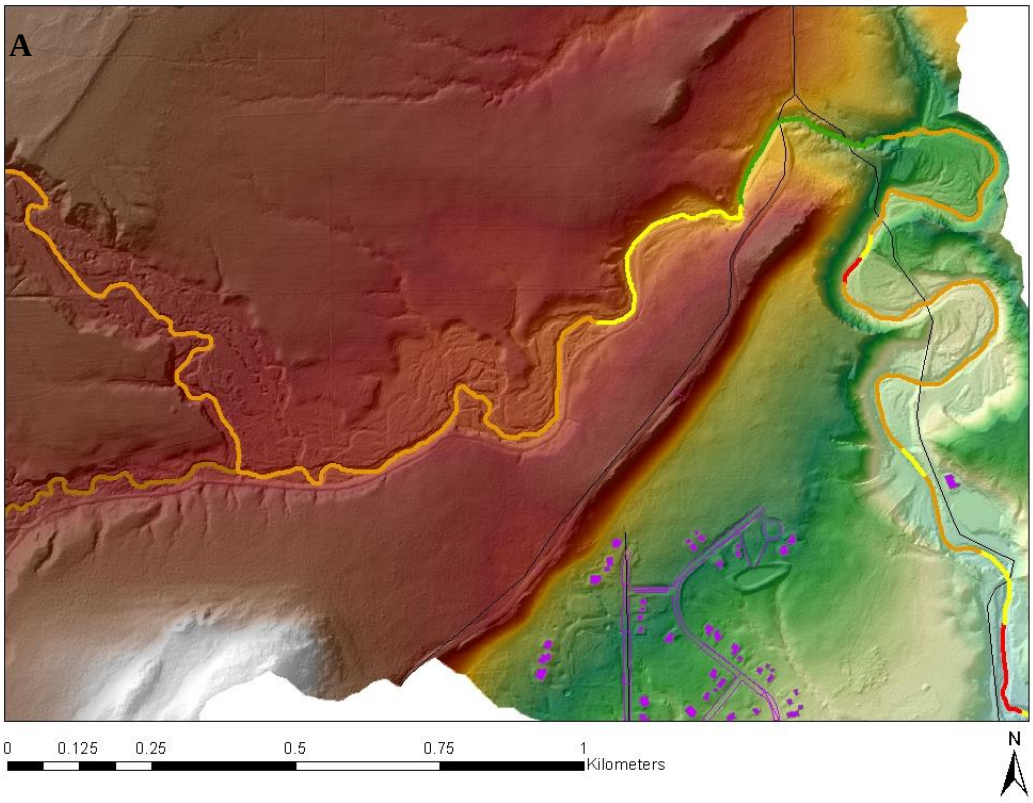


**Figure 15A** Valley types and channel-reach types map of Amity Creek were identified during field observations.

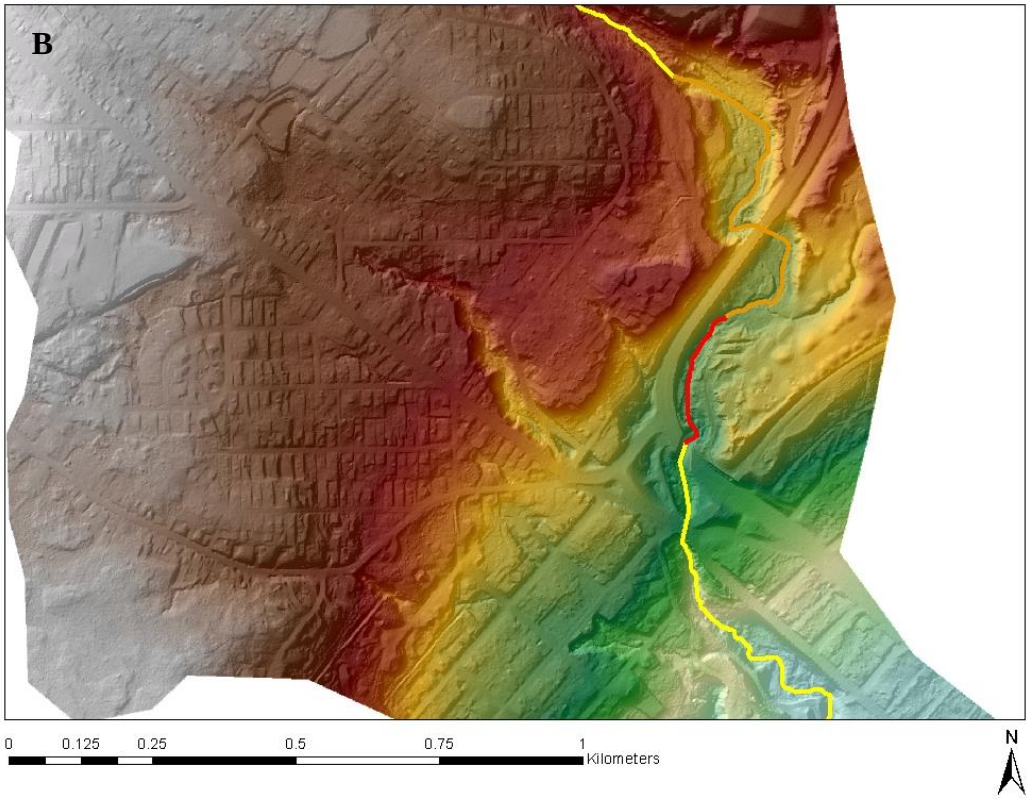


**Figure 15B** Valley types and channel-reach types map of Miller Creek were identified during field observations.

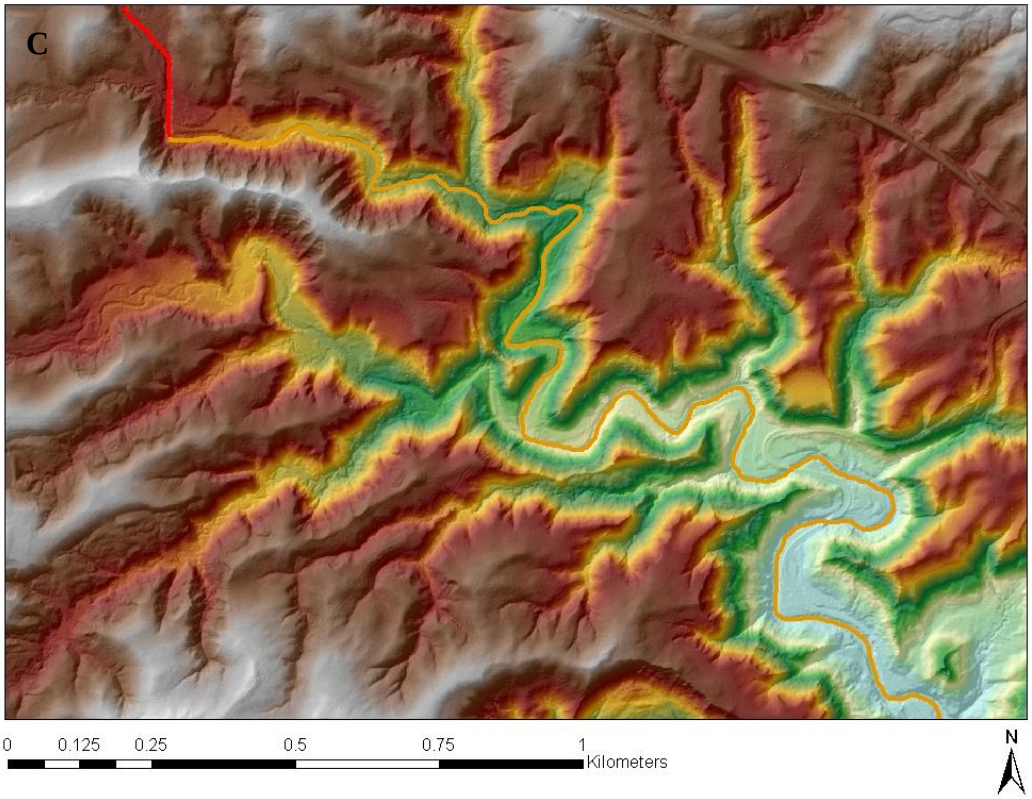


**Figure 15C** Valley types and channel-reach types map of Mission Creek were identified during field observations.

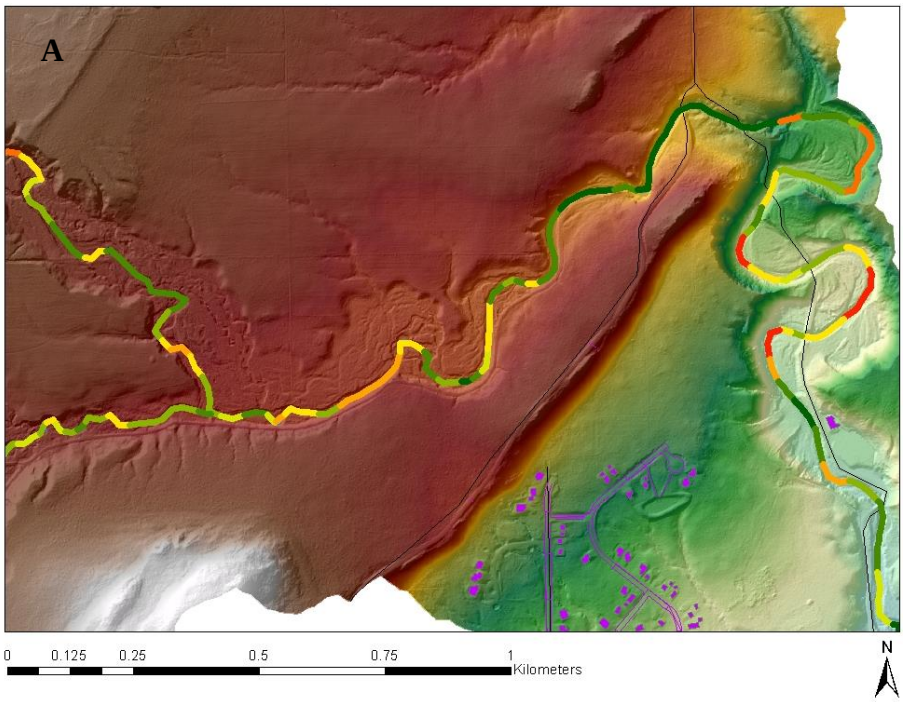


**Legend**

FEI

0 1 2 3 4 5 6 7

Digital Elevation Model (m)

High: 451.178

Low: 191.774

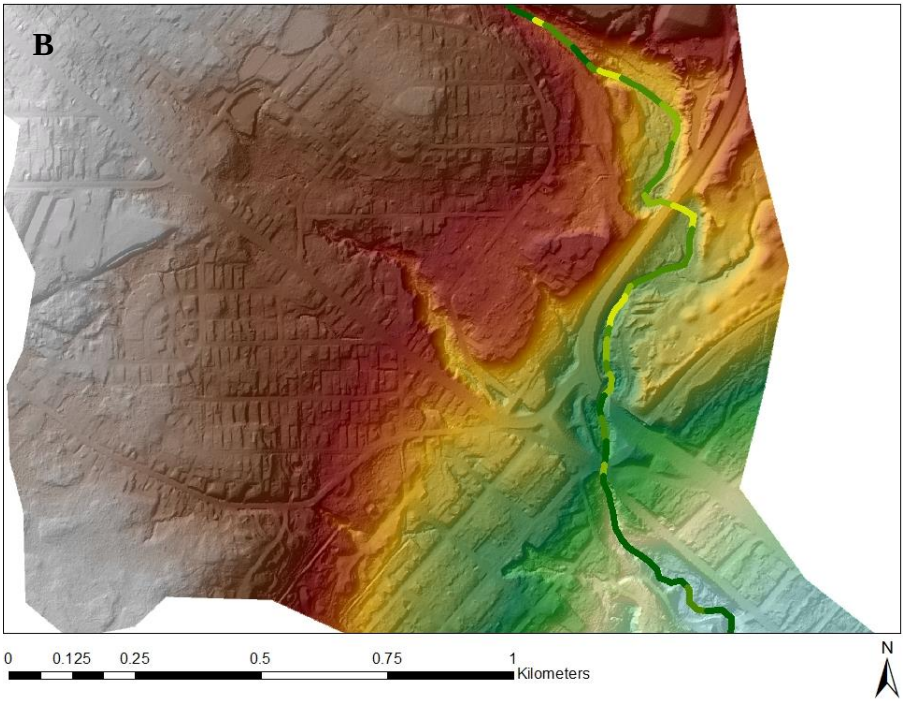


**Legend**

FEI

0 1 2 3 4 5 6 7

Digital Elevation Model (m)

High: 456.614

Low: 181.57

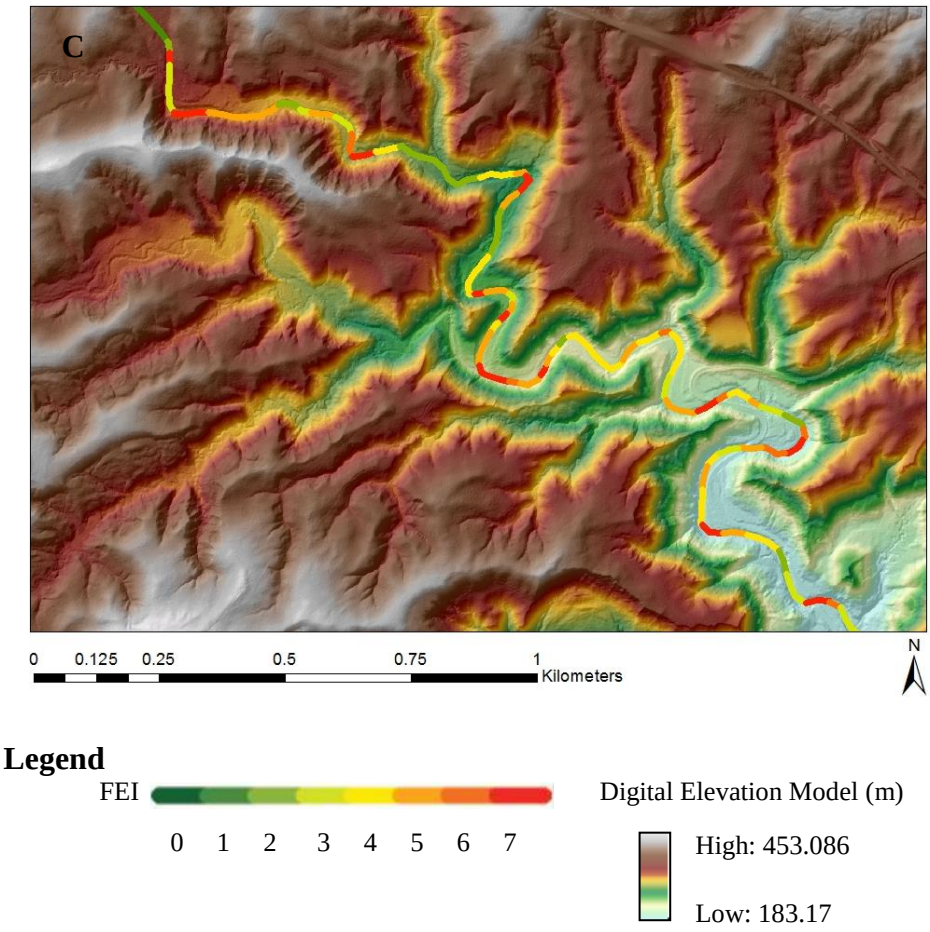


**Figure 16** Field Erosion Index (FEI) of **A.** Amity Creek, **B.** Miller Creek, and **C.** Mission Creek. Definition of each FEI score is shown in Figure 6 (this is shown in ***Methods: Field observations***).

Table 3 and Figure 17 show the percent of points per survey stream length with each FEI score. The percentage indicates the density of each level of erosion in each watershed. In the northern area of Duluth-area streams, the Lester River and Amity Creek experienced more streambank erosion at the toe (FEI 2-3) and slumping (FEI 4-5), whereas Chester Creek and Tischer Creek show fewer FEI ≥ 1 hotspots due to bedrock exposure in the lower reaches. The significant bedrock exposure on bluffs at the central areas of Duluth-area streams means that erosion at reaches with high FEI are rarely found. However, Sargent Creek and Mission Creek significantly experienced erosion as slumping (FEI 4-5) and complete scours (FEI 6-7).

These surveys show a wide range of erosion occurred along the streams. In the lower and middle reaches of Amity Creek and Mission Creek where we conducted the field observations, 56% and 78% of the stream length experienced moderate to high levels of erosion (FEI ≥ 2), respectively, whereas the lower and middle reaches of Miller Creek have only 27% experiencing some levels of erosion. Approximately one-third of survey sites in Amity Creek and half of survey sites in Mission Creek experienced slumping and complete scour (FEI ≥ 4), while there are only few slumps in Miller Creek (Table 3).

**Table 3** Percent of points per survey stream length with each FEI score. The data indicate how much erosion occurred along the streams.

| FEI | Lester | Amity | Tischer | Chester |
|---|---|---|---|---|
| 0 | 21.43 | 18.98 | 63.30 | 31.71 |
| 1 | 12.62 | 25.50 | 16.51 | 23.17 |
| 2 | 16.90 | 21.81 | 11.93 | 18.29 |
| 3 | 11.90 | 4.53 | 3.67 | 11.59 |
| 4 | 15.95 | 15.58 | 3.67 | 9.15 |
| 5 | 13.57 | 7.37 | 0.92 | 4.88 |
| 6 | 3.10 | 3.12 | 0 | 0.61 |
| 7 | 4.52 | 3.12 | 0 | 0.61 |
| **# of survey points** | 420 | 353 | 109 | 164 |
| **Length (km)** | 10.475 | 8.800 | 2.700 | 4.075 |

| FEI | Miller | Merritt | Keene | Kingsbury | Knowlton | Stewart | Sargent | Mission |
|---|---|---|---|---|---|---|---|---|
| 0 | 40.70 | 32.91 | 37.40 | 25.55 | 38.24 | 40.30 | 0 | 0 |
| 1 | 32.66 | 34.18 | 30.08 | 20.44 | 30.39 | 23.88 | 16.56 | 21.74 |
| 2 | 19.10 | 17.72 | 16.26 | 16.79 | 15.69 | 7.46 | 22.70 | 22.98 |
| 3 | 6.03 | 13.92 | 6.50 | 27.01 | 5.88 | 4.48 | 9.82 | 15.84 |
| 4 | 1.51 | 0 | 9.76 | 3.65 | 2.94 | 16.42 | 14.11 | 18.01 |
| 5 | 0 | 1.27 | 0 | 0 | 5.88 | 5.97 | 16.26 | 10.25 |
| 6 | 0 | 0 | 0 | 2.19 | 0 | 0 | 8.28 | 4.66 |
| 7 | 0 | 0 | 0 | 4.38 | 0.98 | 1.49 | 12.27 | 6.52 |
| **# of survey points** | 199 | 79 | 123 | 137 | 102 | 67 | 322 | 326 |
| **Length (km)** | 4.950 | 1.950 | 3.050 | 3.400 | 2.525 | 1.650 | 8.025 | 8.125 |

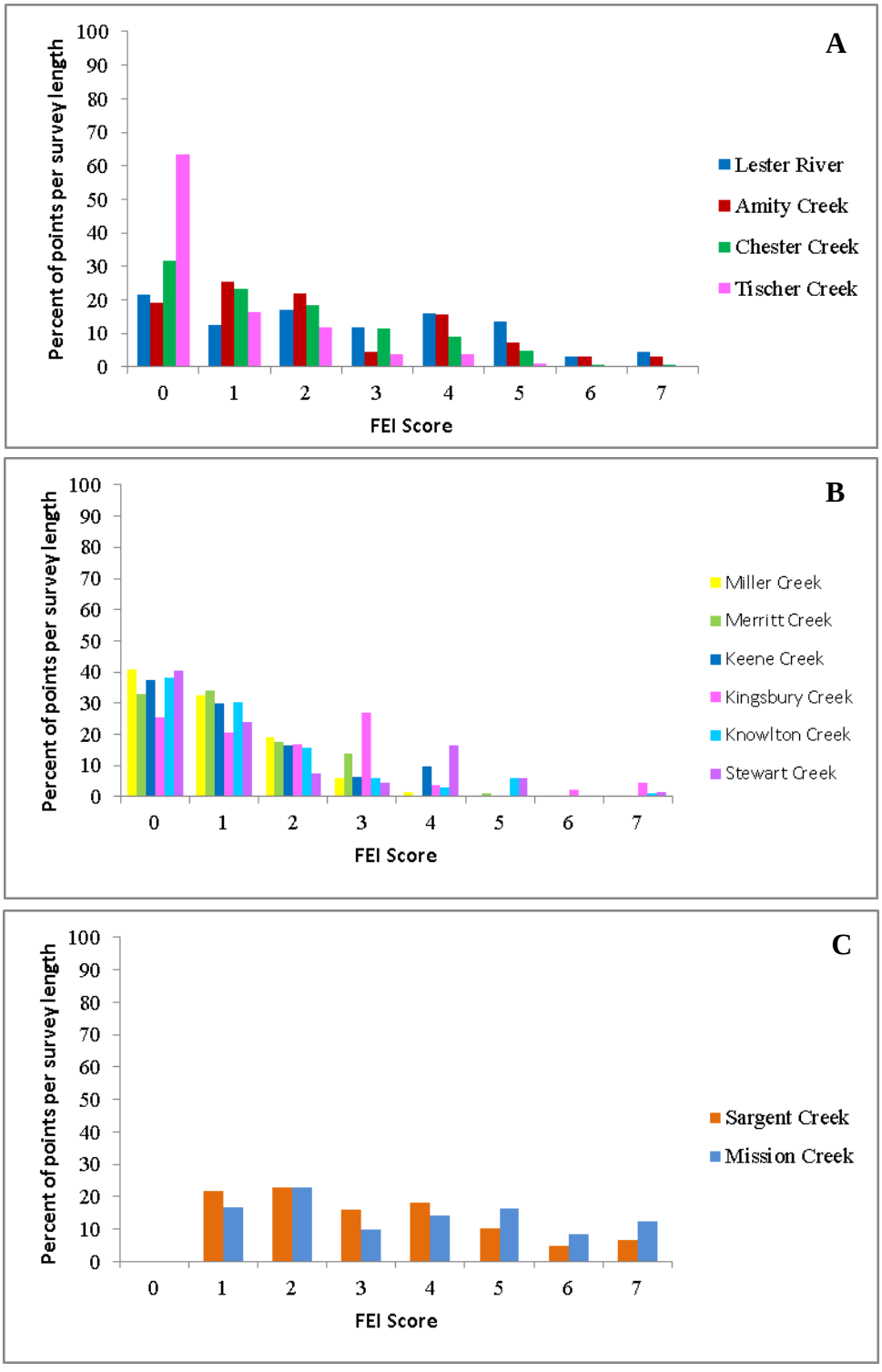


**Figure 17** Percent of points per survey stream length with each FEI score of 12 watersheds, according to Table 3, in different areas of Duluth-area streams: **A.** the northern area, **B.** the central area, and **C.** the southern area.

### *Results: GIS Predictors Compared to Field Observations*

We compared the results of GIS predictors to FEI surveys conducted at points, which are spaced every 25 meters along the lower and middle reaches of Amity Creek, Miller Creek, and Mission Creek where the FEI survey data were collected. Figures 18, 19 and 20 show data comparisons between the GIS predictors and the FEI scores for Amity Creek, Miller Creek, and Mission Creek, respectively. Those plots are also shown with standard error bars from the mean.

In Figures 18, 19, and 20, plot A shows the average SP for each FEI score. Plots B and C show the average AOI and the average bend curvature ratio for each FEI score. Plots D and E show the percent of points near 2 meters and higher bluffs and 4 meters and higher bluffs, respectively, for each FEI score. Plot F shows the percent of points located in combined bedrock exposure locations for each FEI score. The $r^2$ and the p-values, which are shown on plots A, B, C, D, and E, do not include FEI = 0 (bedrock reaches) in calculation. However, the data of FEI = 0 are shown on those plots for a reference; they are bedrock reaches which have low erosion regardless of the stream power, the angle of impingement, the bend curvature ratio, or the bluff proximity.

From Table 4, there is a very significant negative correlation between the average bend curvature ratio and FEI in all three creeks. The percent of points adjacent to 2 meters and higher bluffs with FEI also has a significant correlation. The percent of points adjacent to 4 meters and higher bluffs with FEI has a significant correlation in Amity Creek and Mission Creek, but that is almost significant in Miller Creek. There are no significant correlations between the average SP and FEI, and between the average angle of impingement and FEI, except in Mission Creek. However, stream power as the main driver of erosion is still used to develop the threshold model. Moreover, the percent of points near the combined bedrock exposure location is close to 100% for FEI = 0 because it is defined as a bedrock reach. Likewise, at FEI $\geq$ 1, we would ideally expect 0% of points adjacent to the combined bedrock exposure maps.

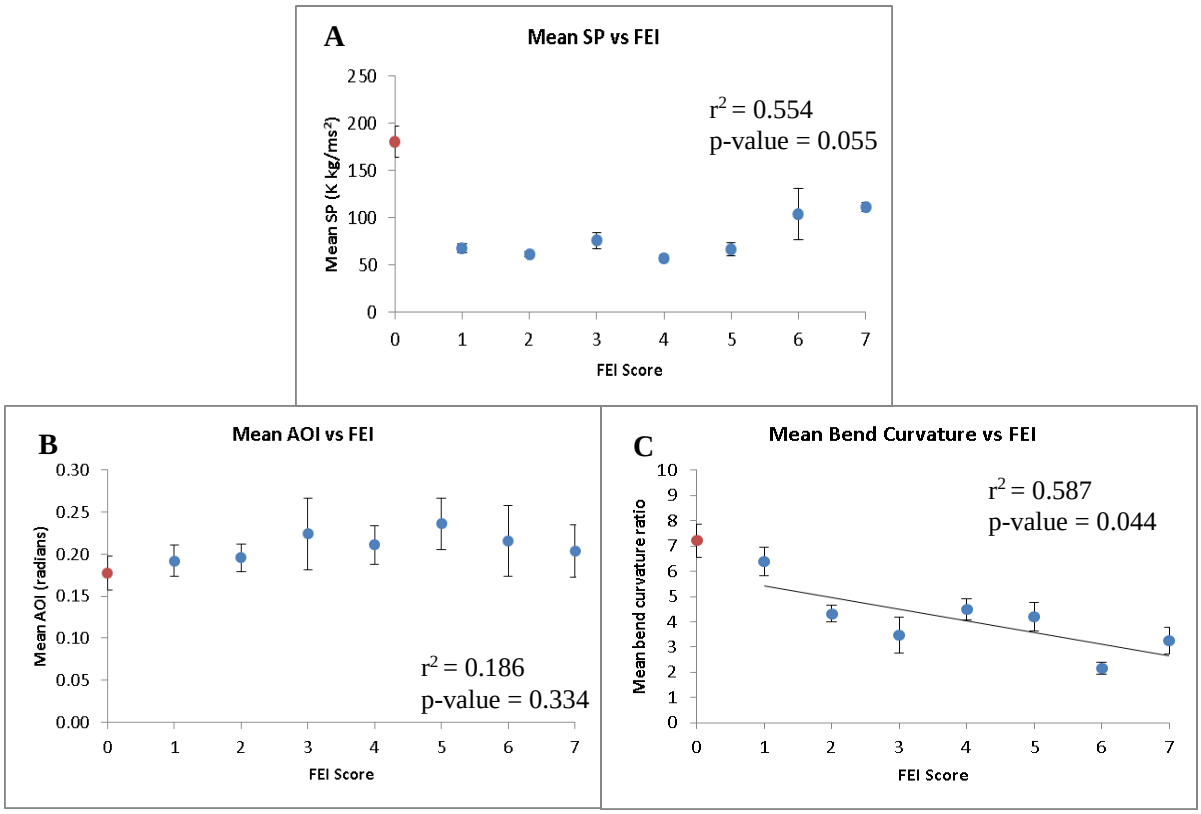


**Figure 18** Comparisons between GIS predictors and FEI surveys on Amity Creek. All data were extracted at points spaced in every 25 meters along the stream network where the FEI survey was conducted. Plots A, B, and C illustrate the average stream power-based erosion index, angle of impingement, and bend curvature ratio, respectively, along with the error bars that indicate one standard error from the mean. Even though FEI = 0 is illustrated on these plots, the linear regressions do not include FEI = 0. Regression lines are illustrated on the significant regression. $r^2$ and p-values are also shown on these plots.

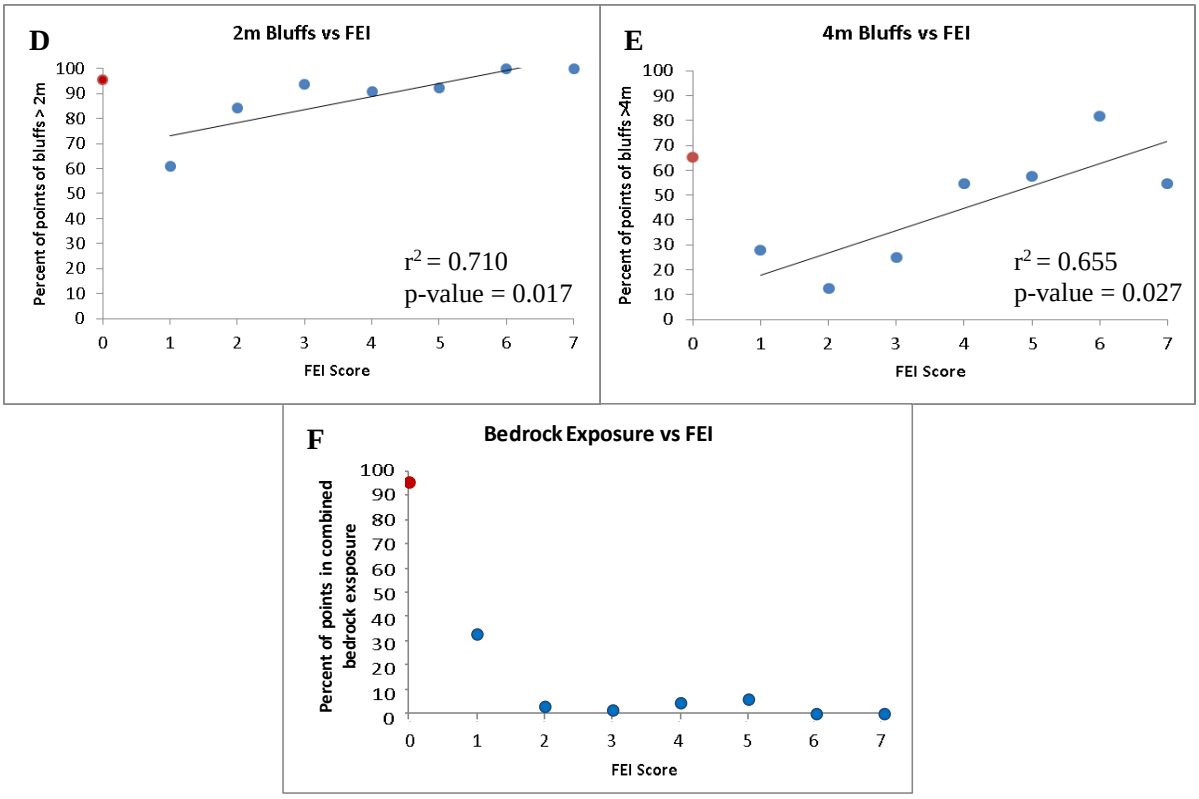


**Figure 18, ctd:** Comparisons between GIS predictors and FEI surveys on Amity Creek. All data were extracted at points spaced in every 25 meters along the stream network where the FEI survey was conducted. Plots D and E illustrate the percent of points of 2 meters and higher bluffs, and 4 meters and higher bluffs, respectively. Plot F illustrates the percent of points within outcrop location as mapped on combined bedrock exposure map. 95 % of the points are located to bedrock at FEI = 0, and less than 20% of the points are adjacent to bedrock for FEI 2-7. $r^2$ and p-values are also shown on plots D and E.

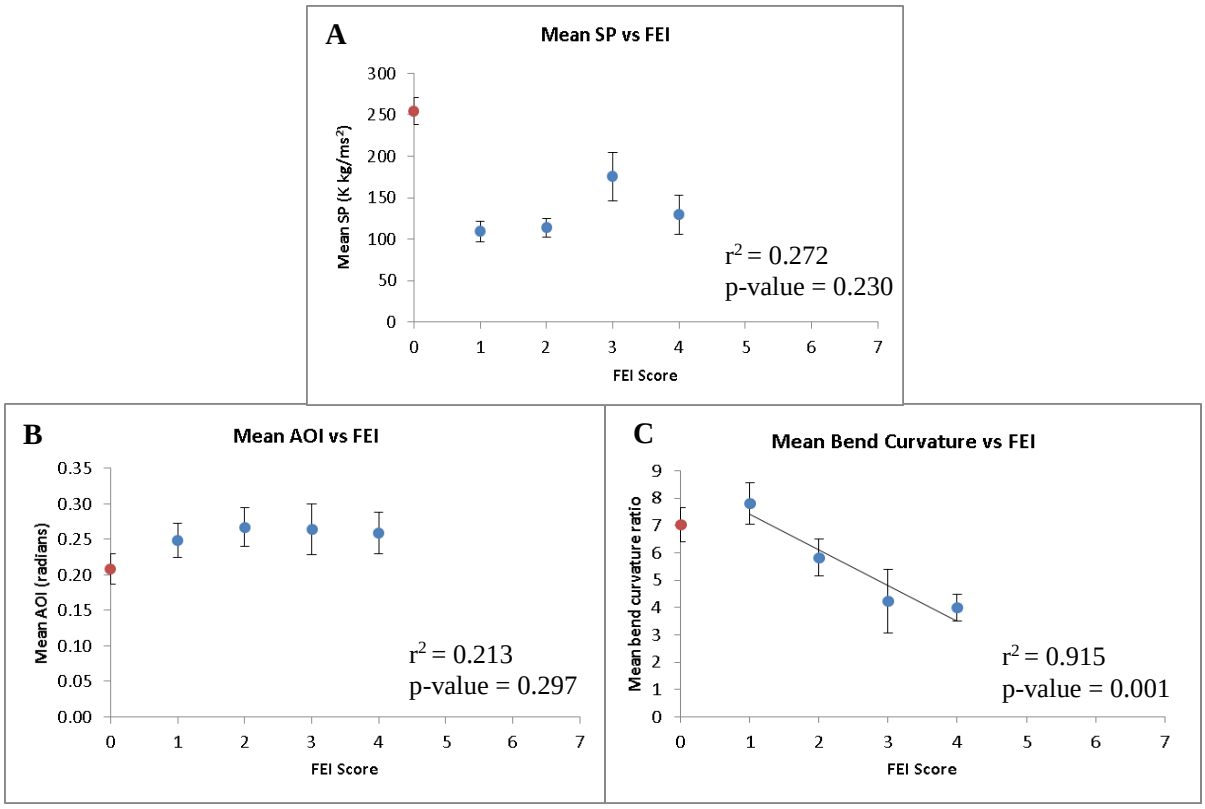


**Figure 19** Comparisons between GIS predictors and FEI surveys on Miller Creek. All data were extracted at points spaced in every 25 meters along the stream network where the FEI survey was conducted. Plots A, B, and C illustrate the average stream power-based erosion index, angle of impingement, and bend curvature ratio, respectively, along with the error bars that indicate one standard error from the mean. Even though FEI = 0 is illustrated on these plots, the linear regressions do not include FEI = 0. Regression lines are illustrated on the significant regression. $r^2$ and p-values are also shown on these plots.

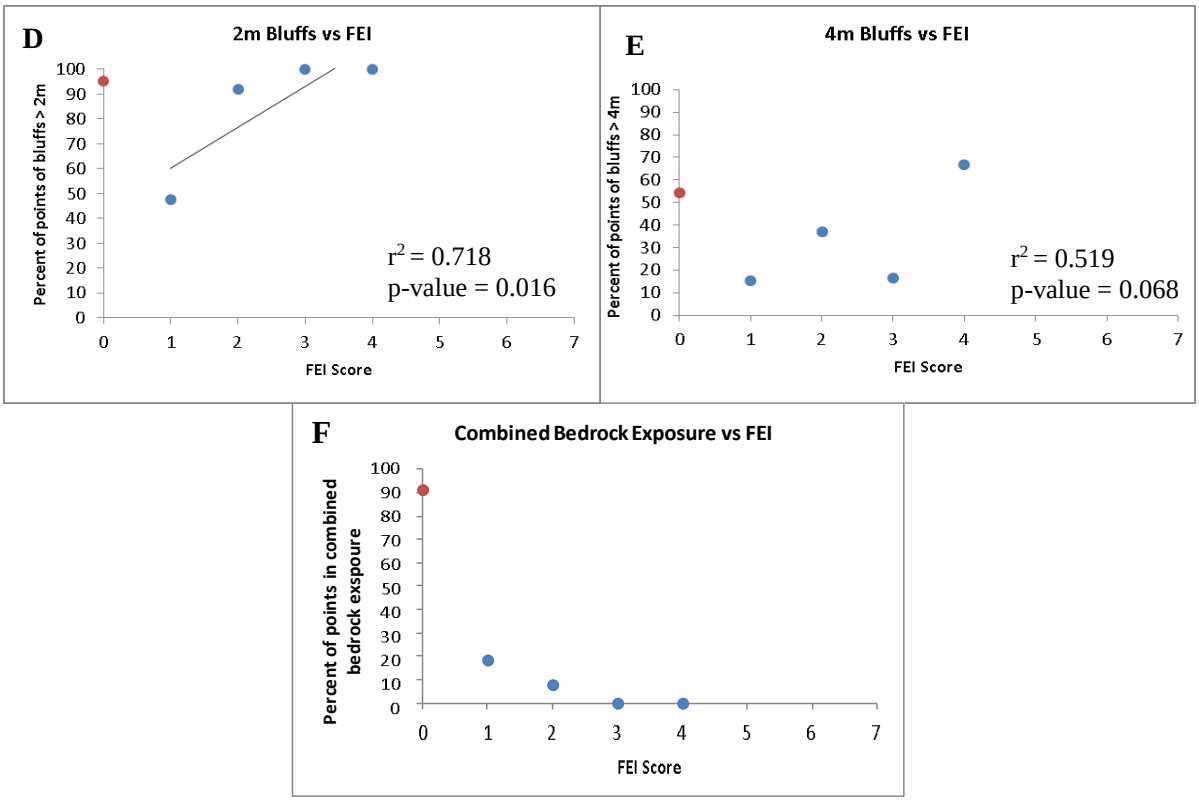


**Figure 19, ctd:** Comparisons between GIS predictors and FEI surveys on Miller Creek. All data were extracted at points spaced in every 25 meters along the stream network where the FEI survey was conducted. Plots D and E illustrate the percent of points of 2 meters and higher bluffs, and 4 meters or higher bluffs, respectively. Plot F illustrates the percent of points within outcrop location as mapped on combined bedrock exposure map. 90 % of the points are located to bedrock at FEI = 0, and 0% of the points are adjacent to bedrock for FEI 3-4. $r^2$ and p-values are also shown on plots D and E.

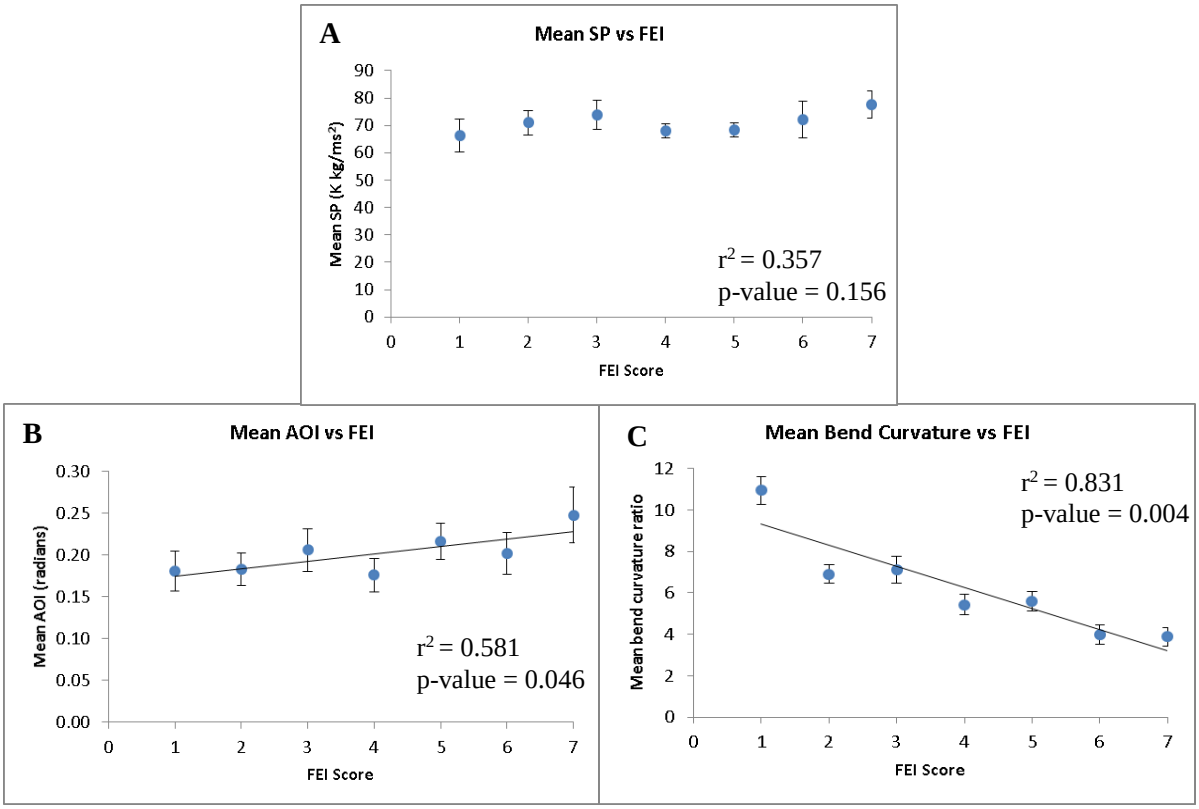


**Figure 20** Comparisons between GIS predictors and FEI surveys on Mission Creek. All data were extracted at points spaced in every 25 meters along the stream network where the FEI survey was conducted. Plots A, B, and C illustrate the average stream power-based erosion index, angle of impingement, and bend curvature ratio, respectively, along with the error bars that indicate one standard error from the mean. Even though FEI = 0 is illustrated on these plots, the linear regressions do not include FEI = 0. Regression lines are illustrated on the significant regression. $r^2$ and p-values are also shown on these plots.

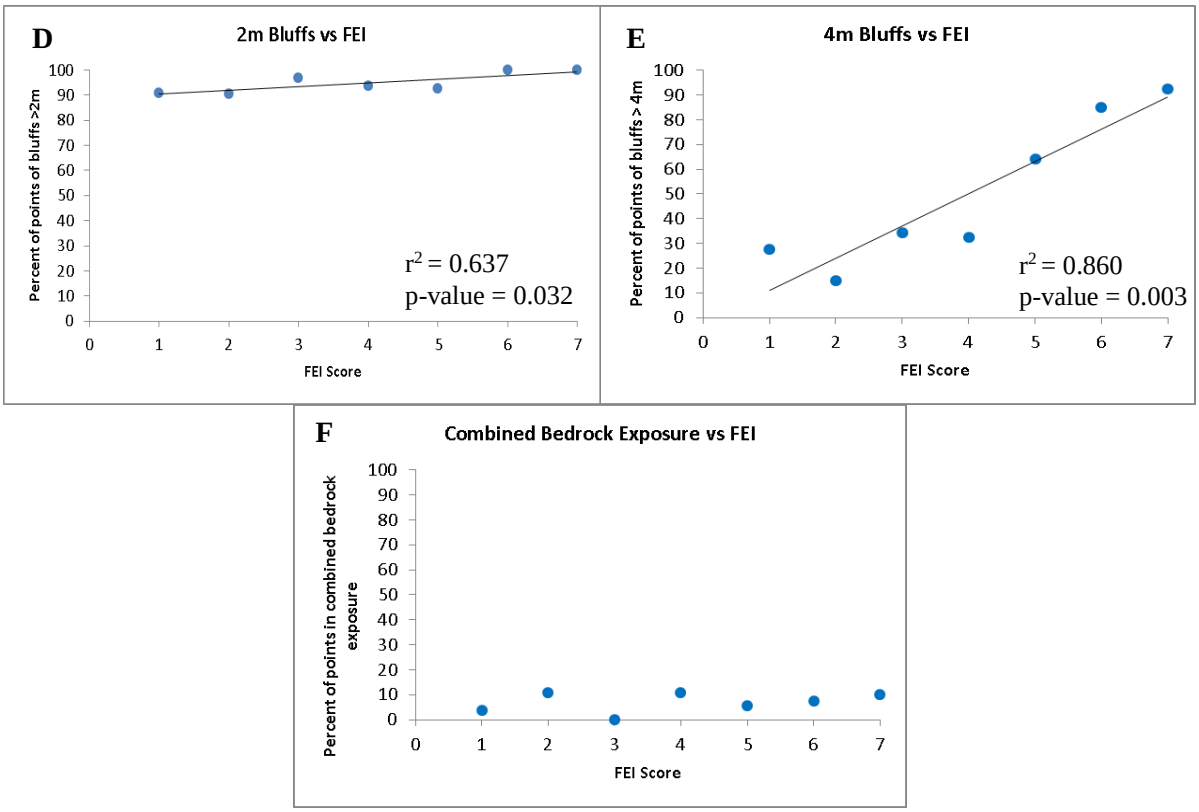


**Figure 20, ctd:** Comparisons between GIS predictors and FEI surveys on Mission Creek. All data were extracted at points spaced in every 25 meters along the stream network where the FEI survey was conducted. Plots D and E illustrate the percent of points of 2 meters and higher bluffs, and 4 meters and higher bluffs, respectively. Plot F illustrates the percent of points within outcrop location as mapped on combined bedrock exposure map. There are no points located to bedrock at FEI = 0, whereas less than 15% of the points are adjacent to bedrock for FEI 1-7. $r^2$ and p-values are also shown on plots D and E.

**Table 4** Predictor vs FEI score regression statistics show $r^2$ and p-values. The bold values are the significant correlations between the predictor and FEI score.

| FEI | Amity Creek | | Miller Creek | | Mission Creek | |
|---|---|---|---|---|---|---|
| | **$r^2$** | **p-value** | **$r^2$** | **p-value** | **$r^2$** | **p-value** |
| Mean SP for each FEI | 0.554 | 0.055 | 0.272 | 0.230 | 0.357 | 0.156 |
| Mean AOI for each FEI | 0.186 | 0.334 | 0.213 | 0.297 | **0.581** | **0.046** |
| Mean BCR for each FEI | **0.587** | **0.044** | **0.915** | **0.001** | **0.831** | **0.004** |
| % Pts Near 2m Bluffs | **0.710** | **0.017** | **0.718** | **0.016** | **0.637** | **0.032** |
| % Pts Near 4m Bluffs | **0.655** | **0.027** | 0.519 | 0.068 | **0.860** | **0.003** |
| Number of Points | 353 | | 199 | | 326 | |

***Results: Threshold Model***

Since many streambanks and bluffs experienced different levels of erosion, according to field-observation based data, we found much more erosion than was predicted from the GIS-based predictive model. We thus made a new threshold model in order to refine the GIS-based predictive model by allowing us to more accurately predict erosional locations in the streams which are prone to be eroded based on comparing the predictor variables with field observations. According to Figure 18-20, we found three GIS predictors have significant correlations, and one of them has almost significant correlations with FEI scores: the SP, the bend curvature ratio, 2 meters and higher bluffs, and 4 meters and higher bluffs. So, reaches with values above the threshold for each predictor could be erosional hotspots (Figure 21).

Theoretically, points that have SP values greater than the threshold are predicted to be erosional hotspots. Likewise, the bend curvature, which is less than the threshold, could be a tight bend and predicted as erosional hotspots. In order to find the most effective threshold, we focused on **the percent accuracy for all points** and **the percent accuracy for FEI ≥ 2**. We also concentrated on **the percent of points over-predicted** (the percent of points that had SP greater than the SP threshold and the bend curvature less than the bend curvature threshold, but FEI =1), and **the percent of points under-predicted** (the percent of points that had SP less than the SP threshold and the bend curvature greater than the bend curvature threshold, but FEI ≥ 2). We started to set the threshold for SP and for bend curvature ratio by choosing a random number for the SP

and the bend curvature ratio. This number must maximize the percent accuracy for all points and for FEI $\geq 2$ and minimize the percent of points over- and under-predicted. We changed and calculated those thresholds several times in order to get the highest percent accuracy for all points and for FEI $\geq 2$, with lowest percent of points over- and under-predicted in the threshold model.

After we calculated each single-predictor threshold model, three multi-predictor threshold models were developed based on reaches that fit all of the following criteria of erosional hotspots. Model 1 included the thresholds for SP, and bend curvature ratio, bluff proximity and lack of bedrock exposure (no bedrock exposed within 5 meters of the point based on the combined bedrock exposure map). Model 2 included the same thresholds but for SP, bluffs, and bedrock exposure only. Model 3 included the same thresholds but for bend curvature ratio, bluffs, and bedrock exposure only. For each of these models, we calculated the same statistics as described above for the single-predictor models to determine their accuracy.

This calculation was first developed in Amity Creek and was applied to Miller Creek but varies the predictor variables by using the threshold values as a fraction of the maximum SP value and as a fraction of the bend curvature ratio value in the watershed. However, we did not apply the same thresholds to Mission Creek due to the difference in ranges of values of predictor variables and bedrock types (fine-grained sedimentary rocks).

For Amity Creek, we found the effective SP threshold was 20,000 kg/ms$^2$ and the effective bend curvature ratio threshold was 10. After developing the threshold model on Amity Creek, we applied the same thresholds to Miller Creek by using the threshold values as a fraction of maximum SP value (3.036%) and as a fraction of bend curvature ratio value (52.7%) in the watershed. The SP thresholds of Miller Creek were reduced to 18,000 kg/ms$^2$, but the bend curvature ratio thresholds were raised to 10.6. Mission Creek, however, was independently developed: The threshold model that the effective SP threshold was 10,000 kg/ms$^2$ and the effective bend curvature ratio threshold was 10 (Table 5).

The threshold model improved upon the GIS-based predictive model; the percent accuracy for all points increased to 80% from the GIS-based predictive models in all streams, and the percent accuracy for FEI ≥ 2 was greater than 80% in Amity Creek and Mission Creek, and greater than 70% in Miller Creek, compared with the GIS-based predictive model. The percent of points over-predicted slightly increased from the GIS-based predictive model, whereas the percent of points under-predicted significantly declined to lower than 10% in all streams.

From this adjustment, the refined threshold model improved the percent accuracy for all points and for FEI ≥ 2 in these three streams. Meanwhile, the percent of points over-predicted and under-predicted were better-adjusted, following the changes in the SP thresholds and the bend curvature ratio thresholds (Figure 21).

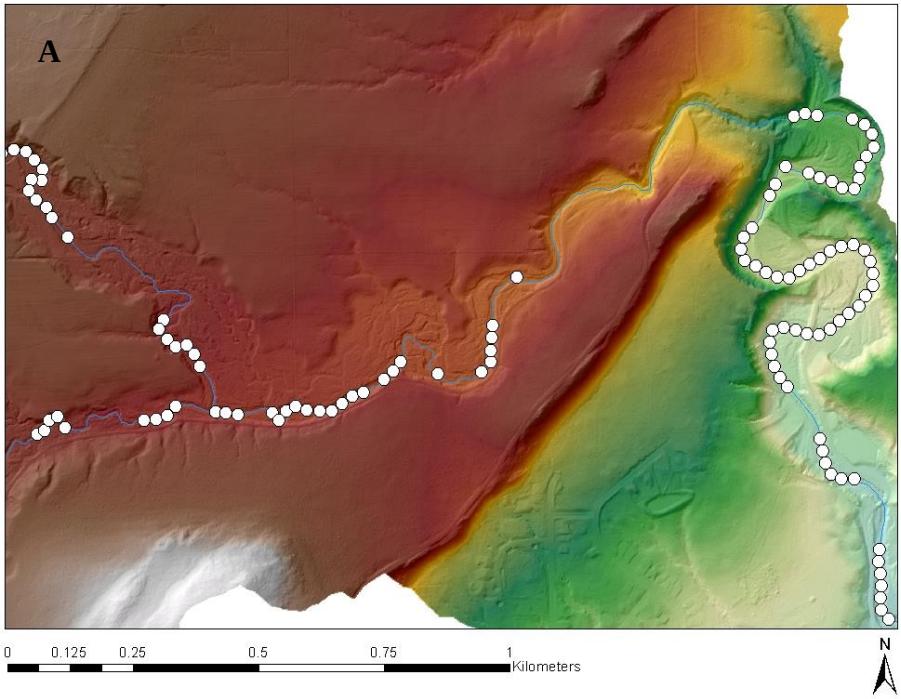


**Legend**

Consecutive Points of High Erosional Potential

Amity Creek

Digital Elevation Model (m)

High: 451.178

Low: 191.774

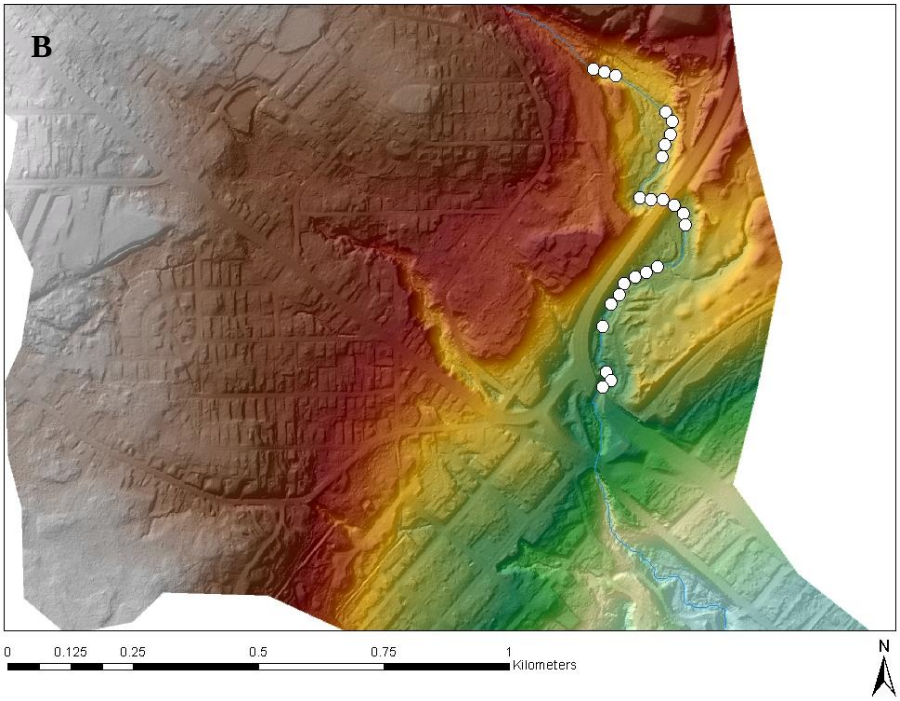


**Legend**

Consecutive Points of High Erosional Potential

Miller Creek

Digital Elevation Model (m)

High: 456.614

Low: 181.57

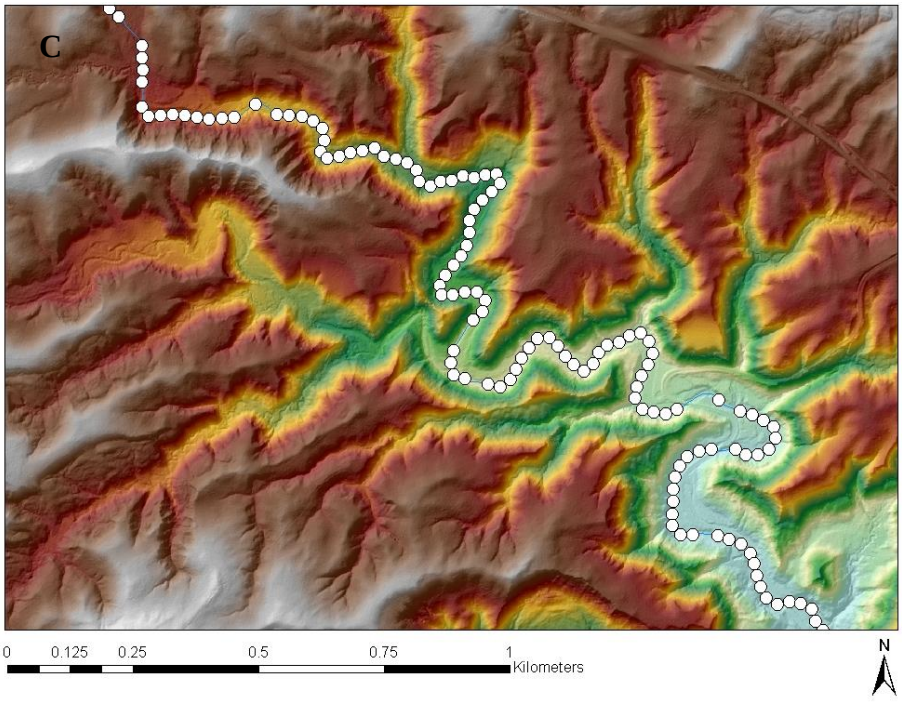


**Figure 21** Results of threshold models for **A.** Amity Creek, **B.** Miller Creek, and **C.** Mission Creek. White dots are erosional hotspots. Lower SP threshold, new bend curvature ratio threshold, 2 meters and higher bluff proximity, and combined bedrock exposure were included in calculation of these threshold models.

**Table 5** A comparison between GIS-based predictive model and refined threshold models, for each statistic is shown under the model details.

| **Amity Creek** | ← **GIS-based** → | ← **Refined** → | | |
|---|---|---|---|---|
| **Model Details** | **Predictive** | **Model 1** | **Model 2** | **Model 3** |
| Stream Power ($kg/ms^2$) | > 71,649 | > 20,000 | > 20,000 | - |
| Angle of Impingement (r) | > 0.5 | - | - | - |
| Bend Curvature | - | < 10 | - | < 10 |
| Bluffs | > 2m, within 7m | > 2m, within 7m | > 2m, within 7m | > 2m,within 7m |
| Bedrock Exposure | not within 5m | not within 5m | not within 5m | not within 5m |
| % accuracy for all points | 54.67 | 87.25 | 84.42 | 88.10 |
| % accuracy for FEI≥ 2 | 19.39 | 83.16 | 83.16 | 84.69 |
| % of points over-predicted | 0.57 | 3.40 | 6.23 | 3.40 |
| % of points under-predicted | 44.76 | 9.35 | 9.34 | 8.50 |
| TOT No. of points | 353 | 353 | 353 | 353 |
| TOT No. of points FEI ≥ 2 | 196 | 196 | 196 | 196 |
| **Miller Creek** | | | | |
| **Model Details** | **Predictive** | **Model 1** | **Model 2** | **Model 3** |
| Stream Power ($kg/ms^2$) | > 134,683 | > 18,000 | > 18,000 | - |
| Angle of Impingement (r) | > 0.5 | - | - | - |
| Bend Curvature | - | < 10.6 | - | < 10.6 |
| Bluffs | > 2m, within 7m | > 2m, within 7m | > 2m, within 7m | > 2m,within 7m |
| Bedrock Exposure | not within 5m | not within 5m | not within 5m | not within 5m |
| % accuracy for all points | 74.90 | 84.92 | 82.41 | 84.92 |
| % accuracy for FEI≥ 2 | 30.19 | 71.70 | 83.02 | 75.47 |
| % of points over-predicted | 1.51 | 7.54 | 13.06 | 8.54 |
| % of points under-predicted | 18.59 | 7.54 | 4.52 | 6.53 |
| TOT No. of points | 199 | 199 | 199 | 199 |
| TOT No. of points FEI ≥ 2 | 53 | 53 | 53 | 53 |
| **Mission Creek** | | | | |
| **Model Details** | **Predictive** | **Model 1** | **Model 2** | **Model 3** |
| Stream Power ($kg/ms^2$) | > 51,798 | > 10,000 | > 10,000 | - |
| Angle of Impingement (r) | > 0.5 | - | - | - |
| Bend Curvature | - | < 10 | - | < 10 |
| Bluffs | >2m,within 20m | >2m,within 20m | >2m,within 20m | >2m,within 20m |
| Bedrock Exposure | not within 5m | not within 5m | not within 5m | not within 5m |
| % accuracy for all points | 40.49 | 84.35 | 82.21 | 84.35 |
| % accuracy for FEI≥ 2 | 29.04 | 88.60 | 97.79 | 88.60 |
| % of points over-predicted | 0.31 | 6.13 | 15.95 | 6.13 |
| % of points under-predicted | 59.20 | 9.51 | 1.84 | 9.51 |
| TOT No. of Points | 326 | 326 | 326 | 326 |
| TOT No. of points FEI ≥ 2 | 272 | 272 | 272 | 272 |

***Results: Data Analysis***

The refined threshold model is an adjusted version of the GIS-based predictive model based on additional field data. The lower SP threshold and the new bend curvature ratio threshold of the refined threshold model maximize the percent accuracy for all points and FEI $\geq 2$, and minimize the percent of points over-predicted, and under-predicted. Reaches that have values greater than thresholds are identified as erosional hotspots with the goal that this refined threshold model more accurately indicates the locations of erosional hotspots.

Erosional hotspots from the refined threshold model were identified based on topography, channel planform, and geology. Streams in the northern and the southern areas of Duluth have major changes in channel slope, substrate materials, channel curvature and sinuosity when they flow directly into Lake Superior. The locations of **topographic erosional hotspots** are strongly affected by topography and channel planform geometry. However, erosion can also occur due to the influences of infrastructure and human modifications, such as road crossings, culverts, or bridges. In places, where topographic erosional hotspots lie in areas of significant anthropogenic influences, they are identified as **topographic/anthropogenic erosional hotspots** which dominate in streams in the central area of Duluth. Moreover, there are additional points that eroded with strong anthropogenic influences that are located in areas not identified as topographic erosional hotspots. These points are identified as **anthropogenic erosional hotspots** due to the direct influences of infrastructure potentially causing erosion.

Table 6 shows the percent of each type of erosional hotpots that is classified based on the influences causing erosion in Duluth-area streams. More than 88% of all erosional hotspots found along the survey sites in the Lester River, Amity Creek, Sargent Creek, and Mission Creek are topographic erosional hotspots, whereas more than 56% of all erosional hotspots found along the survey sites from Tischer Creek to Stewart Creek are topographic/anthropogenic erosional hotspots, except in Knowlton Creek. Some erosional hotspots found in the lower reaches of all streams are anthropogenic erosional hotspots and are shown as a percentage of all sites with anthropogenic influences. Listed are the

proportion of sites that experienced erosion within anthropogenic areas out of all the sites where anthropogenic modifications intersect streams.

When we compare the locations of erosional hotspots with geomorphic segment classification of Duluth-area streams (Table 1), we find that most erosional hotspots are in the middle and lower reaches, which are similar to the potential for geomorphic change in each segment as classified by Fitzpatrick et al. (2006). We also compared erosional hotspots with channel-reach types and valley types (Figure 15), and found that the topographic erosional hotspots are mostly located in pool-riffle reaches within confined and entrenched valleys. These channel-reach types and valley types in Duluth-area streams have high channel sinuosity and often have high relief in erodible substrates. Therefore, they are more susceptible to be eroded than other geomorphic reach types. Table 7 shows the percent of each channel-reach type and each valley type found in Duluth-area streams. The channel-reach types and valley types in this table are also classified as non-eroded (FEI=1) or as eroded (FEI≥2). Figures 22 and 23 show the locations of all erosional hotspots in map view and on longitudinal profiles of Amity Creek, Miller Creek, and Mission Creek, respectively.

**Table 6** Percent of types of topographic and topographic/anthropogenic erosional hotspots classified is based on influences to the causes of erosion. The bold values illustrate the main proportion of the influences to cause erosion in each stream.
*** Anthropogenic erosional hotspots are differently calculated shown as a percentage of sites that eroded out of all the sites with anthropogenic influences (see Appendix 2 for raw data)

| Types / Streams | Topographic Erosional Hotspots | Topographic/Anthropogenic Erosional Hotspots | *** Anthropogenic Erosional Hotspots |
|---|---|---|---|
| Lester | **96.0** | 4.0 | 20.0 |
| Amity | **88.0** | 12.0 | 29.2 |
| Tischer | 10.7 | **89.3** | 27.4 |
| Chester | 9.3 | **91.7** | 26.8 |
| Miller | 43.3 | **56.7** | 40.4 |
| Merritt | 32.3 | **67.7** | 37.5 |
| Keene | 10.0 | **90.0** | 42.3 |
| Kingsbury | 29.1 | **70.9** | 40.0 |
| Knowlton | **70.6** | 29.4 | 50.0 |
| Stewart | 41.7 | **58.3** | 42.8 |
| Sargent | **94.6** | 5.4 | - |
| Mission | **94.6** | 5.4 | 19.0 |

**Table 7** Percent of channel-reach types and valley types found along the survey sites of Duluth-area streams is classified as non-eroded (FEI =1) and eroded (FEI ≥ 2). The bold values illustrate the main proportion of each channel-reach type and valley type to be either non-eroded or eroded (See Appendix 2 for raw data).

| Area and % / Classification | Northern | | Central | | Southern | |
|---|---|---|---|---|---|---|
| | %FEI=1 | %FEI≥2 | %FEI=1 | %FEI≥2 | %FEI= 1 | %FEI≥2 |
| *Reach Types* | | | | | | |
| Artificial (AR) | 25.0 | **75.0** | **65.1** | 34.9 | - | - |
| Cascade (CA) | **94.1** | 5.9 | **66.7** | 33.3 | - | - |
| Colluvial (CO) | - | - | - | - | **62.5** | 37.5 |
| Plane-Bed (PB) | 42.3 | 57.7 | **72.4** | 27.6 | **65.6** | 34.4 |
| Pool-Riffle (PR) | 29.8 | **70.2** | 24.6 | **75.4** | 21.0 | **79.0** |
| Step-Pool (SP) | 43.7 | **56.3** | 30.5 | **69.5** | 34.7 | **65.3** |
| *Valley Types* | | | | | | |
| Alluvial (A) | - | - | 51.1 | 48.9 | 44.1 | **55.9** |
| Confined (C) | 26.4 | **73.6** | 27.5 | **72.5** | 36.9 | **63.1** |
| Entrenched (E) | 35.2 | **64.8** | 46.7 | **53.3** | 19.0 | **81.0** |

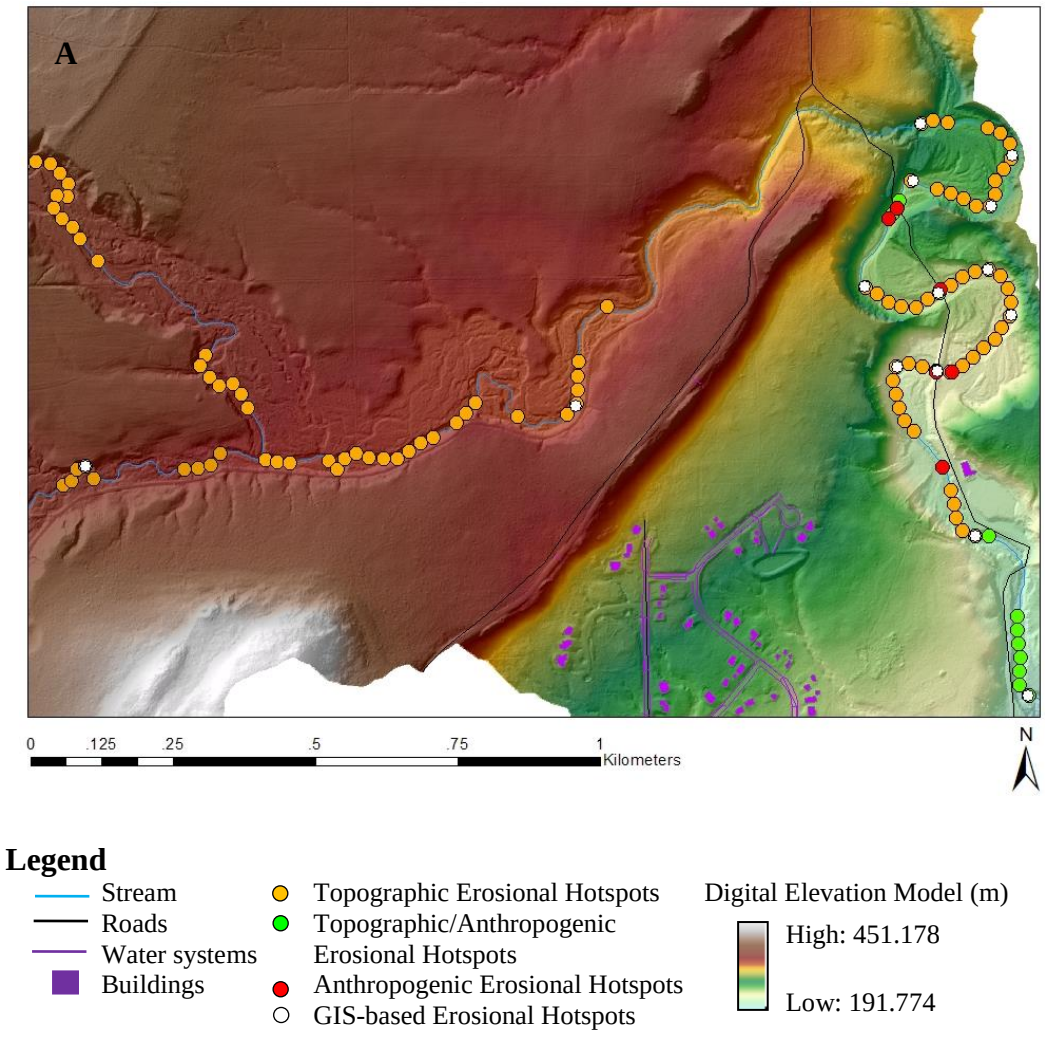


**Figure 22A** Different types of erosional hotspots in Amity Creek from the refined threshold model. The figure also shows a comparison of locations of erosional hotspots between the GIS-based predictive model and the refined threshold model.

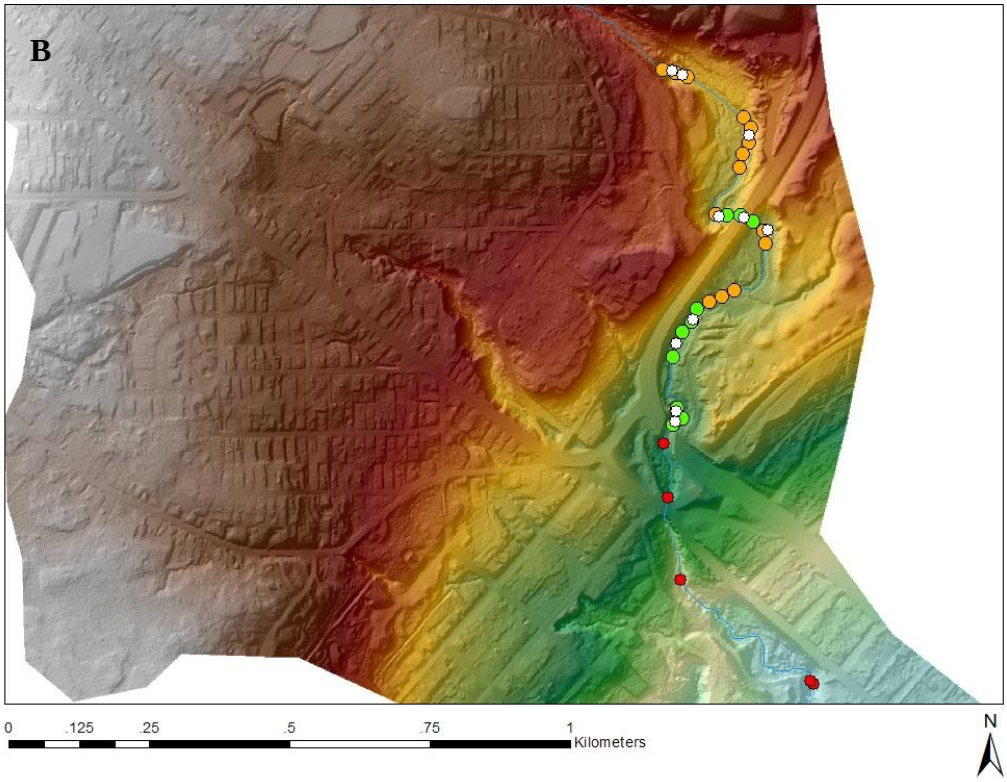


**Figure 22B** Different types of erosional hotspots in Miller Creek from the refined threshold model. The figure also shows a comparison of locations of erosional hotspots between the GIS-based predictive model and the refined threshold model.

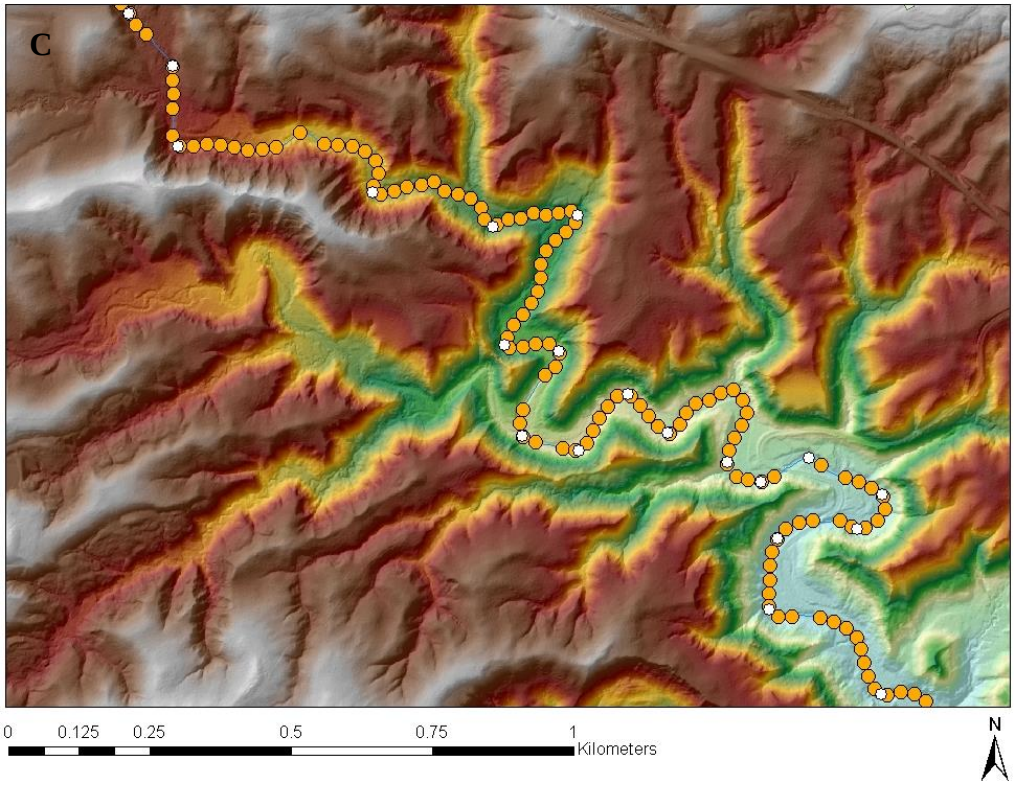


**Figure 22C** Different types of erosional hotspots in Mission Creek from the refined threshold model. The figure also shows a comparison of locations of erosional hotspots between the GIS-based predictive model and the refined threshold model.

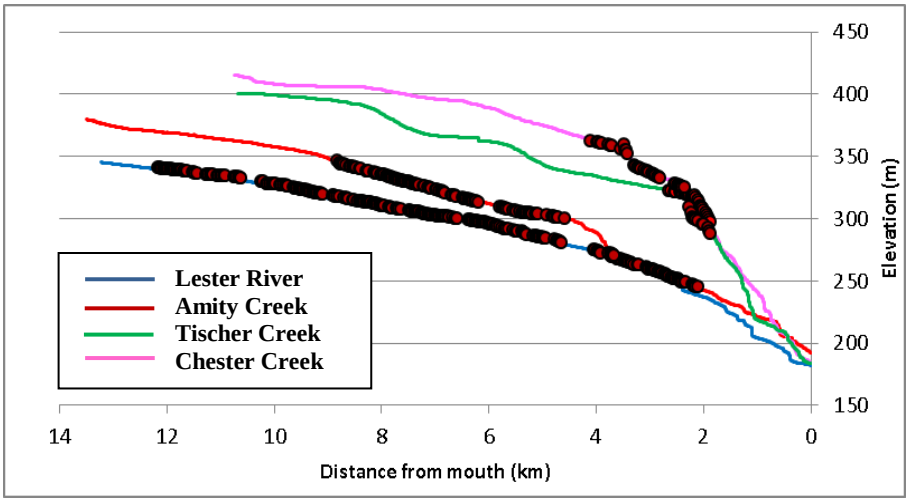


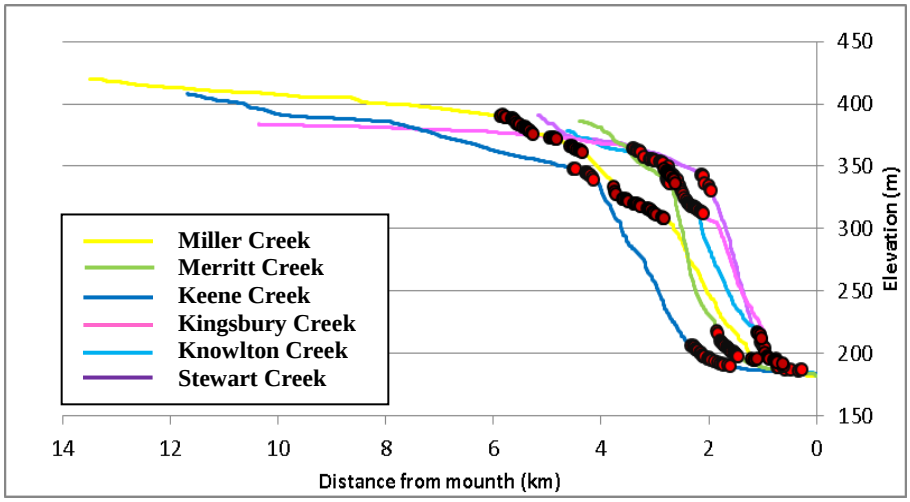


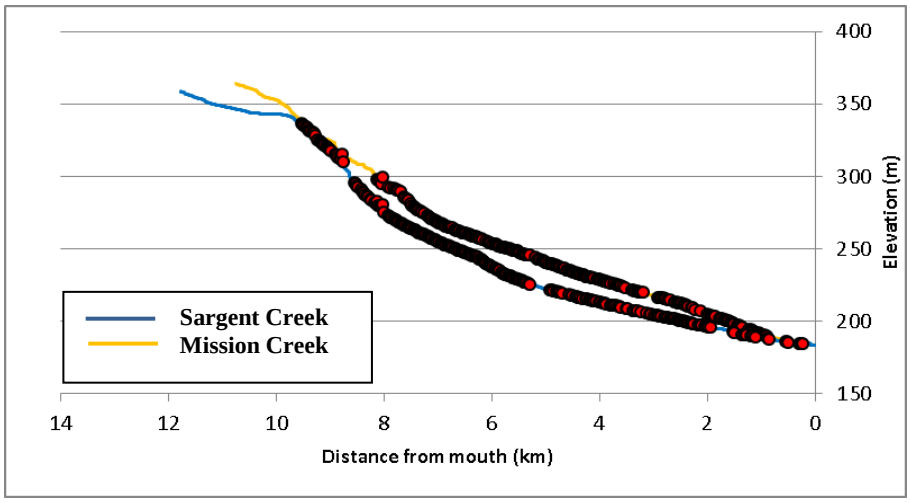


- Topographic and topographic/anthropogenic erosional hotspots

**Figure 23** Erosional hotspots from three different parts of Duluth-area streams are shown on longitudinal profiles: **A.** the northern area, **B.** the central area, and **C.** the southern area (See Appendix 3 for all erosional hotpots in map view)

## *Discussion*

### *Role of Geomorphic Context in Erosion*

Duluth is located on a steep hillside that descends in elevation from inland elevations to Lake Superior. The landscape resulted from the profound effects of the retreat of the Superior lobe 11,500 years before present. The land has been rising up from the isostatic adjustment, and the lake levels have fluctuated throughout Holocene epoch. In other words, the land rose at the same time that lake levels fell, initiating an incision wave. Since the last few thousand years, the lake level has been rising relative to the land elevation, at least in the Duluth-area. The consequence for the isostatic rebound induced the stream networks to flow perpendicularly toward the shoreline of Lake Superior and the St. Louis River estuary. At the same time, rivers started to vertically incise through glacial deposits and bedrock in order to reach the lake level of Lake Superior, exposing the bedrock to the ground surface, and carrying sediments into the lake and the estuary (Saarnisto, 1974).

The distinct geomorphic characteristics in Duluth-area streams play an essential role in controlling the erosional processes, leading to different levels of erosion in different areas of the watershed. In the northern area of Duluth, erosion occurs in the middle and lower reaches of streams in places that lack bedrock exposure. Erosional sites are generally found along steep channel slopes underlain by glacial deposits within entrenched valleys. Erosion in the central area is also found in the middle and lower reaches with influences of anthropogenic modifications. There are few places that experienced high levels of channel erosion in the central area due to the resistant bedrock exposure throughout the watershed. The southern area experiences significant erosion because of fine-grained sedimentary rocks and glacial tills within entrenched valleys. Steep channel slopes with high sinuosity cause high levels of erosion in this particular area due to the increased secondary flow. A large amount of sediments eroded from erodible bluffs in the central and the southern areas of Duluth deposit at the estuary because a low stream power there can no longer move sediments further. As a result, the river outlets at the estuary are generally flat within alluvial valleys (Figures 2B, and 2C).

In Duluth-area streams, pool-riffle reaches within confined and entrenched valleys are most susceptible to erosion, according to the table 7 more than 70 % of all pool-riffle reaches eroded in all streams. These sensitive reaches are typically found in the middle and lower reaches throughout the Duluth watersheds. Because the large-scale flood in 2012 had high stream energy and increased secondary flow to significant erosion at outer banks, erodible substrates at outer banks collapsed and distributed significant volumes of sediment to the streams. The sediments then deposit at inner banks, in Lake Superior, or in the lower reaches within alluvial valleys due to the low gentle channel slopes and wide channels.

*Values of Predictor Variables*

The GIS-based predictive model relied on four predictor variables: stream-power based erosion index, angle of impingement, bluff proximity, and bedrock exposure locations. However, we added the bend curvature ratio in the threshold model for determining the channel planforms and comparing the tightness of meander bends with the angle of impingement.

The stream power-based erosion index is defined as the rate of potential energy expenditure per unit length of channel. The SP values are directly based on upstream areas and channel slopes. Therefore, we predicted that SP values would rise as channel slope increases downstream indicating an increase in the ability of the channel to erode as long as the bed and the banks maintain the same erodibility. High SP values can cause high levels of erosion and move more sediment downstream. Eventually, reaches with high SP values may erode to bedrock, exposing it on the bed and banks, and slowing erosion rates down substantially. According to Figures 18A and 19A, these plots show that locations at FEI=0 (bedrock reaches) usually have high SP values in Amity Creek and Miller Creek. Figure 24 is an example of the relationship between SP values and erosion (shown as FEI score) in Amity Creek where higher SP values cause higher levels of erosion, but the level of erosion dramatically drops in bedrock reaches.

When water reaches a meander bend, the centrifugal force moves water on the surface toward the outside of the bend, raising the water level there. The hydraulic head

is slightly higher near the outer bank than near the inner bank, so, the pressure gradient drives water back towards the inner banks near the bed, causing a secondary flow. This secondary flow moves sediments along the bed of the stream toward the inside of curve, forming a point bar.

Due to secondary flow processes, the channel planform geometry is an important factor that may drive erosion in a particular area. The angle of impingement was one of methods used previously to calculate channel planform geometry. High angle of impingement values occur at tight bends indicating higher erosion potential than a bend that has low angle of impingement values. However, the measurement of angle of impingement is dependent on the length of ruler used. The largest change in an angle should be measured every quarter of a wavelength. If the ruler is smaller than a quarter of a wavelength, the larger meanders are still recorded, but if the ruler is greater than a quarter of a wavelength, the angle of impingement in smaller meanders is underestimated. Because most streams in Duluth have the variable meander wavelength, one ruler is not suitable to measure all meanders for the entire stream (Figure 25).

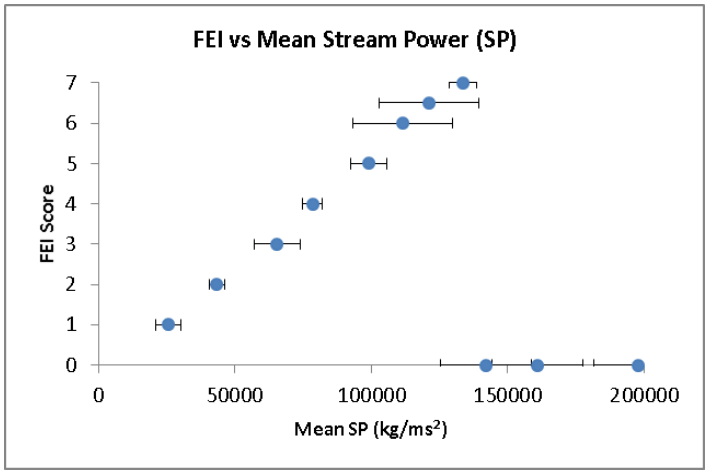


**Figure 24** A relationship between stream power in kg/ms$^2$ and erosion (shown as FEI score) in Amity Creek. Higher SP values cause higher levels of erosion, but the level of erosion dramatically drops in bedrock reaches (FEI=0).

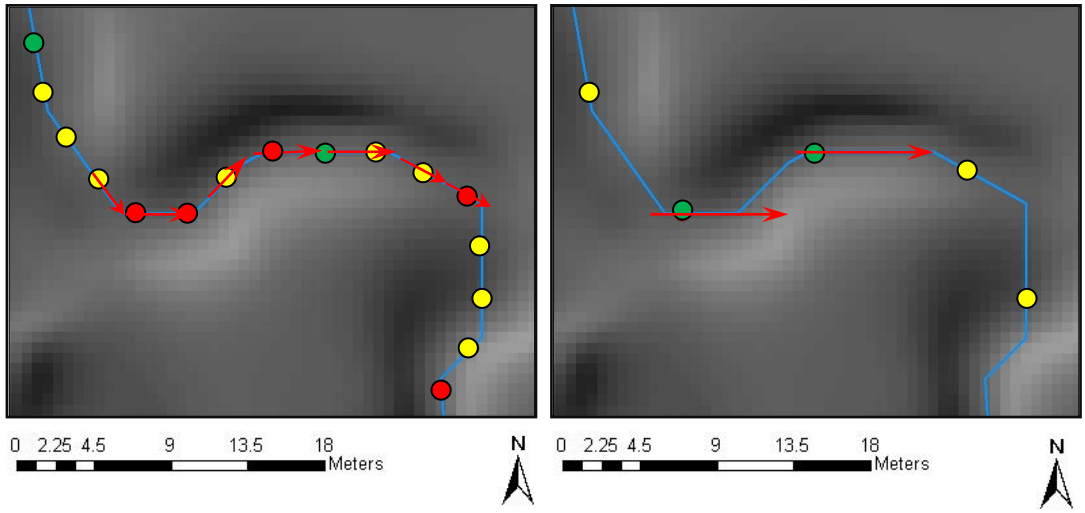


**Legend**

Angle of Impingement Values
Low (0-0.1)
Medium (0.1-0.5
High (>0.5)
Ruler Used
Sargent Creek

Digital Elevation Model (m)
High: 436.631
Low: 183.414

**Figure 25** A different ruler length, or space between points, used to calculate an angle of impingement. It should be less than or equal to a quarter of a wavelength of a meander bend in order to avoid missing a tight bend. However, one ruler length does not fit to the entire stream and the calculation becomes difficult to automate: **A.** the ruler (5 meters spacing) is short enough to measure the meander, **B.** the ruler (15 meters spacing) is too large to measure tight bends resulting in a low angle of impingement.

The bend curvature measurement provided to be more useful as a measure of channel planform geometry than angle of impingement. Manually-drawn circles along the streams can measure the tightness of each meander bend in a reach with variable meander wavelength. Figure 26 is an example of manually-drawn circles measuring meander bends with variable meander wavelength in Sargent Creek.

Erodible streambanks and bluffs can be the sources of sediment when hydraulic action scours at their bases, leading to oversteepening and destabilization. Erosion on the lower banks can lead to slumping on the upper banks. Therefore, during a large-scale flood, erosion rates can be high through the processes of both hydraulic action and mass failure. The particles eroded coupled with high stream energy continue eroding streambanks and bluffs further downstream.

While the large-scale flood can erode bedrock, the timescale for large failure events in bedrock reaches is much greater than in erodible substrates. Due to the strong relationship between flood erosion and substrate, bedrock exposure maps are crucial to predict erosional hotspots accurately over a large area. Bedrock exposure maps downloaded from the Minnesota Geological Survey lack the detail needed to assess bedrock locations at the spatial scale we are working at. So, we augmented the MGS bedrock exposure map by field observations (Figures 14A and 14B). The field observation-based bedrock exposure maps improve upon the MGS bedrock exposure maps to get more accurate bedrock exposure locations. Figures 27A and 27B show that the improvement in mapping FEI=0 locations (bedrock reaches) increases from 87% to 95% in Amity Creek, and from 50% to 90% in Miller Creek.

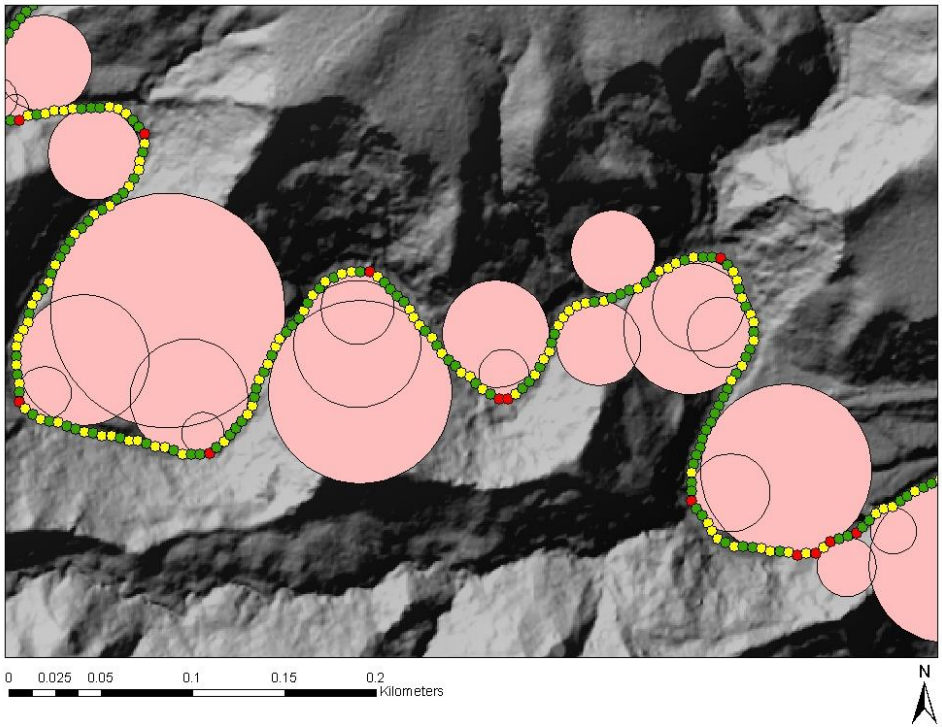


**Figure 26** A comparison between the angle of impingement and the bend curvature in Mission Creek. The assumed ruler can be greater and smaller than a quarter of wavelength. The results from the bend curvature, which are indicated how curve it is, would be more realistic.

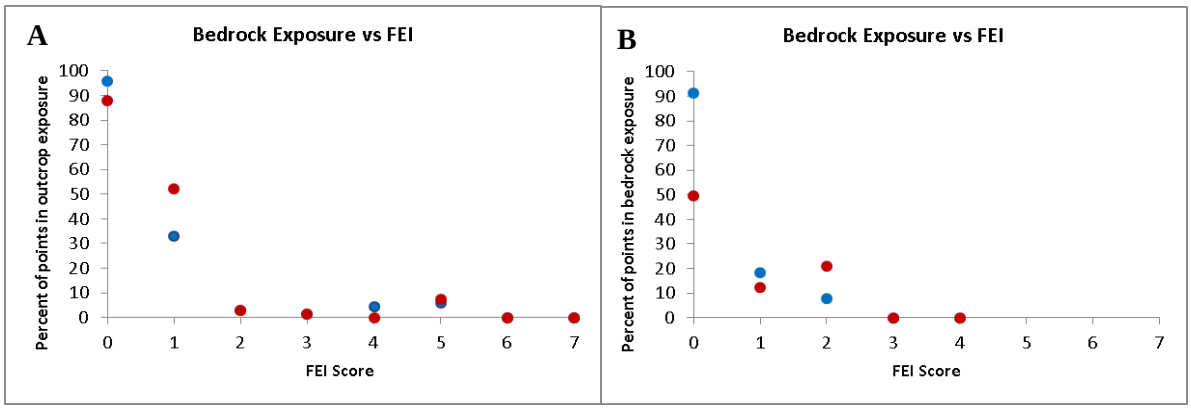


**Figure 27** A comparison of the percent of points of bedrock exposure locations between the MGS bedrock exposure data (red dots) and the combined bedrock based data (blue dots) with each FEI score: **A.** Amity Creek, **B.** Miller Creek. The percent of bedrock reaches (FEI=0) slightly increases in Amity Creek, but considerably rises in Miller Creek.

*Comparison between Prior Work and the Current Work*

Wick (2013) did a previous project in the topic of identifying erosional hotspots in streams along the North Shore of Lake Superior, MN, using high-resolution elevation and soils data. The goal of the previous project was to develop a GIS-based model to predict erosional hotspots at a reach scale in three rivers of the North Shore of Lake Superior. We applied her methodology to predict erosional hotspots in Duluth-area streams. However, the results between two consecutive projects are not exactly the same.

The previous project had no correlation between the angle of impingement and FEI score in part due to the variable meander wavelengths along the channel, and thus had limitation for using channel planform in the resulting model. The current project uses manually-drawn circles to determine the bend curvature of each meander bend in a reach with variable meander wavelength. The new bend curvature methodology can solve the problem of variable meander wavelength. According to Figures 18C, 19C, and 20C, these plots show very significant correlations between bend curvature ratio and FEI score in three example streams. Due to this improvement, bend curvature ratio was added as a predictor to identify erosional hotspots in the refined threshold model.

Field Erosion Index is an assessment of the geomorphic response to change from the 2012 flood. Although the FEI scores are fixed in the specific category (Figure 6), the

scores given in two separate field surveys might not be exactly the same because 1) different observers can visualize different levels of erosion, even if they focus on the same location; 2) a 2-year gap in time between observers means that some erosional sites have recovered by vegetation regrowth on damaged bluffs or have been restored by workers after the flood stopped; and 3) different resolution lidar data provide different spatial details of the relief of streambanks and bluffs. Thus, our assessment may be different from the previous assessment that was conducted with field surveys shortly after the flood stopped. Figure 28 shows the comparison of FEI score assessment between the previous project (Wick, 2013) and the current project. The difference shown was calculated through subtraction of FEI scores between the current project and the previous project. There is a huge positive difference of FEI score assessment at meander bends near Seven Bridges Road due to the continuous slumps and scours, whereas a huge negative difference of FEI score assessment at the channel near Skyline Parkway resulted from vegetation regrowth during a 2-year gap.

The refined threshold model is based on the results of erosion occurring in the streams. The threshold values in this model indicate a given reach which is more prone to erode, based on FEI scores from field observation-based data. The refined threshold model improved the GIS-based predictive model by increasing points which can be erosional hotpots. According to Wick's (2013) project, she set threshold for 3 predictors in Amity Creek: the maximum SP threshold value was at 15,000 $kg/ms^2$; points within 7 meters near 2 meters and higher bluffs; and have no manual bedrock exposure within 5 meters of each point. For our project, we set different thresholds for 4 predictors in Amity Creek: the maximum SP threshold value was at 20,000 $kg/ms^2$; the minimum bend curvature ratio was 10; points within 7 meters near 2 meters and higher bluffs; and have no combined bedrock exposure within 5 meters of each point. Table 8 shows the refined threshold model 1 from two different projects, including all predictors used.

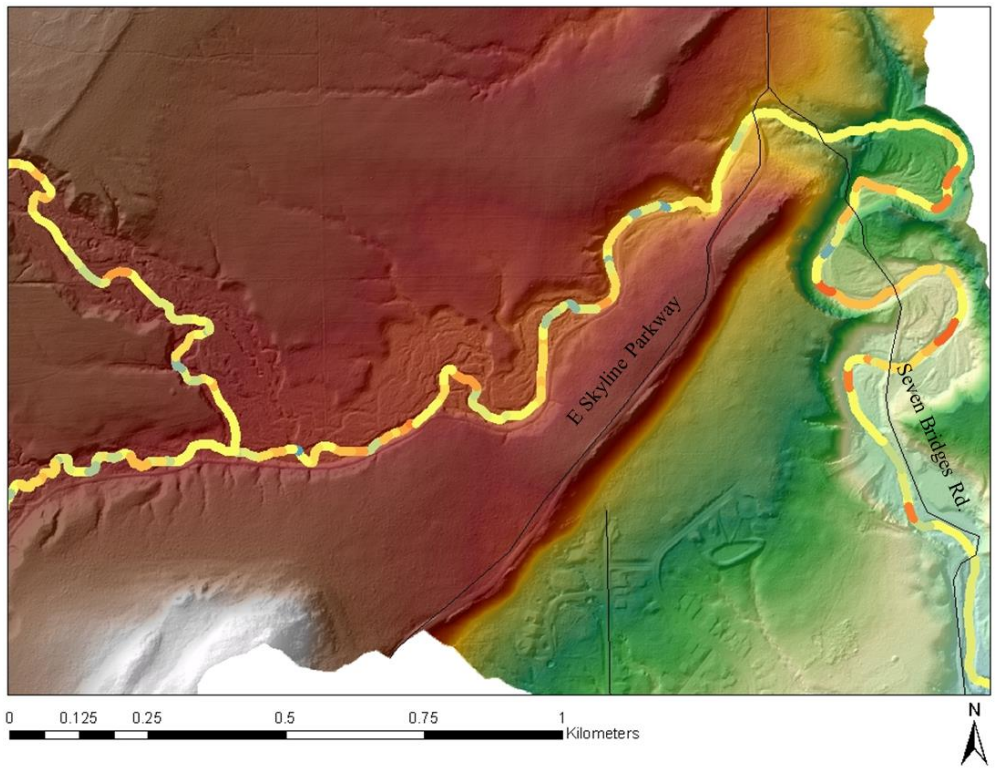


**Legend**

FEI Difference

-7 -6 -5 -4 -3 -2 -1 0 1 2 3 4 5 6 7

Digital Elevation Model (m)

High: 451.178

Low: 191.774

**Figure 28** Difference of FEI score assessment between previous project and current project in Amity Creek. The new scores are resulted from subtraction between $FEI_{current}$ and $FEI_{previous}$. These scores tell how much difference we assess the geomorphic response from two different time periods.

**Table 8** A comparison of the refined threshold model 1 between Wick's (2013) project and our current project. The total numbers of point are different due to points spaced 2 meters apart in the previous threshold model and spaced 25 meters apart in the current threshold model.

| **Amity Creek** | | |
|---|---|---|
| **Model Details** | **Previous threshold model 1** | **Current threshold model 1** |
| Stream Power ($kg/ms^2$) | > 15,000 | > 20,000 |
| Bend Curvature | - | < 10 |
| Bluffs | > 2m, within 7m | > 2m, within 7m |
| Bedrock Exposure | not within 5m of manual | not within 5m of combined |
| % accuracy for all points | 70.70 | 87.25 |
| % accuracy for FEI≥ 2 | 73.40 | 83.16 |
| % of points over-predicted | 12.80 | 3.40 |
| % of points under-predicted | 16.50 | 9.35 |
| TOT No. of points | 6051 | 353 |
| TOT No. of points FEI ≥ 2 | 3742 | 196 |

According to Table 8, Wick's (2013) threshold model has the percent accuracy for all points and for FEI ≥ 2 lower than our threshold model, whereas the percent of points over-predicted and under-predicted in her threshold model are greater than our threshold model. One potential reason for this is the difference in extracting data at points spaced 2 meters apart in her threshold model, and spaced 25 meters apart in our threshold model. The numbers of surveyed points are significantly different and could cause the FEI surveyed data of 2 meters of spacing to change more frequently than that of 25 meters of spacing. Her threshold model has 73.40% of the points that FEI ≥ 2 extracted every 2 meters in Amity Creek, while 83.16% of points extracted every 25 meters had FEI ≥ 2 in the same stream in our threshold model. The different spacing of points also causes a considerable difference in the percent of points over-predicted and under-predicted. Another potential reason is that the difference in bedrock exposure maps, which are based on each investigator's field data, which could lead to misidentify some erosional hotspots located near bedrock exposure from different maps. Therefore, the different bedrock exposure maps directly affect the accuracy of the threshold model to predict erosional hotspots.

*Valley Types and Channel-Reach Types*

Valley types and channel-reach types in Duluth-area streams vary in terms of potential response and susceptibility to the disturbance (flood). According to Figure 2, channels in the upper reach are in flat wetlands, and then steepen toward Lake Superior with different valley types and channel-reach types. Step-pool and pool-riffle reaches within entrenched valleys are found in the middle reaches of all creeks. Cascade and resistant bedrocks within confined valleys are found in the lower reaches of the Lester River to Stewart Creek. However, a few places in the lower reaches close to the St. Louis River estuary are plane-bed reaches or have artificial modifications within alluvial valleys.

According to Fitzpatrick et al. (2006), there is evidence of landslide, bank erosion, and bluff failure found in the middle and lower reaches. Therefore, erosional hotspots would be more dense in these particular areas. Figures 15A, 15B, and 15C are examples of valley types and channel-reach types, which are assessed during field checking. Table 9 is a combination between Tables 6 and 7 that shows the percent of each channel-reach type found in three different areas of Duluth-area streams, classified as non-eroded (FEI=1) and as eroded (FEI $\geq$ 2). Table 9 also shows the percent of types of erosional hotspots classification that is directly from eroded reaches (FEI $\geq$ 2) and is classified based on the influences on erosion.

According to Table 9, pool-riffle and step-pool reaches are the primary channel-reach types that experience erosion (FEI $\geq$ 2) throughout the Duluth watersheds. Plane-bed and artificial reaches are minor channel-reach types that experience erosion. These pool-riffle reaches have significant potential to change and can thus respond to the increasing sediment supply and discharge because they have mobile grain sizes. The step-pool reaches are also more resilient to erosion from increasing discharge and high sediment-supply because of more immobile grain sizes (boulders and cobbles).

According to Table 7, more than 60%, and 50% of confined valleys and entrenched valleys, respectively, experienced erosion in the 2012 flood. These two valley types are susceptible to erosion because the high discharge of the flood has the increased

stream energy and secondary flow that can act on the toe of an erodible bluff, oversteepening, and eventually leading to bank and bluff erosion. They eventually distribute a large amount of sediments to the streams.

**Table 9** Percent of channel-reach types and erosional hotspots types found in different areas of Duluth-area streams, showing in FEI =1, and FEI≥ 2 categories. Percent of types of erosional hotspots, which is from FEI≥ 2, is based on influences on erosion, but anthropogenic erosional hotspots are shown as a percentage of all anthropogenic sites that eroded (see Appendix 2). The bold values illustrate a main proportion of each channel-reach type and erosional hotspot types in different areas of Duluth.

**Northern Area** (Lester River, Amity Creek, Tischer Creek, and Chester Creek)

| % of Classification / Reach Types | %FEI =1 | %FEI≥ 2 | | % Topographic Erosional Hotspots | % Topo/Anthro Erosional Hotspots | % Anthropogenic Erosional Hotspots |
|---|---|---|---|---|---|---|
| Artificial (AR) | 25.0 | **75.0** | | - | **64.3** | 35.7 |
| Cascade (CA) | **94.1** | 5.9 | | 14.3 | 71.4 | 14.3 |
| Colluvial (CO) | - | - | | - | - | - |
| Plane-bed (PB) | 42.3 | **57.7** | | **100.0** | - | - |
| Pool-riffle (PR) | 29.8 | **70.2** | | **78.0** | 12.0 | 10.0 |
| Step-pool (SP) | 43.7 | **56.3** | | 38.7 | **49.3** | 12.0 |

**Central Area** (Miller Creek, Merritt Creek, Keene Creek, Kingsbury Creek, Knowlton Creek, and Stewart Creek)

| % of Classification / Reach Types | %FEI =1 | %FEI≥ 2 | | % Topographic Erosional Hotspots | % Topo/Anthro Erosional Hotspots | % Anthropogenic Erosional Hotspots |
|---|---|---|---|---|---|---|
| Artificial (AR) | **65.1** | 34.9 | | - | 65.1 | 34.9 |
| Cascade (CA) | **66.7** | 33.3 | | 33.3 | 66.7 | - |
| Colluvial (CO) | - | - | | - | - | - |
| Plane-bed (PB) | **72.4** | 27.6 | | 23.5 | 64.7 | 11.8 |
| Pool-riffle (PR) | 24.6 | **75.4** | | 36.7 | **55.4** | 7.9 |
| Step-pool (SP) | 30.5 | **69.5** | | 41.8 | **50.7** | 7.5 |

**Southern Area** (Sargent Creek, and Mission Creek)

| % of Classification / Reach Types | %FEI =1 | %FEI≥ 2 | | % Topographic Erosional Hotspots | % Topo/Anthro Erosional Hotspots | % Anthropogenic Erosional Hotspots |
|---|---|---|---|---|---|---|
| Artificial (AR) | - | - | | - | - | - |
| Cascade (CA) | - | - | | - | - | - |
| Colluvial (CO) | **62.5** | 37.5 | | 60.0 | 40.0 | - |
| Plane-bed (PB) | **65.6** | 34.4 | | 52.9 | 41.2 | 5.9 |
| Pool-riffle (PR) | 21.0 | **79.0** | | **99.5** | - | 0.5 |
| Step-pool (SP) | 34.7 | **65.3** | | **81.7** | 18.3 | - |

*Types of Erosional Hotspots and Anthropogenic Roles in Erosion*

In this project, we classified erosional hotspots from the refined threshold model into 2 types: 1) **topographic erosional hotspots** are erosional hotspots located in areas which tend to have significant changes in topography, substrate materials, and channel planform geometry; and 2) **topographic/anthropogenic erosional hotspots** are topographic erosional hotspots which lie in areas of significant anthropogenic influences. Furthermore, **anthropogenic erosional hotspots** are additional sites which experience some levels of erosion due to significant anthropogenic modifications. These sites are not identified from the refined threshold model, but are only found in the field surveys (Tables 6 and 9).

According to Table 6, and 9, topographic erosional hotspots are primary types found in the northern and southern areas, whereas topographic/anthropogenic erosional hotspots are main types found in the central areas of Duluth. Anthropogenic erosional hotspots are minor types found in lower reaches of all streams, except in Sargent Creek.

Human modifications are important issues causing significant erosion in the lower reach of Tischer Creek to Stewart Creek because these areas are the city center and communities that have a high density of infrastructure and constructions. Those modifications can either increase or decrease the levels of erosion from the 2012 flood.

1) Infrastructure can increase rates of erosion due to channel narrowing at culverts and bridges. When the streams have high discharge during the flood, they flow through narrow channels with a decrease in cross-sectional areas. The mean flow velocity and the erosive potential of the flow considerably increase and can cause erosion at the bed and banks above and below the infrastructure.

2) Some channels have low channel capacity that cannot hold large volumes of flowing water from floods. Because cities have constructed drainpipe networks under roads in order to drain water out of houses and constructions, small channels get high levels of erosion due to an inability to hold the large volumes of the flowing water.

3) A straight channel due to irrigation system and city management can increase channel gradient by shortening a path. Flow velocity and sediment transport capacity will

increase. Therefore, straight reaches can lead to increased erosion, increasing sediment supply further by vertical incision, and triggering the susceptibility of banks to erosion.

4) Riparian vegetation clearance can cause bank erosion due to destabilization of streambanks and bluffs. Riparian vegetation on the bank can strengthen bank stability and roughness. However, since vegetation is removed, or riparian vegetation type and density are changed by humans, the rate of erosion on streambanks will increase and they are possibly no longer able to hold down the substrate materials.

5) Urbanization can lead to increased erosion at the impervious surfaces, which do not allow water to penetrate through the ground, i.e. pavements, roads, parking lots, and compacted soils. During a storm event, runoff with high velocity of water on impervious surfaces reaches channels faster, and may contribute to exceeding the capacity of the channel to hold the large volume of flowing water, leading to high erosion on erodible streambanks and bluffs. The discharge with high velocity, which passes through infrastructure, can impact those constructions, i.e. roadside erosion, bridge collapse, and retaining wall failure. This consequence does not only have effects at a local scale, but it also alters watershed characteristics by increasing lateral erosion, widening a channel or a valley, and increasing the amount of sediment loads downstream.

*Temporal Scales of an Annual Flood and a Large-Scale Flood*

The erosion potential of a reach is dependent in part on the timescale of interest. Because the precipitation that occurred during June 19$^{th}$ to 20$^{th}$, 2012 was an estimated 500-year rainfall event (Graning & Hluchan, 2012; Czuba et al, 2012), it caused a large-scale flood that induced widespread erosion and contributed significant volumes of sediment to streams. The discharge from this large-scale flood was much higher in magnitude than an annual bankfull event.

The FEI assessment in this project is assumed to assess the effects of the 500-year rainfall event. Fundamentally, the typical predictor variables causing erosion should be the same between floods of varying magnitude, i.e. stream power, and streambank and bluff erodibility, but with different magnitudes of erosion between an annual flood and a large-scale flood. Particularly, the stream power of the 2012 flood was much greater than

that of an annual flood due to the significant increase in discharge. This might lead to increase the magnitude, eroding more streambanks and bluffs, cutting off the meanders, and enlarging the channel width through lateral erosion. The high magnitude flood can also cause infrastructure failures where infrastructure interrupts the flow path, such as at road crossings and bridges.

The lower stream power and lower magnitude of an annual flood can also cause erosion because discharge can equal or exceed the effective discharge. At bankfull discharge, many streams have energy to erode streambanks and bluffs at outer banks, forming point bars at inner banks, and moving sediments downstream. In addition, an annual flood can have some small effects to infrastructures, such as culverts and drainage ditches clogged from woody debris.

Furthermore, a large-scale flood has high stream energy to remove riparian vegetation and add large woody debris to streams. These effects may induce high erosion potential and also let more sediment into streams through bank failure, mass wasting, and collapse. However, because large wood debris jams are from different sites rather than from erosional hotspots, they make predicting erosional hotspots in a given event very complicated.

*Lidar Alignment and Improvement*

Minnesota Geospatial Information Office has lidar data available to download to see the topography in great detail. Lidar data in the Arrowhead region collected during spring 2011 and fall 2012 are thus an effective tool to identify erosional hotspots from the 2012 flood. However, it proved to be more complicated to use them to do quantitative analyses of change detection. Since airborne flights flew in different flight directions each time period, the different alignment leads to decreased accuracy due to offsets within a single campaign and between the two campaigns. The poor alignment can cause shifting in either horizontal or vertical direction or both, leading to unrealistic spatial patterns of change, and an inaccurate net volumetric budget change.

There are time-consuming processes being developed to improve alignment by matching individual flightlines and matching based on slope (Streutker et al., 2011), but

given the high stated horizontal error in the Arrowhead data, it is not clear if the vertical error will be improved substantially enough to do quantitative volumetric changes. Because of these issues, we did not use repeat lidar data to quantify how much net volumetric sediment was eroded or deposited, but instead reply upon field observations to assess erosional magnitude from the 2012 flood. The procedures we have done to identify and attempt to fix alignment issues with repeat lidar data are described in Appendix 1.

### *Conclusions*

Many streams in Duluth-area experienced the high magnitude of the 2012 flood. Those streams have reach-scale sites that are highly susceptible to erosion called erosional hotspots. The erosional sites in this project were identified from 1-meter resolution lidar data which are available in Duluth. These lidar-derived DEMs were highly valuable in calculating the predictor variables, leading to identification of erosional hotspots and susceptible reaches.

Duluth-area streams are located in a distinct geomorphic setting where streams in the upper reaches are in flat to low-gradient wetlands, then steepen towards Lake Superior. Based on the geomorphology, the SP values are prone to increase toward the outlets, and are able to drive increasing amounts of erosion in susceptible reaches downstream. The angle of impingement or the bend curvature ratio can specify sites with susceptible reaches at tight bends. Areas with high SP that are also proximal to high bluffs can significantly contribute sediment to the streams. Available bedrock exposure data were combined with the previous predictor variables to predict erosional hotspots in erodible substrates through a GIS-based predictive model. Field-erosion maps were used to verify the locations of erosional hotspots that were predicted from the GIS-based predictive model. The field erosion map was also used to develop the refined model that more accurately located erosional hotspots than the GIS-based predictive model.

The accuracy of the refined threshold model increased to be greater than 80% when thresholds were lowered to more closely match data from field observations. The success of this type of model is related to 1) the decrease of threshold values in the refined threshold model in order to best fit field-mapped erosional zones; 2) the new

channel curvature measurement from the bend curvature ratio which is more accurate than the angle of impingement as measured previously; and 3) the improved bedrock exposure maps verified by the field observation-based data.

Pool-riffle reaches in confined and entrenched valleys were the most sensitive channel-reach type to changes in the 2012 flood because small and mobile grain sizes can easily respond to high discharge events. In confined and entrenched valleys, there is more access to potential sediment sources as erodible substrates on banks and bluffs that are eroded, and then collapse into the streams. Most erosional hotspots within the susceptible reach type located in the middle and lower reaches are classified as topographic erosional hotspots. In the central areas of Duluth-area streams, most erosional hotspots are classified as topographic/anthropogenic erosional hotspots due to the infrastructure surrounding streams in this area.

The limitation of erosional hotspots identification in this project is from the difference in erosion between a large-scale flood event and an annual flood event. The predictive model may overestimate the locations that would experience erosion in a typical bankfull event. However, these are the areas that would be expected to have the most erosion and the most dynamic channels over time.

The threshold model from this study more accurately identifies erosional hotspots and the susceptible reaches, and flood-damaged area assessment during the 2012 flood due to the improvement of the GIS-based predictive model based on the field data. Thus, the results from the threshold model could be beneficial for the City of Duluth, MN as people can monitor these susceptible sites and efficiently restore them for the benefits of their communities and ecological systems.

For future investigation, the errors in horizontal and vertical alignment from lidar generated before- and after-2012 flood should be addressed to assess how much channel change occurred on banks and bluffs in these catastrophic events. Another future effort might adapt this GIS-based predictive model to measure the erosion from less frequent flood conditions by adjusting the threshold values of parameters fitted to lower magnitude of floods. In addition, since infrastructure can influence the geomorphic

characteristics in a particular area, the model should incorporate those anthropogenic effects to further investigate and measure the changes near those constructions.

***References***


Agarwal, P. K., Arge, L., and Danner, A. (2006). From point cloud to grid DEM: A scalable approach. In A. Riedl, W. Kainz, and G. A. Elmes (Eds.), *Progress in spatial data handling:12th international symposium on spatial data handling* (771-788). New York, NY: Springer.

American Society of Civil Engineers (ASCE) Task Committee on Hydraulics, Bank Mechanics, and Modeling of River Width Adjustment. (1998). River width adjustment. I: Processes and mechanisms. *Journal of Hydraulic Engineering, 124*(9), 881-902.

Attig, J. W., Clayton, L., and Mickelson, D. M. (1985). Correlation of late Wisconsin glacial phases in the Western Great Lakes area. *Geological Society of America Bulletin, 96*(12), 1585-1593.

Bandara, K. R. M. U., Samarakoon, L., Shrestha, R. P., and Kamiya, Y. (2011). Automated generation of digital terrain model using point clouds of digital surface model in forest area. *Journal of Remote Sensing, 3*(5), 845-358.

Begin, Z. B. (1981). Stream curvature and bank erosion: A model based on the momentum equation. *The Journal of Geology, 89*(4), 497-504.

Boerboom, T. J. (2009). C-19 geologic atlas of Carlton County, Minnesota [part A]. Retrieved from http://purl.umn.edu/58760

Bull, W. B. (1979). Threshold of critical power in streams. *Geological Society of America Bulletin, 90*(5), 453-464.

Cannon, W. F. (1994). Closing of the midcontinent rift-a far-field effect of grenvillian compression. *Geology, 22*(2), 155-158.

Czuba, C. R., Fallon, J. D., and Kessler, E. W. (2012). *Floods of June 2012 in Northeastern Minnesota*. Reston, VA: U.S. Geological Survey.

Ferguson, R. I. (2005). Estimating critical stream power for bedload transport calculations in gravel-bed rivers. *Geomorphology, 80*(5), 33-41.

Fitzpatrick, F. A., Peppler, M. C., DePhilip, M. M., and Lee, K. E. (2006). *Geomorphic characteristics and classification of Duluth-area streams, Minnesota.* Reston, VA: United States Geological Survey.

Forsman, B. (2014). Flood response: Lake Superior's dark surprise. *Minnesota Sea Grant.* Retrieved from http://www.seagrant.umn.edu/newsletter/2014/02/flood_response_lake_superiors_dark_surprise.html

Furbish, D. J. (1988). River-bend curvature and migration: How are they related?. *Geology*, *16*(8), 752-755.

Graning, A., and Hluchan, R. (2012). Summary of Duluth flash flood event, June 19th-20th, 2012. Retrieved from http://www.crh.noaa.gov/images/dlh/StormSummaries/2012/June19_flood/DuluthSummary.pdf

Grant, G. E., Swanson, F. J., and Wolman, M. G. (1990). Pattern and origin of stepped-bed morphology in high-gradient streams, Western Cascades, Oregon. *Geological Society of America Bulletin*, *102*(3), 340-352.

Green, J. C. (1983). Geologic and geochemical evidence for the nature and development of the middle proterozoic (keweenawan) midcontinent rift of North America. *Tectonophysics*, *94*, 413-437.

Hobbs, H. C. (2004). Late Wisconsinan superior-lobe deposits in the Lake Superior Basin Northeast of Duluth. In M. J. Severson, and J. Heinz (Eds.), *Proceedings of the Institute on Lake Superior Geology, 50th Annual Meeting, Field Trip Guidebook, Volume* 50 (86–98). Thunder Bay, ON: The 50th Institute on Lake Superior Geology.

Hobbs, H. C. (2009a). M-186 surficial geology of the Duluth Heights Quadrangle, St. Louis County, Minnesota. Retrieved from http://purl.umn.edu/58229

Hobbs, H. C. (2009b). M-187 surficial geology of the Duluth Quadrangle, St. Louis County, Minnesota. Retrieved from http://purl.umn.edu/58230

Hobbs, H. C. (2009c). M-188 surficial geology of the West Duluth Quadrangle, St. Louis County, Minnesota. Retrieved from http://purl.umn.edu/58231

Hodgson, M. E., and Bresnahan, P. (2004). Accuracy of airborne lidar-derived elevation: Empirical assessment and error budget. *Photogrammetric Engineering & Remote Sensing*, *70*(3), 331-339.

Hooke, J. M. (1979). An analysis of the processes of river bank erosion. *Journal of Hydrology*, *42*, 39-62.

Knighton, A. D. (1973). Riverbank erosion in relation to stream flow conditions, River Bollin-Dean, Cheshire. *East Midland Geographer, 6*, 416-426.

Knighton, A. D. (1974). Variation in width-discharge relation and some implications for hydraulic geometry. *Geological Society of America Bulletin, 85*(7), 1069-1076.

Knighton, D. (1998). *Fluvial forms and processes*: a new perspective. New York, NY: John Wiley & Sons Inc.

Lauer, J. W. (2006). Channel planform statistic: An ArcMAP project. Retrieved from http://www.nced.umn.edu/content/tools-and-data

Leopold, L. B., and Maddock, Jr., T. (1953). *The hydraulic geometry of stream channels and some physiographic implications*. Washington, DC: U.S. Government Printing Office.

Leopold, L. B., Wolman, M. G., and Miller, J. P. (1964). *Fluvial processes in geomorphology*. San Francisco, CA: W. H. Freeman and Company.

Lusardi. B.A. (1997). Minnesota at a glance: Quaternary glacial geology. Minnesota Geological Survey, University of Minnesota. Retrieved from http://www.d.umn.edu/prc/fieldcamp/Forms/Mn_Quaternary.pdf

Miller, J. D., Green, J. C., Severson, M. J., Chandler, V. W., and Peterson, D. M. (2001). M-119 geologic map of the Duluth Complex and related rocks, Northeastern Minnesota, scale 1:200,000. Retrieved from http://conservancy.umn.edu/handle/11299/183

Montgomery, D. R., and Buffington, J. M. (1997). Channel-reach morphology in mountain drainage basins. *Geological Society of America Bulletin, 109*(5), 596-611.

Montgomery, D. R., and Buffington, J. M. (1998). Channel processes, classification, and response. *River Ecology and Management*, *112*, 1250-1263.

Nagel, D. E., Buffington, J. M., Parkes, S. L., Wenger, S., and Goode, J. R. (2014). *A landscape scale valley confinement algorithm: Delineating unconfined valley bottoms for geomorphic, aquatic, and riparian applications*. Fort Collins, CO: U.S. Department of Agriculture, Forest Service, Rocky Mountain Research Station.

Nanson, G. C., and Hickin, E. J. (1986). A statistical analysis of bank erosion and channel migration in Western Canada. *Geological Society of America Bulletin, 97*, 497-504.

National Oceanic and Atmospheric Administration. (2013). What is LIDAR?. Retrieved from http://oceanservice.noaa.gov/facts/lidar.html

Neitzel, G. (2013). Monitoring event-scale stream bluff erosion with repeat terrestrial laser scanning; Amity Creek, Duluth, MN (Master's Thesis). University of Minnesota, Duluth.

Nieber, J. L., Wilson, B. N., Ulrich, J. S., Hansen, B. J., and Canelon, D. J. (2008). *Assessment of streambank and bluff erosion in the Knife River watershed*. St. Paul, MN: University of Minnesota

Ojakangas, R. W. (2009). *Roadside geology of Minnesota*. Missoula, MT: Mountain Press Publishing Company.

Ojakangas, R. W., and Matsch, C. L. (1982). *Minnesota's geology*. Minneapolis, MN: University of Minnesota Press.

Passalacqua, P., Trung, T. D., Foufoula-Georgiou, E., Sapiro, G., and Dietrich, W. E. (2010). A geometric framework for channel network extraction from lidar: Nonlinear diffusion and geodesic paths. *Journal of Geophysical Research*, *115*, F01002, doi:10.1029/2009JF001254

Passalacqua, P., Tarolli, P., and Foufoula-Georgiou, E. (2010). Testing space-scale methodologies for automatic geomorphic feature extraction from lidar in a complex mountainous landscape. *Water Resources Research*, *46*, W11535, doi:10.1029/2009WR008812

Rinaldi, M., and Casagli, N. (1998). Stability of streambanks formed in partially saturated soils and effects of negative pore water pressure: The Sieve River (Italy). *Journal of Geomorphology*, *26*, 253-277.

Saarnisto, M. (1974). The deglaciation history of Lake Superior region and its climatic implication. *Quaternary Research*, 4(3), 316-339.

Schwartz, J. (2012). Cost of Minnesota flood estimated at $100 million. *New York Times*. Retrieved from http://www.nytimes.com/2012/06/23/us/millions-in-damage-from-duluth-flooding.html

Streutker, D. R., Glenn, N. F., and Shrestha, R. (2011). A slope-based method for matching elevation surfaces. *Photogrammetric Engineering & Remote Sensing*, *77*(7), 743-750.

Van Schmus, W. R. (1992). Tectonic setting of the midcontinent rift system. *Tectonophysics*, *213*, 1-15.

Wick, M. J. (2013). Identifying erosional hotspots in streams along the North Shore of Lake Superior, Minnesota using high-resolution elevation and soils data (Master's Thesis). University of Minnesota, Duluth.

## *Appendices*

### *1. Lidar Alignment and Improvement*

Lidar is a remote sensing technology that uses light in the form of a pulse laser to examine the surface of the earth. It has been widely used in recent years for a growing number of multidisciplinary applications. However, spatial accuracy is limited by positional error and point labeling error as described in ***Background****: Light Detection and Ranging (lidar).* For instance, our study area in the Arrowhead region has lidar images generated from different flightline pathways; an airplane flew in north-south to generate pre-flood lidar images, and another flew either northwest-southeast or northeast-southwest to generate post-flood lidar images (Figure 29). So, this can cause vertical and horizontal shifts, exposing offsets everywhere in lidar images.

We did several tests to assess the offsets and attempt to improve the alignments between 2 campaigns:

1) we used a least-squares matching technique that was a conventional approach to shift each pixel in both the horizontal and vertical directions (Streutker et al., 2011). To do this, we made a small rectangle at a stable point (building, road, and outcrop) in both pre-flood and post-flood lidar images. We then clipped them out, manually shifting x and y coordinates of the post-flood lidar images, subtracting adjusted post- and pre-flood lidar images, and making a cross-section to see how elevation differences changed after the adjustment. We reiterated those steps until those two images had the least offsets of elevation difference. We then applied the adjustment to other areas on the same flightline (Figure 30). However, this method was a time-consuming process that we had to spend lots of time randomly shifting the post-flood lidar images in order to fit to the pre-flood lidar image and the flightline alignment issues.

2) we used GeoNet to smooth the lidar images. After doing this, the high-frequency errors were smoothed, while the landscape features were preserved (Figure 4). However, the offsets due to the horizontal and vertical shifts still persisted.

3) we used a slope-based method for matching elevation surfaces (Streuker et al., 2011) to improve the lidar misalignment in our areas. We started to select an area in two overlapping flightlines, plotting the two elevation profiles from each flightline, plotting the elevation difference between those two profiles, and plotting local slope along the length of the profiles. Figure 31B shows the vertical offset between the pre- and post-lidar images of approximately 15 centimeters on the road, and greater than that on a valley side. The horizontal offset between them was 1-2 meters. Figures 31C and 31D show no correlation between the elevation difference and the local slope.

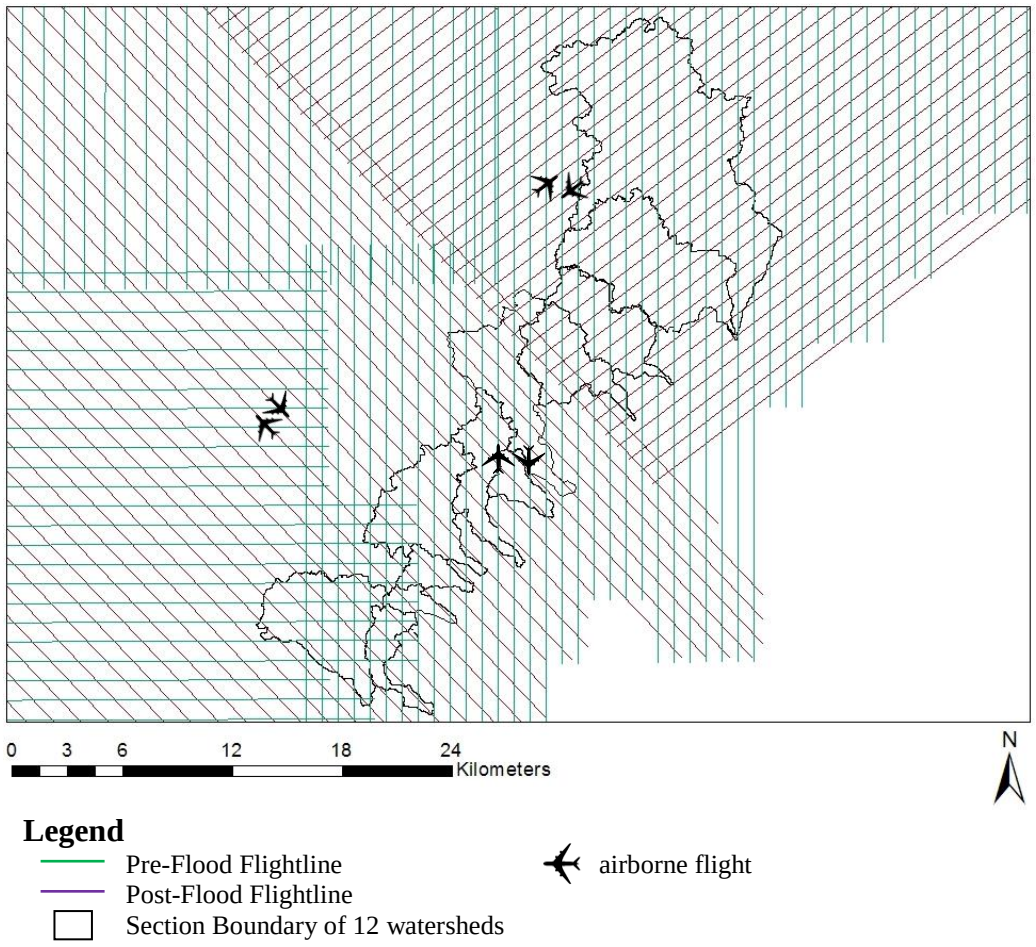


**Figure 29** Different flightlines in the Arrowhead region and in Duluth-area streams; an airplane flew in north-south to generate pre-flood lidar images (green lines), and another flew either northwest-southeast or northeast-southwest to generate post-flood lidar images (purple lines).

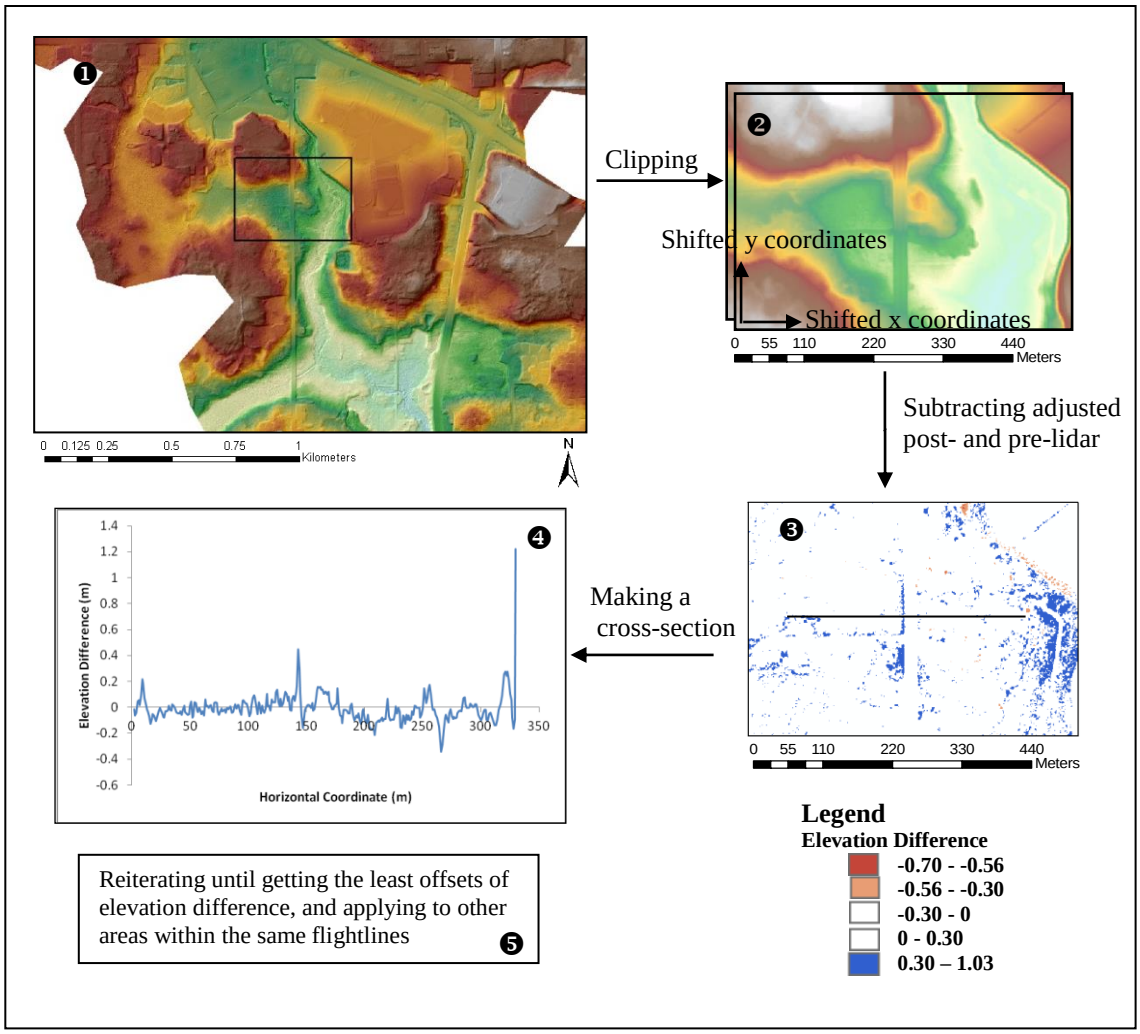


**Figure 30** Steps of a least-squares matching method to adjust lidar alignment.

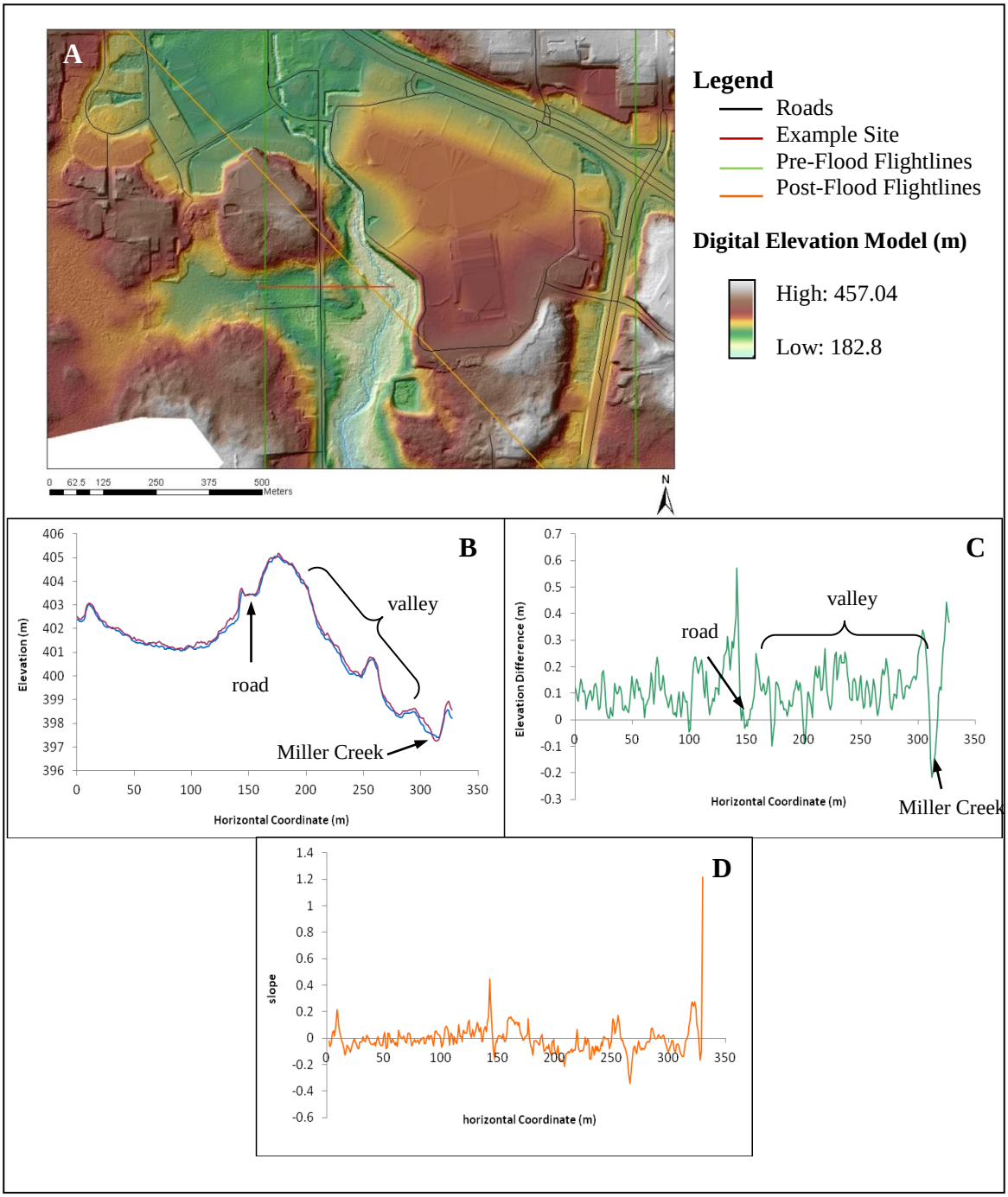


**Figure 31** Procedures of a slope-based method for matching elevation surface in a particular area: **A.** a map showing the location of the profile (red line) and two overlapping flightlines, **B.** a cross-section profile showing elevation of two overlapping flightlines in the selected area, blue and red lines are the elevations from pre- and post-flood lidar images, respectively, **C.** a graph showing elevation difference of the areas within two flightlines, and **D.** a graph showing the local slope along the length of the profiles.

As the slope increases, the vertical shift will grow larger. We used a one-dimensional diagram (Figure 32) and the equation (5) to find the values of offsets:

$$\Delta z = z_{offset} - (x_{offset} \cdot m_x) \qquad (5)$$

where $z_{offset}$ is the vertical offset, $x_{offset}$ is the horizontal offset, $m_x$ is the local slopes, and $\Delta z$ is the elevation difference (Streutker et al., 2011).

However, the elevation difference and the local slope, which are shown in Figures 31C and 31D, have no correlation and are difficult to identify the values. We thus repeatedly used the least-squares methods as described in 1) by manually adjusting lidar alignment.

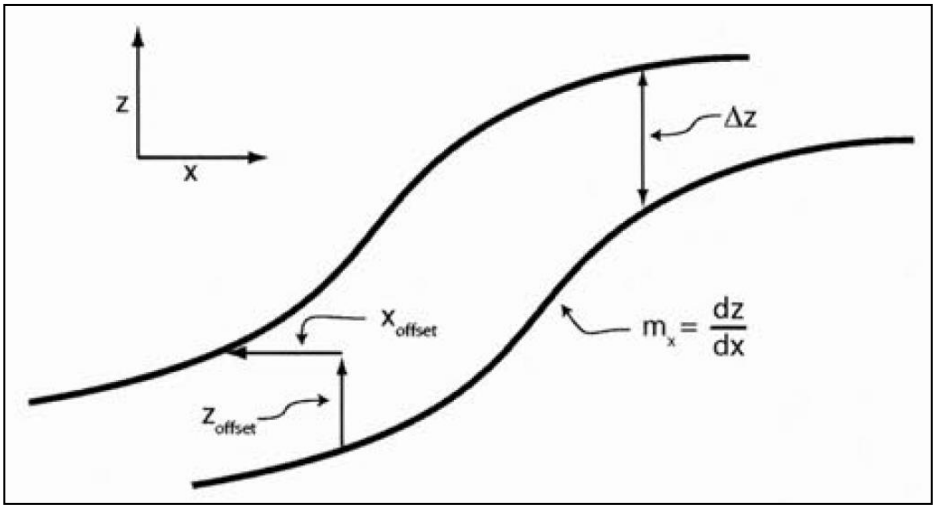


**Figure 32** A diagram illustrates the relationship between horizontal offset ($x_{offset}$) and vertical offset ($z_{offset}$), and the apparent elevation difference ($\Delta z$) between the two liens (the picture modified from Streutker et al., 2011)

4) A LAS tile file is a specific format that stores lidar point cloud data records from a lidar survey. Point cloud data were used to generate new raster files in this project. We used the LAS toolbox which was available to download from the rapidlasso GmbH (http:// http://rapidlasso.com/). This toolbox contained useful tools for lidar processing. Initially, we had an intention to shift the alignment of the LAS data in horizontal and vertical directions with some distances, and then generate new raster files. However, there were no functional tools in LAS toolbox and in ArcMap available to shift alignment of LAS data. So, we started to change the LAS files to point cloud data which contained GPS date-stamps. These date-stamps allowed us to know the time data for each point cloud. Those points generated from post-flood LAS files were horizontally shifted to change x coordinates, and vertically shifted to change z coordinates. After doing this, we converted those points into TIN and DEM, respectively. However, we were not satisfied the results from this shifting processes because new DEMs still yielded the larger offsets in both directions.

After we have done all procedures, the offsets of lidar alignment still existed in both horizontal and vertical directions. Therefore, we did not use lidar images to compare what geomorphic characteristics and how much erosion and deposition occurred along the streams from the 2012 flood due to those offsets that we could not fix.

| Watershed / Reach Types | FEI | Lester River | Amity Creek | Tischer Creek | Chester Creek | Miller Creek | Merritt Creek | Keene Creek | Kingsbury Creek | Knowlton Creek | Stewart Creek | Sargent Creek | Mission Creek |
|---|---|---|---|---|---|---|---|---|---|---|---|---|---|
| Artificial (AR) | =1 | 3 | - | - | - | 12 | 2 | 20 | 16 | 6 | - | - | - |
| | ≥2 | 9 | - | - | - | 4 | 2 | 11 | 12 | 1 | - | - | - |
| Cascade (CA) | =1 | 1 | 15 | - | - | - | 2 | - | - | - | - | - | - |
| | ≥2 | 1 | 0 | - | - | - | 1 | - | - | - | - | - | - |
| Colluvial (CO) | =1 | - | - | - | - | - | - | - | - | - | - | - | 5 |
| | ≥2 | - | - | - | - | - | - | - | - | - | - | - | 3 |
| Plane-Bed (PB) | =1 | 24 | - | - | 17 | 1 | 16 | - | 3 | - | 22 | 44 | 17 |
| | ≥2 | 45 | - | - | 11 | 5 | 1 | - | 6 | - | 4 | 21 | 11 |
| Pool-Riffle (PR) | =1 | 54 | 110 | 18 | 4 | 23 | 0 | 6 | 8 | 11 | 4 | 57 | 51 |
| | ≥2 | 152 | 246 | 14 | 26 | 40 | 22 | 20 | 38 | 26 | 13 | 193 | 212 |
| Step-Pool (SP) | =1 | 18 | 4 | 22 | 8 | 6 | 1 | 11 | 0 | 3 | 4 | 24 | 9 |
| | ≥2 | 21 | 14 | 15 | 17 | 19 | 4 | 17 | 2 | 8 | 7 | 48 | 14 |

| Watershed / Valley Types | FEI | Lester River | Amity Creek | Tischer Creek | Chester Creek | Miller Creek | Merritt Creek | Keene Creek | Kingsbury Creek | Knowlton Creek | Stewart Creek | Sargent Creek | Mission Creek |
|---|---|---|---|---|---|---|---|---|---|---|---|---|---|
| Alluvial (A) | =1 | - | - | - | - | 13 | 18 | 20 | 16 | 13 | 12 | 58 | 28 |
| | ≥2 | - | - | - | - | 9 | 19 | 28 | 10 | 10 | 12 | 61 | 48 |
| Confined (C) | =1 | 9 | 2 | 17 | 13 | 25 | 2 | 9 | 11 | 7 | 3 | 24 | 14 |
| | ≥2 | 18 | 24 | 28 | 44 | 39 | 13 | 22 | 40 | 24 | 12 | 48 | 17 |
| Entrenched (E) | =1 | 94 | 128 | - | 18 | 19 | - | - | 2 | - | - | 37 | 40 |
| | ≥2 | 207 | 225 | - | 10 | 19 | - | - | 5 | - | - | 153 | 175 |

### *2. Raw Data of the Surveys in Each Stream*

**Table 10** Number of surveyed points in Duluth-area streams classified as non-erosion (FEI=1) and as erosion (FEI≥ 2) in different categories: **A.** channel-

| Watershed / Reach Types | Lester River | | | Amity Creek | | | Tischer Creek | | | Chester Creek | | | Miller Creek | | | Merritt Creek | | |
|---|---|---|---|---|---|---|---|---|---|---|---|---|---|---|---|---|---|---|
| | T | T/A | A | T | T/A | A | T | T/A | A | T | T/A | A | T | T/A | A | T | T/A | A |
| Artificial (AR) | - | 9 | - | - | - | - | - | - | - | - | - | 5 | - | 4 | 7 | - | 2 | 1 |
| Cascade (CA) | 1 | - | - | - | - | - | - | - | - | 1 | 10 | - | - | - | - | 1 | 2 | - |
| Colluvial (CO) | - | - | - | - | - | - | - | - | - | - | - | - | - | - | - | - | - | - |
| Plane-Bed (PB) | 45 | - | - | - | - | - | - | - | - | - | - | - | - | 5 | - | - | - | 1 |
| Pool-Riffle (PR) | 149 | - | 6 | 215 | 20 | 10 | - | 13 | 20 | 4 | 24 | 11 | 20 | 18 | 2 | 9 | 13 | 2 |
| Step-Pool (SP) | 22 | - | - | 4 | 10 | - | 3 | 12 | 3 | - | 15 | 6 | 9 | 11 | 1 | - | 4 | 1 |

| Watershed / Reach Types | Keen Creek | | | Kingsbury Creek | | | Knowlton Creek | | | Stewart Creek | | | Sargent Creek | | | Mission Creek | | |
|---|---|---|---|---|---|---|---|---|---|---|---|---|---|---|---|---|---|---|
| | T | T/A | A | T | T/A | A | T | T/A | A | T | T/A | A | T | T/A | A | T | T/A | A |
| Artificial (AR) | - | 11 | 3 | - | 10 | 3 | - | 1 | 1 | - | - | - | - | - | - | - | - | - |
| Cascade (CA) | - | - | - | - | - | - | - | - | - | - | - | - | - | - | - | - | - | - |
| Colluvial (CO) | - | - | - | - | - | - | - | - | - | - | - | - | - | - | - | 3 | 2 | - |
| Plane-Bed (PB) | - | - | - | 4 | 2 | 1 | - | - | - | - | 4 | - | 18 | 3 | - | - | 11 | 2 |
| Pool-Riffle (PR) | - | 19 | 4 | 12 | 25 | 2 | 17 | 7 | 1 | 3 | 10 | 2 | 193 | - | - | 212 | - | 2 |
| Step-Pool (SP) | 5 | 15 | 2 | - | 2 | - | 7 | 2 | 1 | 7 | - | - | 37 | 11 | - | 12 | - | - |

**Table 11** Number of erosional hotspots (FEI≥ 2) in Duluth-area streams classified as
1) topographic erosional hotspots (T)
2) topographic/anthropogenic erosional hotspots (T/A)
3) anthropogenic erosional hotspots (A)

### *3. Erosional Hotspots in the Large-Scale Maps*

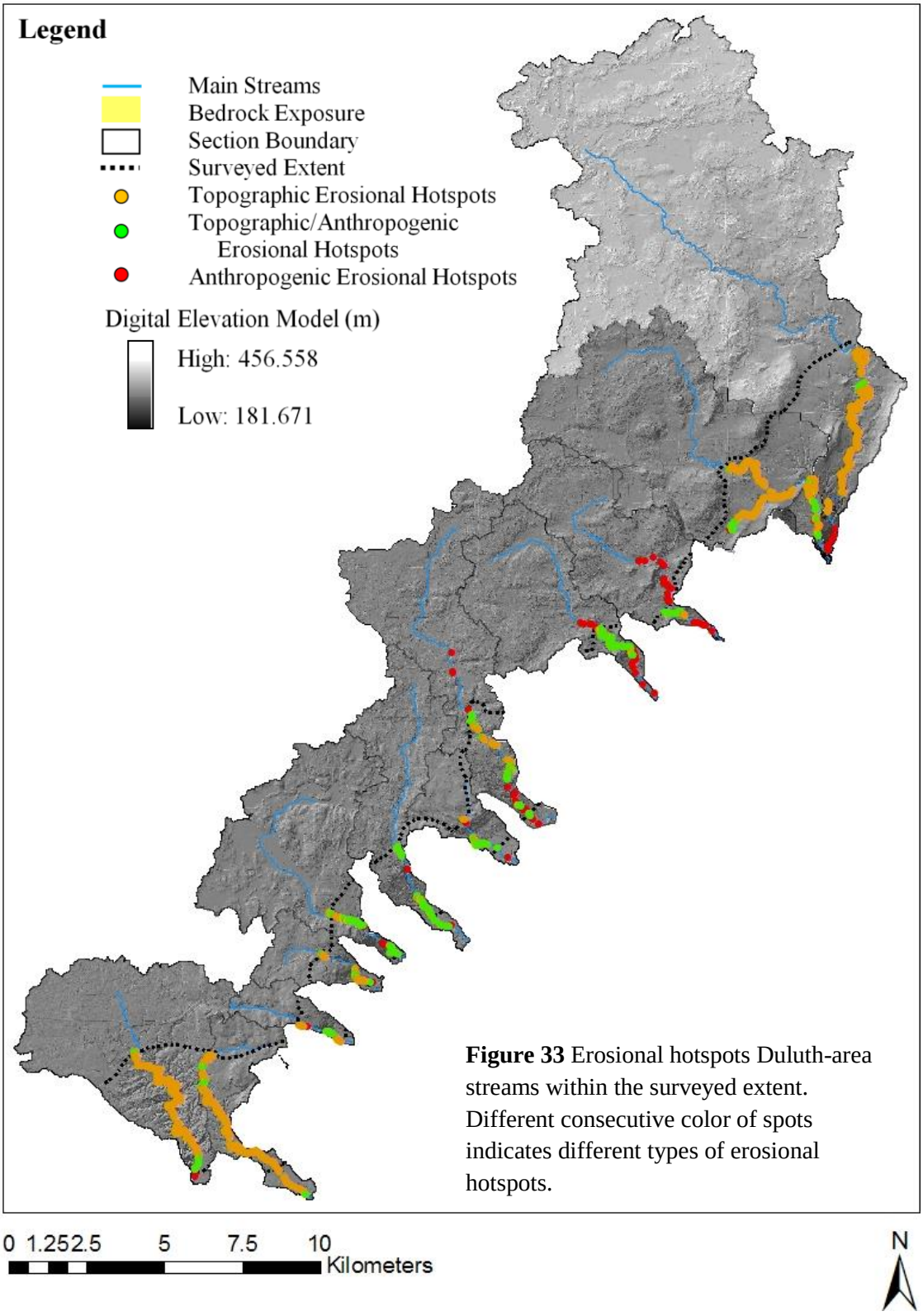


**Figure 33** Erosional hotspots Duluth-area streams within the surveyed extent. Different consecutive color of spots indicates different types of erosional hotspots.

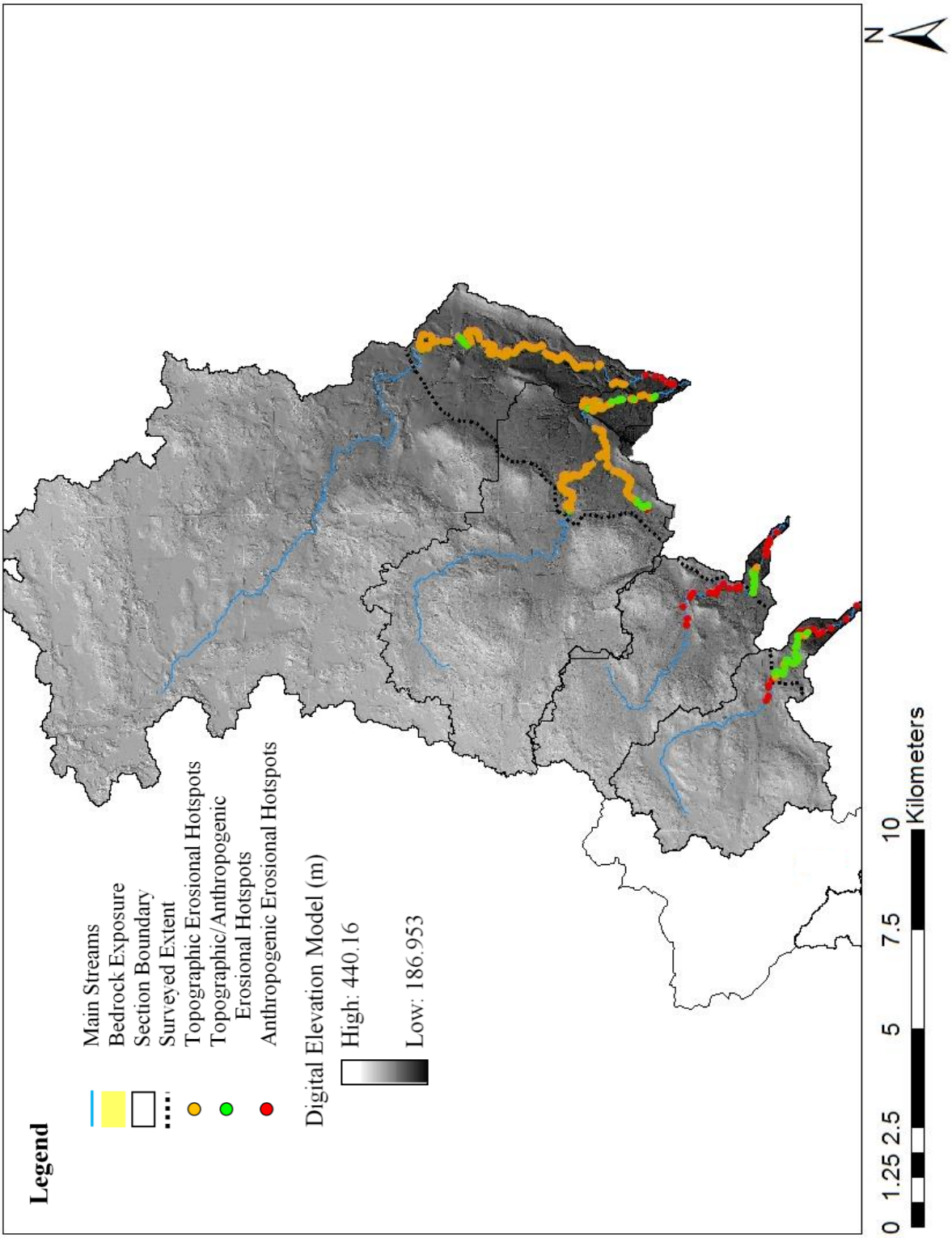


**Figure 34** Erosional hotspots in the northern area of Duluth-area streams within surveyed extent. Different consecutive color of spots indicates different types of erosional hotspots.

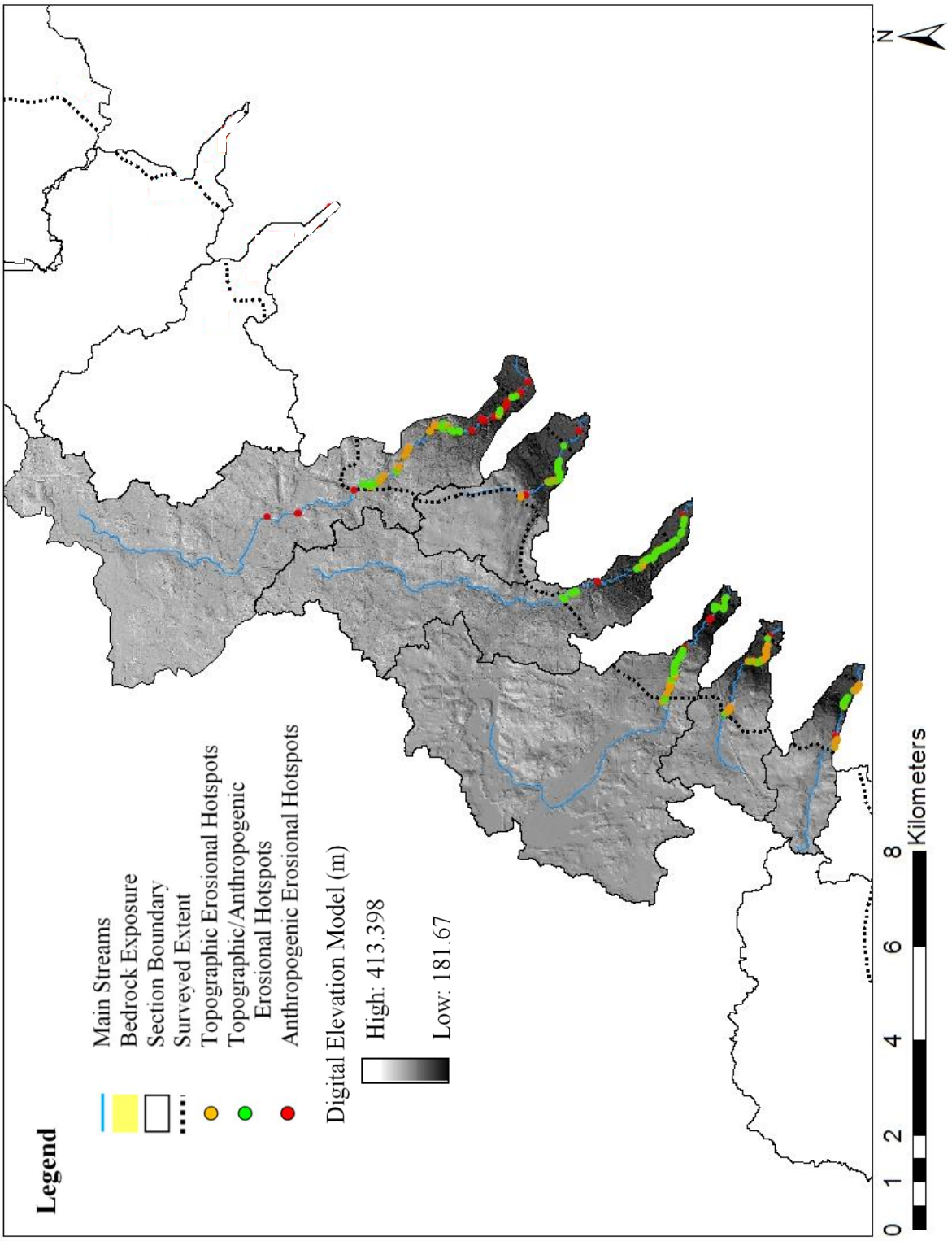


**Figure 35** Erosional hotspots in the central area of Duluth-area streams within the surveyed extent. Different consecutive color of spots indicates different types of erosional hotspots.

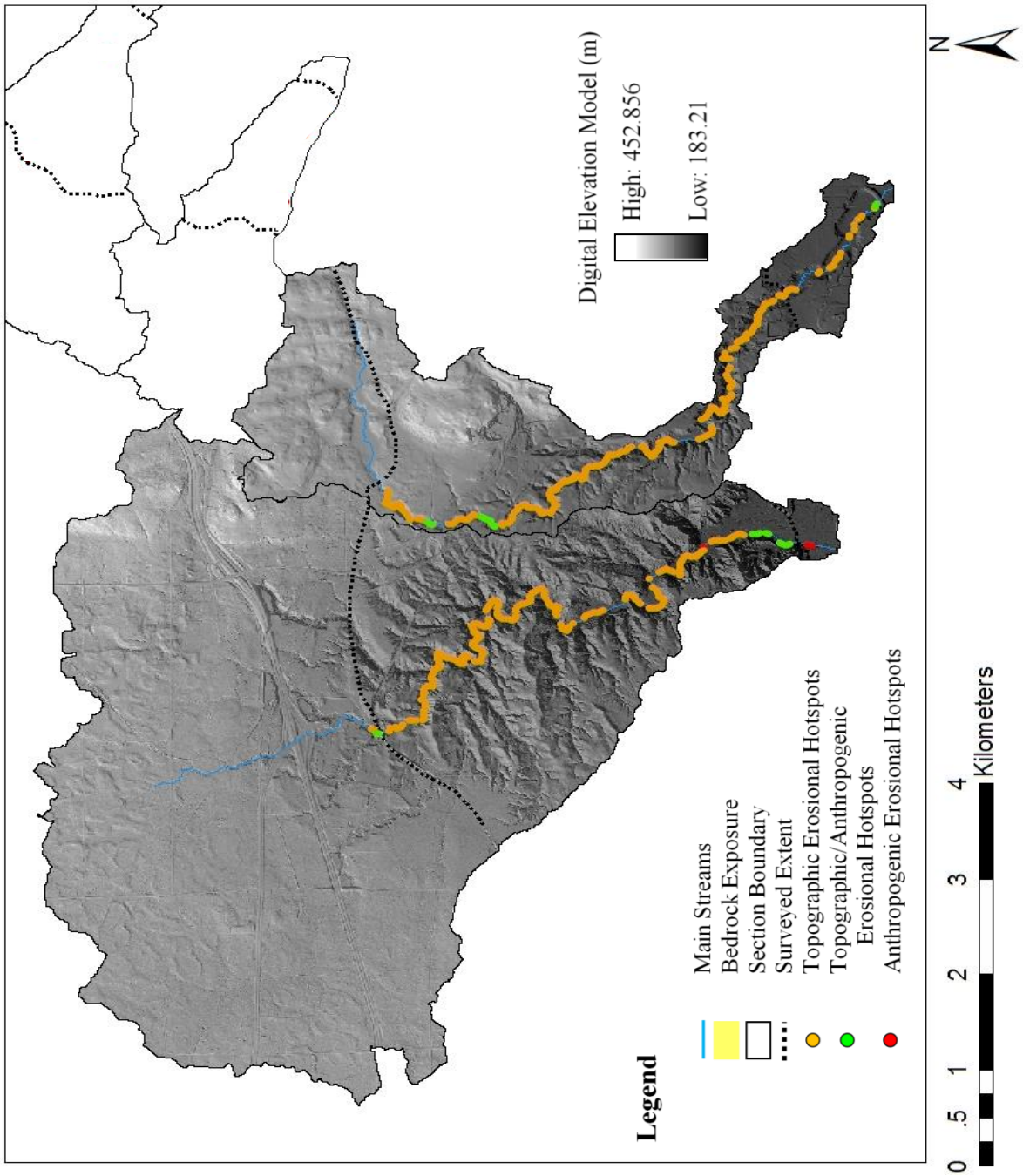


**Figure 36** Erosional hotspots in the southern area of Duluth-area streams within the surveyed extent. Different consecutive color of spots indicates different types of erosional hotspots.